NANOSCALE CONFINEMENT EFFECTS BETWEEN THIN METALLIC

SURFACES: FUNDAMENTALS AND POTENTIAL APPLICATIONS

A Dissertation

by

GUSTAVO EMILIO RAMIREZ CABALLERO

Submitted to the Office of Graduate Studies of
Texas A&M University
in partial fulfillment of the requirements for the degree of

DOCTOR OF PHILOSOPHY

December 2011

Major Subject: Materials Science and Engineering

Nanoscale Confinement Effects between Thin Metallic Surfaces: Fundamentals and

Potential Applications

NANOSCALE CONFINEMENT EFFECTS BETWEEN THIN METALLIC

SURFACES: FUNDAMENTALS AND POTENTIAL APPLICATIONS

A Dissertation

by

GUSTAVO EMILIO RAMIREZ CABALLERO

Submitted to the Office of Graduate Studies of
Texas A&M University
in partial fulfillment of the requirements for the degree of

DOCTOR OF PHILOSOPHY

Approved by:

Chair of Committee,	Perla B. Balbuena
Committee Members,	Tahir Cagin
	Raymundo Arroyave
	Jaime C. Grunlan
Intercollegiate Faculty	
Chair,	Ibrahim Karaman

December 2011

Major Subject: Materials Science and Engineering

ABSTRACT

Nanoscale Confinement Effects between Thin Metallic Surfaces: Fundamentals and

Potential Applications. (December 2011)

Gustavo Emilio Ramirez Caballero, B.A., Universidad Industrial de Santander

Chair of Advisory Committee: Dr. Perla B Balbuena

Density functional theory is used to study the physico-chemical effects of two metallic thin films separated by distances in a range of 4-10 Å. In this condition, the electrons from the metallic thin film surfaces tunnel through the energy barrier existing between the separated thin films, creating an electronic distribution in the gap between films. The characteristics and features of this electronic distribution, such as energy, momentum, and number of electrons, can be traced by quantum mechanical analyses. These same features can be tuned by varying metallic thin film properties like thickness, separation between films, and film chemical nature. The possibility to tune the physical properties of the electrons located in the gap between thin films makes the studied systems promising for applications that range from catalysis to nano-electronics.

Molecular oxygen, water, and ethylene were located in the gap between thin films in order to study the physical and chemical effects of having those molecules in the gap between thin films. It was observed that the electron structure in the gap modifies the geometric and electronic structure of those molecules placed in the gap. In the case of molecular oxygen, it was found that the dissociation energy can be tuned by changing

the separation between thin films and changing the chemical nature of the surface and overlayer of the thin film. For water, it was found that by tuning the chemical nature of the surface and sub-surface of both metallic thin films, molecular water dissociation can occur. When ethylene was located in the gap between Ti/Pt thin films, the molecule converts in an anion radical adopting the geometry and structure of the activated monomer necessary to initiate chain polymerization.

Regarding magnetism, it was found that by the surface interaction between Ti/Pt and Pt thin films, the magnetic moment of the system decreases as the separation between thin films decreases. The phenomenon was explained by changes observed in the number of electronic states at the Fermi level and in the exchange splitting as a function of separation between films. Finally, a system that resembles a p-n junction was proposed and analyzed. The system is a junction of two metallic thin films with different electronic density in the gap between surfaces. These junctions can be the building blocks for many electronic devices.

DEDICATION

To my father, sister, and wife for their unconditional love and support and in memory of

my mother

ACKNOWLEDGEMENTS

NOMENCLATURE

DFT   Density functional theory

STM   Scanning Tunneling Microscopy

SET   Single electron transistor

CMOS   Complementary metal-oxide-semiconductor

ORR   Oxygen reduction reaction

TABLE OF CONTENTS

LIST OF FIGURES

LIST OF TABLES

1. INTRODUCTION

Nanotechnology studies materials structures, functionality and properties at dimensions from sub-nanometer to several hundred nanometers. At this scale, quantum mechanics effects are predominant; therefore nanomaterials exhibit different physical properties from those of the bulk. One of the challenges of nanotechnology is the design of nanoparticles with tunable shapes and sizes, and therefore to obtain tunable physical and chemical properties that can be useful for technological applications.

The systems studied in this work are composed of two metal thin films separated at sub-nanometer distances. At these distances, the metal thin films have an interaction between them, but not as strong as to become a single film; that is, the system is in a transition from two non-interacting surfaces separated by long distances to a bulk system without surfaces. This transition zone is characterized by an interaction between the two metal thin films that can be explained by a quantum mechanics effect called electron tunneling, where electrons tunnel through the energy barrier located in the gap that separates both metallic surfaces. On the grounds of these phenomena, questions were posed in this work on how to tune the amount of electrons located in the gap between metallic thin films, as well as their energies and momentums and, what possible technological applications may emerge from the system under study.

_____

This dissertation follows the style of *Physical Chemistry Chemical Physics*

It was found that features of the system such as film thickness, separation between thin films, and thin film chemical nature modify the amount and physical properties of the electrons in the gap between thin films. The areas of catalysis and nano-electronics were explored for possible technological applications. In catalysis, the gap between metallic surfaces can be considered as a reactor in which the equilibrium electronic and geometric structures of the molecules are distorted by the electrons filling the gap. Under these conditions, the energy barriers for occurrence of chemical reactions (activation energy) may be modified thus resulting in a new path for the reaction, that is, the system acts as a catalyst. In nano-electronics, the interaction between metallic surfaces separated by a short distance plays a role in the energetic competition between the electron-electron exchange and the kinetic energy of electrons that defines the magnetic properties. This is the case of Pt/Ti systems where the magnetic moment changes with the gap size. This magnetic moment behavior could be used for applications, for instance, magnetic storage of information. Other applications are in the formation of metallic p-n junctions. It is possible to modify the density of electrons in the gap between metallic surfaces, and devices such as the junction of two systems with different density of electrons inside the gap may be arranged resembling a p-n junction. These junctions can be the building blocks for many electronic devices.

The results presented in this work may serve to explain experimental results published in the literature, as it is shown in Section 3. That is the case of enhancement of reactivity of metal porous systems formed after dealloying metal nanoparticles in acid medium [1-4]; the high activity of platinum nanotubes as fuel cell electrodes in which

the chemical reactions may occur both outside and inside the tube; the polymerization of polydiacetylene using an STM tip[5, 6] resembling two metallic surfaces separated by a short distance (the tip surface and the substrate surface) that form a gap where an anion radical initiates the polymerization that continues as a chain reaction, and the evidence of confinement effects in the enhanced rate of reaction of the reduction of 4-nitrophenol with sodium borohydride, where the catalytic reaction takes place in cavities of nanoparticles [7]. In the area of plasmonics, it has been experimentally observed that it is possible to tune the optical response of nanoparticle aggregates by varying the distance between nanoparticles; when the particles are nearly touching. The physical properties described in this work may help to explain the phenomena[8].

This is a theoretical work, where several metallic systems were simulated solving the Schrödinger equation using density functional theory. As in the case of every experimental and theoretical work, the calculations performed in this work have some approximations in the method and in the use of numerical tools that allows the implementation of codes for computer simulations.

This Dissertation is organized in seven Sections. The first one is devoted to establish antecedents, which actually were significant in developing this Dissertation, such as the recently published literature on the field and the theoretical background and computational methods used to obtain the results and conclusions. Section 2 includes an analysis of the role that variables such as chemical nature, thickness of the films, and separation between thin films play in the physical properties of the electrons located in the gap between thin films. Section 3 is a study of the confinement effects of Pt thin

films in the surface-subsurface distance, on the variation in the adsorption energy of atomic oxygen, O, and molecular oxygen, O_2, and dissociation of molecular oxygen, when the separation between surfaces becomes lower than particular threshold distances. Section 4 deals with the characterization of the reactivity in systems confined between alloy surfaces; exploring the geometric and electronic properties of interacting surfaces with different chemical element surfaces. Additionally, the dissociation of molecular oxygen and water systems under confinement is studied. Section 5 is a study of the geometric and electronic properties changes of an ethylene molecule confined between two metal surfaces, and its conversion into a radical anion monomer ready to react forming a polymer chain. Section 6 presents the study of the magnetic properties of a Ti monolayer over Pt when it is brought in contact with a Pt surface, at distances of 4 to 12 Å. Section 7 is a study of systems having gap regions in contact with different electronic densities forming different electrostatic potential energies. These gap regions are formed by different metallic overlayer surfaces and are analogous to p-n junctions in semiconductors materials. The conclusions of this work are summarized in Section 8.

2. THEORETICAL BACKGROUND, COMPUTATIONAL METHODS AND LITERATURE SEARCH

This work is based on quantum mechanics and a computational method, namely DFT, to approximate a solution of Schrödinger's equation. Also a very rich literature is available dealing with each of the particular phenomena treated in this work and will be presented in the respective Section. In section 2.2, a discussion is presented about literature on the general phenomena of energetic effects in the gap between surfaces.

2.1 Theoretical background and computational methods

The theoretical background of this work is based on the solution of the many body Schrödinger equation which requires the use of computational methods due to the complexity of the systems under study. Like every theoretical and experimental work, there are some limitations in the results presented in this work; in this specific case, the limitations are due to the approximations done to solve the many body Schrödinger equation and the numerical methods used to implement the solution of that equation as an algorithm for computational results. In this section a description of the approaches used to solve the many body Schrödinger equation and the computational methods is presented. The aim of this section is the demarcation of the theoretical region where the conclusions of this work rest.

The general physical system under study consists of electrons and nuclei moving in a field generated in conjunction. The Hamiltonian that describes this system with N electrons and K nuclei is:

$$H = \sum_{i=1}^{N} \frac{p_i^2}{2m} + \sum_{n=1}^{K} \frac{P_n^2}{2M_n} + \frac{1}{4\pi\varepsilon_0} \frac{1}{2} \sum_{i,j=1;i\neq j}^{N} \frac{e^2}{|r_i - r_j|} - \frac{1}{4\pi\varepsilon_0} \sum_{n=1}^{K}\sum_{i=1}^{N} \frac{Z_n e^2}{|r_i - R_n|} + \frac{1}{4\pi\varepsilon_0} \frac{1}{2} \sum_{n,n'=1;n\neq n'}^{K} \frac{Z_n Z_{n'} e^2}{|R_n - R_{n'}|} \quad (2-1)$$

The first two terms describe the kinetic energies of electrons and nuclei respectively, the third term the coulomb interaction between electrons, the fourth term the coulomb interaction between electrons and nuclei, and the fifth term the coulomb interaction between nuclei. This equation is extremely difficult to solve even with the best computers available, therefore, it is necessary to make a first approximation. Based on the fact that nuclei are much heavier than electrons, about 1800 times, the motion of the nuclei are separated from the motion of electrons, splitting the degrees of freedom of both particles. This approximation is known as the Born-Oppenheimer approximation:

$$H = \sum_{i=1}^{N} \frac{p_i^2}{2m} + \frac{1}{4\pi\varepsilon_0} \frac{1}{2} \sum_{i,j=1;i\neq j}^{N} \frac{e^2}{|r_i - r_j|} - \frac{1}{4\pi\varepsilon_0} \sum_{n=1}^{K}\sum_{i=1}^{N} \frac{Z_n e^2}{|r_i - R_n|} \qquad (2-2)$$

Within this approximation, the total energy of the systems is the sum of the energy of the electrons added to the electrostatic energy of the nuclei neglecting their motion. This approximation omits the correlated dynamics of nuclei and electrons making impossible the physical description of the following phenomena: polaron-induced

superconductivity, dynamical Jahn-Teller effect at defects in crystals, some phenomena of diffusion in solids, non-adiabaticity in molecule-surface scattering and chemical reactions, relaxation and some transport issues of charge carriers (e^- or h), etc.

Despite of the Born-Oppenheimer approximation, the simpler form of the Schrödinger equation, which is the time-independent, nonrelativistic Schrödinger equation, $H\psi = E\psi$, bares the difficulties of the many-body problem in the term describing the electron-electron interaction, since an individual electron wave function $\psi_i(r)$ can't be found without knowing simultaneously the individual electron wave function of the other electrons in the system.

The electronic structure calculations done in this work from the many body Schrödinger equation after the Born-Oppenheimer approximation are based on density functional theory. This theory resulted from the work of Hohenberg, Kohn and Sham [9, 10]. The first proved theorem says that: "The ground-state energy from Schrödinger's equation is a unique functional of the electron density" and the second theorem defines a property of the functional: "The electron density that minimizes the energy of the overall functional is the true electron density corresponding to the full solution of the Schrodinger equation". This approach has become popular since it postulates that the electronic orbitals are solutions of the Schrodinger equation that depend on the electronic density; and the right electronic density can be found by an equation that only involves a single electron (3 degrees of freedom), reducing in this way the degrees of freedom in comparison with traditional wave-function based methods, such as the

Hartree-Fock method, where the wave function has 3N degrees of freedom with N the number of electrons in the system. The equation is called the Kohn-Sham equations:

$$\left[-\frac{\hbar^2}{2m}\nabla^2 + V(r) + V_H(r) + V_{XC}(r)\right]\psi_i(r) = \varepsilon_i\psi_i(r) \qquad (2-3)$$

The first term of the equation describes the kinetic energy, the second term represents the interaction between an electron and the collection of nuclei, the third term is called the Hartree potential which is the Coulomb repulsion between the electron and the total electron density defined by all electrons in the system:

$$V_H(r) = e^2 \int \frac{n(r')}{|r - r'|} d^3r' \qquad (2-4)$$

This term is unphysical since part of its calculation involves the coulomb interaction between the electron and itself, the so called self-interaction contribution. Finally the fourth term, the exchange correlation potential that includes all the many-body effects: the corrections necessary for the introduction of self-interaction contributions, and exchange and correlation effects, it is formally defined as:

$$V_{XC}(r) = \frac{\delta E_{XC}(r)}{\delta n(r)} \qquad (2-5)$$

This is the main result of DFT: the exchange correlation potential depends only on the electron density, $n(r) = 2\sum_i \psi_i^*(r)\psi_i(r)$, yielding the exact ground state energy and density. Hohenberg-Kohn theorem simplifies the solution of the Schrödinger equation since the ground state of a system can be found by minimizing the energy of an energy functional which can be done by finding the self-consistent solution to a single particle equation described in equation (3). However, at this point, the form of the exchange-correlation functional, $E_{XC}[\{\psi_i\}]$, which existence is guaranteed, is not known.

In all the calculations done in this work the exchange correlation potential is approximated by a functional that has been found to give good results in a large variety of physical problems, this functional uses information of the local electron density and local gradient in the electron density, it is called the generalized gradient approximation (GGA). There are many ways to include the gradient of the electron density in the GGA functional, in this work was used the Perdew-Burke-Ernzerhof functional (PBE)[11].

The different systems used in this work have a large number of electrons which prohibits the direct solution of the Schrödinger equation. Fortunately, the crystals have periodical symmetries that can be used mathematically to convert an otherwise infinite system in a finite system. This is done using the Bloch's theorem that allows the solution of the Schrödinger equation in a finite unit cell applying boundaries conditions that take advantage of the periodicity of the crystal, the so called Bloch boundary conditions. The solutions are expressed as sum of term with form:

$$\phi_k(r) = \exp(ik \cdot r) u_k(r) \qquad\qquad (2-6)$$

Where the term $\exp(ik \cdot r)$ is a plane wave function used as a basis function for the electronic structure calculations, and $u_k(r)$ is periodic with the same periodicity as the unit cell that defined the crystal.

During the calculations of the crystal systems, several integrals inside the Brillouin zone of the system covering possible values of k are performed. In order to efficiently evaluate these kind of integrals, it is important to choose efficiently the values of k. The calculations presented in this work were performed using a widely use method developed by Monkhorst and Pack in 1976[12].

All systems studied in this work are metals, the simulation of this systems require special attention in the zone of transition between occupied and unoccupied electrons, the so called Fermi surface. The reason is that during the simulations the functions that have been integrated are continuous, and this feature makes difficult the simulation of the discontinuity between occupied and unoccupied electrons. The approach followed in the calculations presented in this work forces the functions to be continuous by smearing the discontinuity. The method used was developed by Methfessel and Paxton[13].

In all simulations an energy cutoff was introduced. The reason is that the form of the solutions of the Schrödinger equation for a unit cell presented in equation (6) has the periodic term $u_k(r)$ equal to:

$$u_k(r) = \sum_G c_G \exp[iG \cdot r] \qquad (2-7)$$

where G is a vector defined by $G = m_i b_i$ in reciprocal space. Thus, combining equation (7) and (6) gives:

$$\phi_k(r) = \sum c_{k+G} \exp[i(k+G)r] \qquad (2-8)$$

This equation is a sum that at specific k point can be done for an infinite number of possible values of G. Therefore, in order to compute the calculations the truncation of the sum is necessary. Since the kinetic energy is expressed as:

$$E = \frac{\hbar^2}{2m}|k+G|^2 \qquad (2-9)$$

The sum expressed in equation (8) is truncated by including only G values that give kinetic energies less than some cutoff value:

$$E_{cut} = \frac{\hbar^2}{2m}G_{cut}^2 \qquad (2-10)$$

One of the main problems of calculating band structures of crystals is that close to the nuclei the coulomb potential is deep causing rapid oscillations that complicate the calculations. A way to solve this problem followed in this work is the use of pseudopotentials. The use of this method is supported in the idea that core electrons are not especially important defining the physical properties of the material in contrast of valence electrons that define those properties. The pseudopotentials are weak potentials that outside the core region are the same as a full potential. In this way, the oscillatory behavior close to the nuclei is removed and the valence electrons are described in the same way as a full potential.

There are two important situations where DFT is less accurate: in the estimation of band gaps in semiconducting and insulating materials, and in the estimation of weak van der Waals attractions between atoms and molecules. In order to have accurate results in these situations it is necessary to use high level wave function based methods that describes better the long range electron correlation. There is a very active field of research improving functionals to overcome the mentioned limitations; for instance, the recently available in VASP gradient corrected functional AM05[14] and PBEsol[15], and Hybrid functional PBE0[16] and HSE06[17] that have proved excellent performance in solids, surfaces and better band gap estimations.

In summary, in this work, the first approximation done to solve the Schrödinger is the Born-Oppenheimer approximation; after decoupling electrons from nuclei, the electronic Hamiltonian applied to the Schrödinger equation is solved using DFT. This theory guaranties an exact solution of the ground-state energy from Schrödinger's

equation but the unique functional of the electron density necessary to solve the equation is unknown. In the Kohn-Sham equation the term that is unknown is the exchange correlation potential. Therefore, an approximate functional is used that is based on local electron density and gradient-corrected electron density, GGA, included in the -Burke-Ernzerhof functional (PBE). The periodic symmetries of the crystal system studied allow the use of Bloch's theorem which reduces an infinite system to a finite system applying boundary conditions. The base functions used as solutions of the Schrödinger equation are plane waves multiplied by a periodic function. During the calculation, it is necessary to solve integrals in the reciprocal space that requires efficient values of k; the method developed by Monkhorst and Pack was used. The discontinuities of the electron density in metals are treated by smearing methods developed by Methfessel and Paxton. The infinite sums involved in the calculations are truncated by introducing a cutoff base on values of the kinetic energy. And finally, the interactions between ions are described by pseudopotentials that remove oscillations close to the nuclei and focus in the right description of valence electrons.

2.2 Literature search

Previous research on the topic of this work has been triggered by its importance in technological applications associated with metal-metal or metal-semiconductor contacts, crack formation, wear and friction.[18, 19] The basic understanding of the physical phenomena occurring in the gap between surfaces can be summarized using a descriptive model of energy distribution in that region, depending on the separation

between surfaces. Three situations have been defined, with the first occurring at long separations, where no interaction occurs between both surfaces. A second scenario is defined by surface-surface distances of about 4 to 10 Å, where there is an interaction driven by the presence of electrons migrating from the surfaces into the gap. A third picture emerges at very short surface-surface distances, for which there is an avalanche phenomenon where the surfaces collapse.

Rose et al. [20, 21] discovered a universal relationship between scaled binding energy and separation between bimetallic surfaces, the so called universal binding energy relation (UBER). The found relation is said to be universal in as much as by a simple scaling, a unique curve is found to match the energy-distance dependence for different metals. Moreover, this universal relationship is a common template to study diverse phenomena such as chemisorptions, reaction kinetics on metallic surfaces, and others. Amitava et al. [22] later provided an explanation of the origin of UBER considering the electron density distribution as the key linking energy and distance in a metallic surface. This electron density distribution was found to follow a simple exponential decay function. Finally, Smith et al.[23] found a tendency to avalanche if two surfaces are brought together. Atomic layers collapse or avalanche together if the surfaces approach each other to a critical distance. This tendency is explained as a result of a competition of adhesive energy between surfaces and binding energy of the surface layer to the corresponding substrate.

Experimental studies using Atomic Force Microscopy (AFM) and Scanning Tunneling Microscopy (STM) have complemented the ab initio and density functional

theory (DFT) approaches giving support to the UBER concept. Taylor et al[24] studied adhesive avalanche by both DFT and AFM. Corma et al.[25], based on a theoretical study suggested that spatial confinement of electrons in zeolites might contribute to explain their catalytic activity. Some years later, this same group [26] showed spectroscopic evidence supporting the molecular orbital confinement in zeolites as a contribution for catalytic enhancement.

The energy-distance relationship has been also applied to the study of the fracture of crystals. Carter et al. [27] found that a universal function can be established between energy and crack opening displacement. Based on DFT calculations, Lazar et al. [28] studied cleavage under loading in a mode in which atomic layers are allowed to relax after a crack opening. These authors derived a simple analytical relationship between cohesion energy and stress for relaxed cleavage as a function of crack opening.

Were experimentally investigated by Atay et al. [29], the optical response of gold nanoparticles in pairs by varying the interparticle separation. At nanometer scale, they observed abrupt and large changes in the renormalization and splitting of the surface plasmon polariton energy. Zuloaga et al. [30], using time-dependent density functional theory studied the plasmon resonances in a nanoparticle as a function of interparticle separation. They showed that at interparticle separations below 1nm, there are optical responses and electromagnetic field enhancements drastically different than the classical predictions. Several other studies Principi et al., Shao et al., Mani et al., and Chen et al. [1-4] have reported enhancement of reactivity of metal porous systems formed after dealloying metal nanoparticles in acid medium, these metal porous resembles two

metallic surfaces separated by a short distance. El-Sayed et al. [7] reported experimental evidence of confinement effects in the enhanced rate of reaction for the reduction of 4-nitrophenol with sodium borohydride, where the catalytic reaction takes place in cavities of nanoparticles. Okawa et al. reported polymerization using an STM tip[5, 6] resembling two metallic surfaces separated by a short distance (the tip surface and the substrate surface) that form a gap where an anion radical initiates the polymerization that continues as a chain reaction.

This literature search highlighted some important theoretical and experimental research works that support the results obtained in this Dissertation work.

3. ELECTRONIC CONFINEMENT BETWEEN METAL SURFACES AT SUB-NANOMETER DISTANCES

3.1 Summary

When two metallic thin films become close to each other at distances where the surfaces interact, there are changes in electronic and magnetic properties of the films and in the gap separating them which strongly affect molecules present in the gap inducing new chemical reactions. Variables such as chemical nature and thickness of the films, and separation between the thin films influence such phenomena. This work aims to quantify and understand the effect of these variables on the electronic distribution inside the films and within the gap that separates both films. We present extensive analyses based on two models: a simple one-dimensional Kronig-Penney model and a more complete solution using density functional theory to represent the 3-dimensional system. It is concluded that changes in the thin film thickness modify the allowed energy bands for electrons, electrons energy and momentum, and the probability of having electrons at specific energy and momentum in the gap between films, with thinner films being more affected by migration of electrons to the gap. Changing the separation between films, the electronic properties and distribution are practically constant, with the consequence that shorter separations lead to an increase of the electronic density. Modifying the film chemical nature yields small changes in the electrons energy and momentum, but the number of allowed energy bands may change significantly, and the electronic distribution in the gap correlates with the location of each element in the periodic table.

Findings from these analyses suggest using the distance between surfaces and, or, film thickness as well as chemical composition of the films as control variables for tuning specific catalytic or sensor properties among other applications.

3.2 Introduction

Phenomena associated with metallic surfaces such as adhesion, cohesion, adsorption, catalysis, fracture, and others have been subjects of research for decades due to their related fundamental problems, and because of the technological applications that can be derived of the understanding of these phenomena. Systematic studies have been reported from different points of view and using multidisciplinary approaches: mechanics, physics, chemistry, thermodynamics and quantum mechanics. Ab initio calculations have become an essential tool to study these nano-scale phenomena especially during the last fifteen years.

It is well-known that the structure of materials, mainly composition and surface defects, play significant roles on the physicochemical properties of the material and hence on its mechanical and chemical behavior. A deep study of the environment in the gap between metallic surfaces may lead to a basic understanding of the phenomena occurring at electronic level in order to explain and take advantage of the observed effects. Previous research on this topic has been triggered by its importance in technological applications associated with metal-metal or metal-semiconductor contacts, crack formation, wear and friction.[18, 19] The basic understanding of the physical phenomena occurring in the gap between surfaces can be summarized using a

descriptive model of energy distribution in that region, depending on the separation between surfaces. Three situations have been defined: one, occurring at long separations, where no interaction occurs between both surfaces. A second scenario is defined by surface-surface distances of about 4 to 10 Å, where there is an interaction driven by the presence of electrons migrating from the surfaces into the gap. A third picture emerges at very short surface-surface distances, for which there is an avalanche phenomenon where the surfaces collapse.

Rose et al. [20, 21] discovered an universal relationship between scaled binding energy and separation between bimetallic surfaces, the so called universal binding energy relation (UBER). The found relation is said to be universal in as much as by a simple scaling, a unique curve is found to match the energy-distance dependence for different metals. Moreover, this universal relationship is a common template to study diverse phenomena such as chemisorptions, reaction kinetics on metallic surfaces, and others. Amitava et al.[22] provided an explanation of the origin of UBER considering the electron density distribution as the key linking energy and distance in a metallic surface. This electron density distribution was found to follow a simple exponential decay function. Smith et al. [23] found a tendency to avalanche if two surfaces are brought together. Atomic layers collapse or avalanche together if the surfaces approach each other at a critical distance. This tendency is explained as a result of a competition of adhesive energy between surfaces and binding energy of the surface layer to the corresponding substrate. Experimental studies using Atomic Force Microscopy (AFM) and Scanning Tunneling Microscopy (STM) have complemented the ab initio and

density functional theory (DFT) approaches giving support to the UBER concept. Taylor et al (1991)[24] studied adhesive avalanche by both DFT and AFM.

The energy-distance relationship has been also applied to the study of fracture of crystals. Carter et al.[27] found that a universal function can be established between energy and crack opening displacement. Lazar et al.[28] based on DFT calculations studied cleavage under loading in a mode in which atomic layers are allowed to relax after a crack opening. The authors derived a simple analytical relationship between cohesion energy and stress for relaxed cleavage as a function of crack opening.

The described phenomena may also affect the chemistry of atoms or molecules introduced in the confined region. Corma et al.[25], based on a theoretical study suggested that spatial confinement of electrons in zeolites might contribute to explain their catalytic activity. Some years later, Corma et al.[26] showed spectroscopic evidence supporting the molecular orbital confinement in zeolites as a contribution for catalytic enhancement. El-Sayed et al.[7] reported experimental evidence of confinement effects in the enhanced rate of reaction for the reduction of 4-nitrophenol with sodium borohydride, where the catalytic reaction takes place in cavities of nanoparticles.

In all these systems there is always a surrounding medium that acts as a "cage" providing geometric and electronic confinement. However, a complete analysis of the structural and electronic changes occurring in the "cage" and their potential effects on the confined molecules or atoms has not yet been reported. Moreover, understanding details of this phenomenon can lead us to engineering devices with specific functions.

This study focuses on thin metallic films separated by surface-surface distances of about 4 to 10 Å, where the interaction driven by the presence of electrons tunneling from the surfaces into the gap causes the emergence of interesting physical and chemical features. Questions arise on the causes, nature, and properties of this system, and the variables defining its structure and properties. Careful examination is done on the most adequate modeling techniques for simulating the phenomena occurring in the gap.

On these grounds, this work starts with an analysis based on the simplest model able to describe the system of two films separated by a gap: the Kronig-Penney model.[31] Following this model, conclusions are made regarding the variables that define the physical and chemical behavior of the system such as thickness and chemical nature of each film, and separation between films. After discussing the analysis from the simplest model, a more complete model is investigated using the Vienna ab initio simulation package (VASP), which offers the possibility to study the electronic structure of a complex system closer to a real one. Findings from these analyses suggest using the distance between surfaces and, or, film thickness as well as the chemical composition of the films as control variables for tuning specific catalytic or sensor properties among others. A brief introduction to possible technological applications is offered as a final section.

3.3 Computational methods

The simplest model that describes the system under study is the Kronig-Penney model [31]. This is a one dimensional model that considers the electrons free to move

within the metal, and the gap between films is a potential barrier as shown in Figure 3-1.

The film thickness is a, the films separation is b, and V_0 the energy barrier.
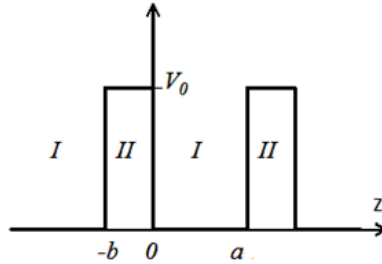
Figure 3-1. One-dimensional potential distribution used to solve the Schrödinger equation. Region I represents the thin film, and region II the gap between films.

The Schrödinger equation for the Kronig-Penney model assumes the following form for the region inside the metal (I) and in the gap (II):

$$\text{(I)} \quad \frac{d^2\Psi}{dz^2} + \frac{2m}{\hbar^2}E\Psi = 0 \quad \text{(II)} \quad \frac{d^2\Psi}{dz^2} + \frac{2m}{\hbar^2}(E\text{-}V_0)\Psi = 0 \tag{3-1}$$

Solving simultaneously both equations using a Bloch function[32], and applying boundary conditions that guarantee the continuity of the wave function in both regions, the solution of the Schrödinger equation in the system exists only if the following condition is satisfied:

$$\frac{(\gamma^2-\alpha^2)}{2\cdot\alpha\cdot\gamma}\sinh(\gamma\cdot b)\cdot\sin(\alpha\cdot a)+\cosh(\gamma\cdot b)\cos(\alpha\cdot a)=\cos\big(k(a+b)\big) \quad (3\text{-}2)$$

where $\alpha^2=\frac{2m}{\hbar^2}E$, and $\gamma^2=\frac{2m}{\hbar^2}\big(V_0\text{-}E\big)$.

In this work we use condition (2) as a design equation, describing the system allowed discrete energy bands, (E, k), at specific film thickness (a), film-film separation (b), and film chemical nature (V_0).

The probability to find an electron with specific energy and k point is given by the relation $\psi\psi^*$, which is normalized by the integral $\int_{-b}^{a}\psi\psi^*dz=1$. The total probability inside the material for specific system is defined as $\int_{0}^{a}\psi\psi^*dz$, and the total probability inside the gap between thin films is defined as $\int_{-b}^{0}\psi\psi^*dz$. The probability distribution inside the material is oscillatory whereas in the gap it always decays exponentially from the surfaces of the material, reaching its minimum in the middle of the gap. When two metallic surfaces interact, it is possible to find electrons in both regions: inside the metal and in the gap between films. This phenomenon is the basic concept that governs the physical and chemical behavior of two films separated by short distances and molecules confined in the gap between the films.

A more complex model, which may describe the real system more accurately, can be studied by DFT calculations, performed using the Vienna ab initio simulation package, VASP.[33-36] Using this software we calculated the charge distribution between thin films separated by a short distance. The new model is three dimensional and it considers electrons inside the material strongly bound to the nuclei, and individual

potentials from each lattice site overlap with each other. The metal slab model consists of a periodically repeated fcc (111) structure (Figure 3-2) composing of Cu, Ag, Au, Co, Pd, Pt, Ni, Rh, and Ir. It was taken as infinite in the x and y directions and finite in z direction. It was simulated using a 2×2 unit cell with different number of layers of metal atoms, and also for various separations between films to account these effects on the electronic structure of the system. All atoms in the system were fixed at positions according to the optimized lattice constant which was determined from bulk calculations. The calculated lattice constants for Cu, Ag, Au, Co, Pd, Pt, Ni, Rh, and Ir were 3.64, 4.16, 4.18, 3.52, 3.96, 3.98, 3.53, 3.84, and 3.88 Å respectively. Spin-polarized DFT calculations were performed with the exchange-correlation functional Perdew-Burke-Ernzerhof (PBE) [11] described within the generalized gradient approximation, with $9 \times 9 \times 1$ k-points in the surface Brillouin zone using Monkhorst-Pack [12] mesh sampling. The plane-wave cutoff energy was optimized at 350 eV. The results were checked for convergence with respect to energy cutoff and number of k-points. Spin polarization was taken into account and the Methfessel-Paxton smearing [13] of order 2 with a value of smearing parameter σ of 0.2 eV was applied. The reported total charge in the gap between films was calculated as the sum of the charges in a region defined from a distance after the position of the surface atoms equals to half of the interlayer distance in the material.
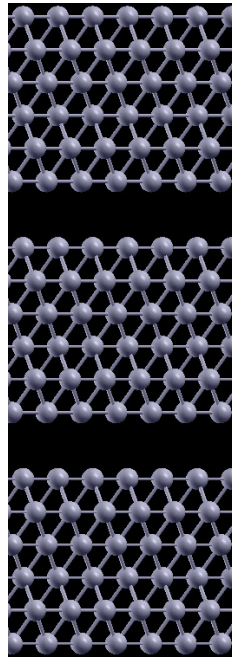
Figure 3-2. The metal slab model consists of a periodically repeated fcc (111) structure. It was taken as infinite in the x and y directions and finite in z direction. It was simulated using a 2 × 2 unit cell with different number of layers of metal atoms, and also for various separations between films to account these effects on the electronic structure of the system.

3.4 Results and discussion

The objective of studying two models with different degrees of complexity is to elucidate the phenomena from two different perspectives, and establish the bases on which possible technological applications may be built on. The simplified 1-D model allows us to rapidly draw many qualitative conclusions which are useful for a first analysis; the 3-D model introduces additional complexities and allows a more detailed

understanding and even the evaluation of metamaterials with specific properties. Thus is important to establish that the results from both models are consistent with each other. In the following sections, thin film thickness and chemical nature, and separation between films are analyzed separately by varying only one variable of interest while fixing the other two.

3.4.1 Film thickness

The mathematical condition for real solutions of the Kronig-Penney model expressed by equation (2) implies that for specific film thickness, film separation, and gap energy barrier an electron can only occupy *certain allowed energy bands*. At fixed films separation and gap energy barrier, but different film thickness, there are changes in the number of allowed energy bands, the energy of each n band, and the width of the bands. For an interval of energy of 10 eV, Table 1 shows the initial and final energy and k point per allowed energy band as well as the energy difference of each energy band for three Iridium systems where each film is composed by 2, 5, and 10 layers of thickness respectively, and 4 Å of separation between films. The energy barrier V_0 for each thin film was calculated using VASP yielding 14.96eV, 14.99eV, and 15.03eV for 2, 5, and 10 layers respectively. It is observed from the results that as the thin film thickness decreases the number of allowed energy bands decreases. For instance, a system with 2, 5, and 10 layers has 2, 6, and 11 allowed energy bands respectively; the maximum k point from each energy band increases as the thin film decreases, being around 0.37, 0.21, and 0.12 for 2, 5, and 10 layers respectively. The difference between the highest

and lowest energy allowed for each band is small but increases at higher energy bands, for instance for the 10 layers system, the first energy band (n=1) has an energy width of 3.57E-5eV whereas the last energy band (n=11) has an energy width of 1.75E-2eV. Finally, each system with specific thickness has different energy band values. In summary, the condition for existence of real solution, equation (2), given by the Kronig-Penney model predicts that the thickness of the film changes the energies, momenta, and number of energy bands of electrons located in the gap between thin films.

Table 3-1. Allowed energy bands and k points calculated from the condition of existence of a real solution expressed in equation (3-2) as a function of film thickness. E_i is the lowest energy, k_i is the initial k point, E_f is the highest energy, and k_f is the final k point of the respective energy band. The energy and k point precision is of 1×10^{-7}.

n	2 layers			5 layers			10 layers		
	$\begin{pmatrix} E_i \\ k_i \end{pmatrix}$	$\begin{pmatrix} E_f \\ k_f \end{pmatrix}$	$E_f - E_i$	$\begin{pmatrix} E_i \\ k_i \end{pmatrix}$	$\begin{pmatrix} E_f \\ k_f \end{pmatrix}$	$E_f - E_i$	$\begin{pmatrix} E_i \\ k_i \end{pmatrix}$	$\begin{pmatrix} E_f \\ k_f \end{pmatrix}$	$E_f - E_i$
1	1.243148	1.244028	8.80E-4	0.252672	0.2527354	6.34E-5	0.2750397	0.2750754	3.57E-5
	1.78952E-3	0.3685845		3.81447E-3	0.2062334		0.1180221	2.691248E-3	
2	4.8799917	4.8884867	8.49E-3	1.0092037	1.0095059	3.02E-4	0.6186274	0.6187144	8.70E-5
	0.3700441	5.562232E-4		0.2057000	8.959737E-4		1.963655E-3	0.1173781	
3				2.2647887	2.2657052	9.17E-4	1.0992411	1.0994143	1.73E-4
				1.321987E-3	0.2065381		0.1175298	1.092863E-3	
4				4.0099824	4.0125010	2.52E-3	1.7164384	1.7167520	3.14E-4
				0.2060871	3.563559E-4		4.759987E-4	0.1179144	
5				6.2272784	6.2344131	7.13E-3	2.4695962	2.4701386	5.42E-4
				4.769945E-4	0.2065457		0.1180931	9.667265E-4	

Table 3-1 continued

n	2 layers			5 layers			10 layers		
	$\begin{pmatrix}E_i\\k_i\end{pmatrix}$	$\begin{pmatrix}E_f\\k_f\end{pmatrix}$	$E_f - E_i$	$\begin{pmatrix}E_i\\k_i\end{pmatrix}$	$\begin{pmatrix}E_f\\k_f\end{pmatrix}$	$E_f - E_i$	$\begin{pmatrix}E_i\\k_i\end{pmatrix}$	$\begin{pmatrix}E_f\\k_f\end{pmatrix}$	$E_f - E_i$
6				8.8810760 / 0.2066512	8.9038025 / 2.965625E-5	2.27E-2	3.3578553 / 6.466638E-4	3.3587774 / 0.1189091	9.22E-4
7							4.3800286 / 0.1187796	4.3815973 / 4.82805E-4	1.57E-3
8							5.5344429 / 9.869133E-5	5.5371528 / 0.1189934	2.71E-3
9							6.8186460 / 0.1187688	6.8234611 / 2.94691E-4	4.81E-3
10							8.2288142 / 6.447677E-5	8.2377375 / 0.1188810	8.92E-3
11							9.7583997 / 0.1189991	9.7759374 / 1.78978E-4	1.75E-2

Since systems with different thin film thicknesses have different allowed energies, it is expected that the probability distribution to find an electron at specific allowed energy and k point as a function of film thickness varies in both regions: inside the material and in the gap. Figure 3-3 shows the probability distribution of Iridium thin films with separation between films of 4 Å and film thickness of 2, 3, and 5 layers respectively. The energies and k-points for probability calculations of the depicted systems were chosen as (4.88, 0.37), (9.64, 0.29), and (8.88, 0.21) for 2, 3, and 5 layers respectively, which correspond to the lowest energy with its k point of the highest energy band within an interval of energy of 10 eV.

Figure 3-3. The top graph is the probability distribution to find an electron with specific energy and k point in both regions of the system: inside the material and in the gap between Iridium films for three different film thicknesses. The bottom graph is the probability distribution to find an electron with a specific energy and k point in the gap between films. The probability distribution changes inside the material and in the gap between films as a function of film thickness.

Table 3-2 shows the total probability to find an electron with specific energy and momentum inside the thin film material and the total probability in the gap between thin films. As expected, the total probabilities vary as a function film thickness since each system has different allowed energies, as explained before. An interesting result is that the total probability to find an electron in the gap between thin films at specific energy

and momentum has local maxima and minima depending on the thin film thickness. As mentioned before, the specific energies and momenta chosen were the lowest energy and its k point corresponding to the highest energy band within an interval of energy of 10 eV.

Table 3-2. Total probabilities inside the thin film and in the gap between thin films as a function of film thickness.

System: Ir, b=4Å	Total probability inside the thin film: $\int_0^a \psi\psi^* dz$	Total probability in the gap between thin films: $\int_{-b}^0 \psi\psi^* dz$
2 layers	0.93	0.07
3 layers	0.87	0.13
5 layers	0.92	0.08
10 layers	0.95	0.05

From the DFT results calculated using VASP, we obtained the total charge distribution regardless of the specific electronic energy. It is observed that the charge distribution as a function of film thickness in the system is practically constant, whereas the total charges in the system change. As an example, Figure 3-4 shows the charge distribution of Iridium films separated by 4.0 Å having films thickness of 10, 5, and 2 layers. These findings suggest that systems with smaller thickness are more affected by giving electrons to the gap which may be reflected in its physical behavior in comparison with those with larger thickness. In the specific region of the gap between films, the results of the calculations show that the charge is practically the same at different film thicknesses. However, since the thickness of the film changes, the number

of atoms and total valence electrons of the system also change; thus, the total charge in the gap between the films with respect to the total charge in the system increases as the film thickness decreases. For instance, in thin films of Ir with films separation of 4.0 Å, the total charge of a system of 2 layers and 5 layers is 72 and 180 valence electrons, respectively; and the total charge for both systems in the gap is 3.07 electrons. Therefore, the percentage of charge in the gap with respect to the total charge of the system is 4.26% for the system of 2 layers and 1.70% for the system of 5 layers, see Table 3-3.
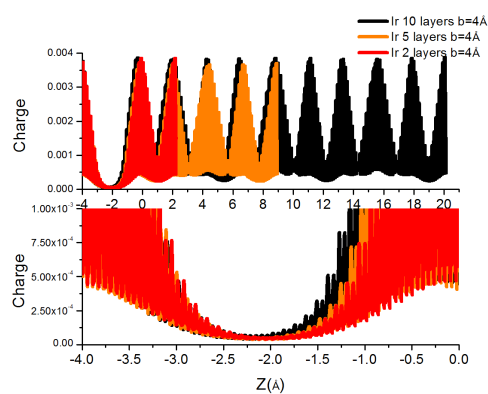
Figure 3-4. The top graph is the charge distribution in both regions of the system: inside the material and in the gap between films for Iridium with three different film thicknesses. The bottom graph is the charge distribution in the gap between films. The charge distribution in the gap between films is constant whereas the total number of valence electrons in the system changes. Some filtering has been done to the extensive calculated data.

Table 3-3. Calculated total valence charge in the system and total charge in the gap between films as a function of film thickness.

System: Ir, b = 4Å	Total valence charge in the system	Total charge in the gap between films	Total charge in the gap per total valence charge in the system
2 layers	72	3.07	4.26%
5 layers	180	3.07	1.70%
10 layers	360	3.10	0.86%

The above analysis was done for the total charge distribution in the systems disregarding the energies of the charges. Using the Kronig-Penney model, it was shown that the electrons in the gap have specific energies and k points. In the more complex system using DFT, since energy bands overlap, it is harder to evaluate the probability at a specific energy band, but it is possible to calculate the charge distribution in an interval of energy and the total probability as the total charge in the gap over the total charge in the specific interval of energy. Figure 3-5a shows this probability, the total charge in the gap between films per total charge for an interval of energy as a function of film thickness. The interval of energy is located 0.1 eV below the Fermi energy level of the Iridium system. The relation between the number of electrons in the gap and the total number of electrons in the system having energies in the selected interval varies as a function of film thickness. This implies that the electrons in the gap have different energies and k points depending on the film thickness. The conclusion agrees with the analysis done using the Kronig-Penney model.
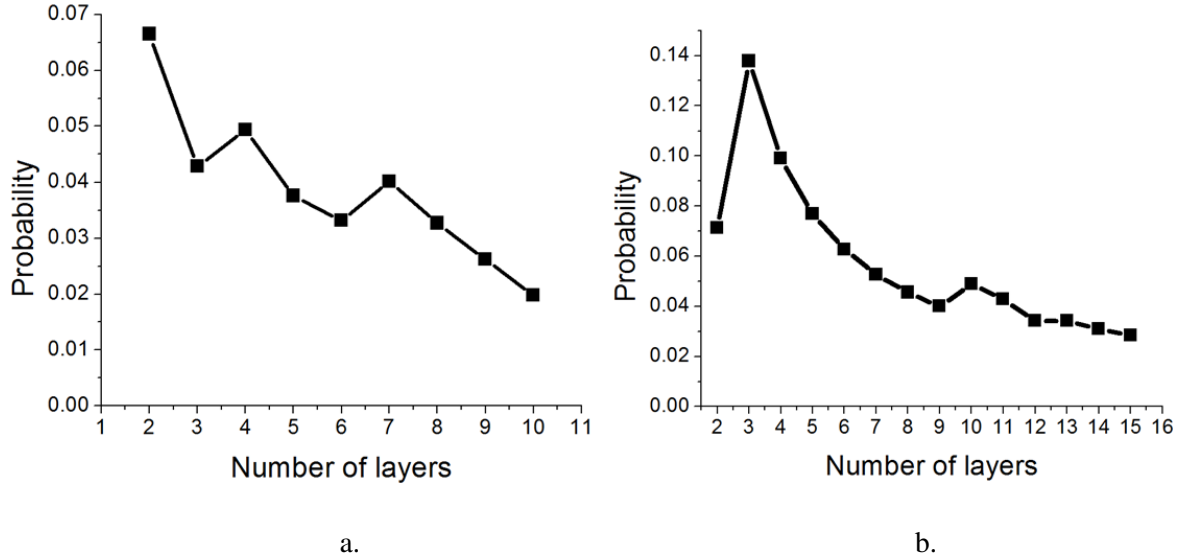
Figure 3-5. a. Total charge in the gap per total charge in an interval of 0.1eV below the Fermi energy versus thin film thickness calculated using DFT in VASP. b. Total probability (as in Table 3-2) to find an electron in the gap between films as a function of film thickness calculated using the Kronig-Penney model.

3.4.2 Separation between films

Using the mathematical condition for real solutions of the Kronig-Penney model expressed in equation (2) we change the separation (b) between Ir films at fixed film thickness of 5 layers and gap energy barrier of 14.99eV. It is found that the number of allowed energy bands in the system is constant, the energy of each energy band slightly changes and the maximum k point for each energy band diminishes as the separation between films increases, see Table 3-4.

Table 3-4. Allowed energy bands and k points calculated from the condition of existence of real solution expressed in equation (3-2) as a function of separation between films. E_i is the lowest energy, k_i is the initial k point, E_f is the highest energy, and k_f is the final k point of the respective energy band.

n	b = 4.0 Å			b = 4.5 Å			b = 5.0 Å		
	$\begin{pmatrix} E_i \\ k_i \end{pmatrix}$	$\begin{pmatrix} E_f \\ k_f \end{pmatrix}$	$E_f - E_i$	$\begin{pmatrix} E_i \\ k_i \end{pmatrix}$	$\begin{pmatrix} E_f \\ k_f \end{pmatrix}$	$E_f - E_i$	$\begin{pmatrix} E_i \\ k_i \end{pmatrix}$	$\begin{pmatrix} E_f \\ k_f \end{pmatrix}$	$E_f - E_i$
1	0.252672	0.2527354	6.34E-5	0.2526919	0.2527155	2.36E-5	0.2526993	0.2527081	8.80E-6
	3.81447E-3	0.2062334		7.67744E-03	0.194477857		9.86394E-03	0.18801033	
2	1.0092037	1.0095059	3.02E-4	1.00929699	1.0094128	1.16E-4	1.0093326	1.00937709	4.44E-5
	0.2057000	8.959737E-4		0.197350271	1.59509E-03		0.19153589	5.43666E-03	
3	2.2647887	2.2657052	9.16E-4	2.2650633	2.2654307	3.67E-4	2.26517339	2.26532069	1.47E-4
	1.321987E-3	0.2065381		2.05976E-03	0.19854494		2.5400E-04	0.19094336	
4	4.0099824	4.0125010	2.52E-3	4.01070289	4.01178059	1.08E-3	4.0110110	4.01147229	4.61E-4
	0.2060871	3.563559E-4		0.19908517	9.56135E-04		0.193549978	1.24772E-03	
5	6.2272784	6.2344131	7.13E-3	6.22917150	6.2325143	3.34E-3	6.2300591	6.2316253	1.57E-3
	4.769945E-4	0.2065457		5.88756E-04	0.199696055		7.86373E-04	0.1935451	
6	8.8810760	8.9038025	2.27E-2	8.886357	8.8984295	1.21E-2	8.8891723	8.8955855	6.41E-3
	0.2066512	2.965625E-5		0.199972673	3.47900E-04		0.19396695	4.41070E-04	

Since energy and k point from each allowed energy band are similar regardless of separation between films, it is expected to find similar values of probability distribution for finding an electron at a specific allowed energy and k point as a function of films separation. Figure 3-6 shows similar values of probability distribution in both regions, inside the material and in the gap between films for separation between films of 4.0, 4.5, and 5.0 Å.
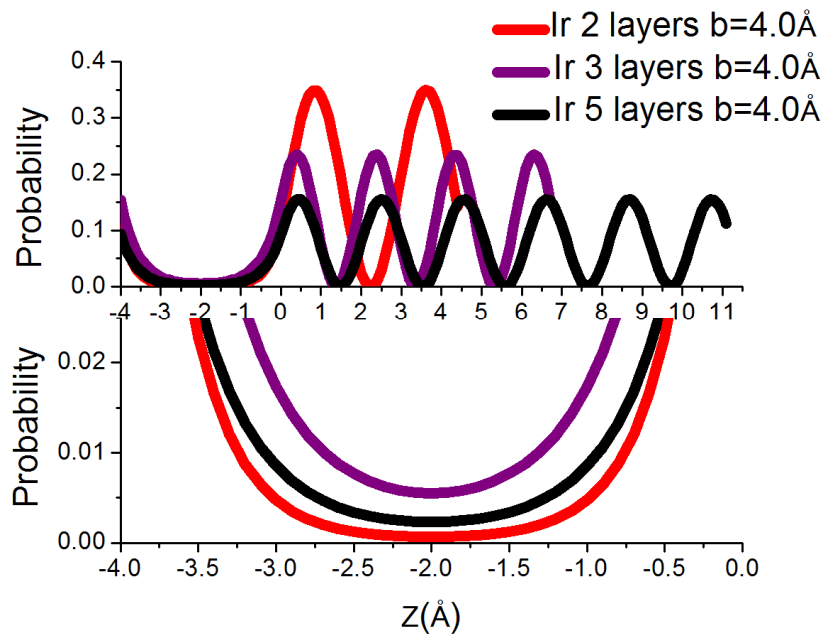
Figure 3-6. The top graph is the probability distribution to find an electron with specific energy and k point in both regions of the system, inside the material and in the gap between films for a thin film of Iridium with three different film separations. The bottom graph is the probability distribution to find an electron with specific energy and k point in the gap between films. The probability distribution practically remains constant with the films separation, but the length of the gap changes; thus, the total probability in the gap per total probability of the system increases as the films separation decreases.

Table 3-5 shows the total probabilities inside the material and in the gap between films. The total probability in the gap between films is practically constant regardless of the separation between films; however, the length of the gap is changing. Therefore, the variable that is changing as a function of separation between films is the total probability in the gap per length of the gap, see Table 3-5.

Table 3-5. Total probabilities inside the thin film and in the gap between films calculated using the Kronig-Penney model. The probabilities remain practically constant with respect to the separation between films.

System: Ir, 5 layers	Total probability inside the thin film: $\int_0^a \psi\psi^* dz$	Total probability in the gap between thin films: $\int_{-b}^0 \psi\psi^* dz$	Total probability in the gap per length of the gap
b=4.0Å	0.922	0.078	1.95%
b=4.5Å	0.924	0.076	1.69%
b=5.0Å	0.925	0.075	1.50%

DFT calculations showed that the total charges inside the material and in the gap between films, regardless of the charge energies, are practically constant as a function of separation between films. Figure 3-7 shows the charge distribution in three systems with the same thin film thickness of 5 layers but with 4, 4.5, and 5 Å separation between films.
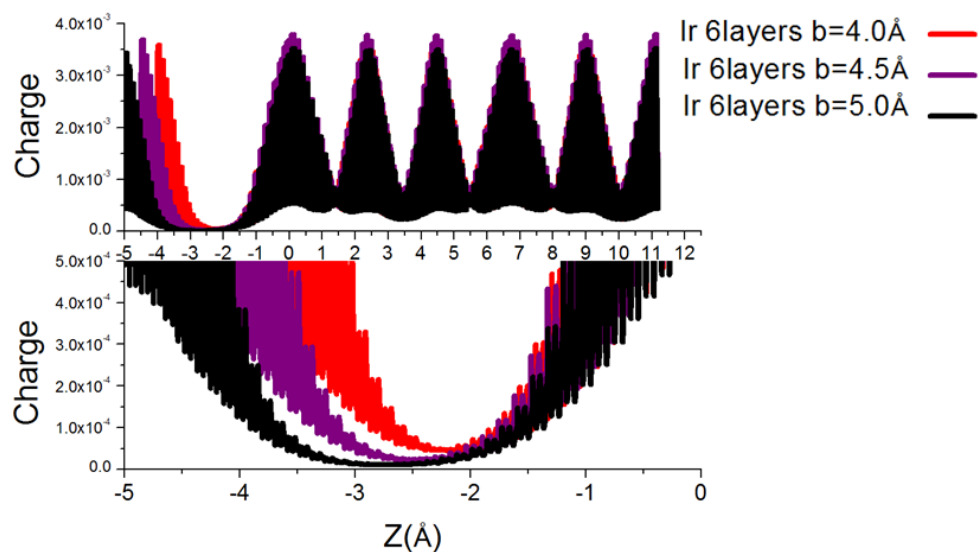
Figure 3-7. The top figure shows the total charge distribution of three Iridium thin films with film thickness of 6 layers and different films separation. The bottom figure shows the charge distribution in the gap between films. The total charge distribution and charge in the gap between films is practically the same for all systems. However, the volume of the gap between films changes with the films separation. For that reason, the total charge in the gap between films per volume of the gap (i.e. the electronic density) increases as the films separation decreases.

The total charge in the systems is constant regardless of the separation between films since the number of atoms is fixed. The results presented in Table 3-6 show that the total charge in the gap between films is practically constant, but the volume in the

gap is changing. This means that as the separation between films decreases the charge in the gap is constant but more confined, therefore denser.

Table 3-6. Total valence charge in the system and in the gap between films. The total charges remain practically constant with respect to the separation between films.

System: Ir, 6 layers	Total valence charge in the system	Total charge in the gap between films	Total charge in the gap per volume in the gap
b = 4.0Å	216	3.05	11.3%
b = 4.5Å	216	3.07	10.1%
b = 5.0Å	216	3.06	9.1%

3.4.3 Films chemical nature

Table 3-7 shows the first four allowed energy bands and k points obtained by using the mathematical condition for real solutions of the Kronig-Penney model expressed in equation (2) of several films with different chemical nature. The separation between films is fixed (b=4.0Å), the film thickness is 11.19Å, and gap energy barriers of 7.36, 9.74, 10.13, 8.23, 7.47, 9.53, 12.65, 12.24, and 14.99eV correspond to Ag, Au, Co, Cu, Ni, Pd, Pt, Rh, and Ir respectively.

Table 3-7. First four allowed energy bands and k points calculated from the condition of existence of real solution expressed in equation (3-2) as a function of gap energy barrier. E_i is the lowest energy, k_i is the initial k point, E_f is the highest energy, and k_f is the final k point of the respective energy band.

n	Cu		Ag		Au	
	$V_0 = 8.23\ eV$		$V_0 = 7.36\ eV$		$V_0 = 9.74\ eV$	
	$\begin{pmatrix} E_i \\ k_i \end{pmatrix}$	$\begin{pmatrix} E_f \\ k_f \end{pmatrix}$	$\begin{pmatrix} E_i \\ k_i \end{pmatrix}$	$\begin{pmatrix} E_f \\ k_f \end{pmatrix}$	$\begin{pmatrix} E_i \\ k_i \end{pmatrix}$	$\begin{pmatrix} E_f \\ k_f \end{pmatrix}$
1	0.23824480	0.238866	0.23511481.0	0.2360048	0.2426788	0.2430271
	1.2473E-03	0.20530852	4951E-03	0.205514779	1.39249E-03	0.2057935
2	0.94950289	0.95256589	0.9363563	0.94077059	0.9679953	0.9696966
	0.206375	7.09099E-04	0.206364299	4.31492E-04	0.20607468	1.87547E-04
3	2.1216633	2.1315555	2.0891564	2.1035668	2.1667138	2.1721145
	3.6808E-04	0.2066409	3.30514E-04	0.20653238	4.99876E-04	0.2066291
4	3.7264914	3.7565737	3.65807139	3.70263999	3.81854799	3.8345222
	0.2066897	1.98905E-04	0.2067811	1.48601E-04	0.20671220	1.63469E-04

n	Ni		Pd		Pt	
	$V_0 = 7.47 eV$		$V_0 = 9.53\ eV$		$V_0 = 12.65\ eV$	
	$\begin{pmatrix} E_i \\ k_i \end{pmatrix}$	$\begin{pmatrix} E_f \\ k_f \end{pmatrix}$	$\begin{pmatrix} E_i \\ k_i \end{pmatrix}$	$\begin{pmatrix} E_f \\ k_f \end{pmatrix}$	$\begin{pmatrix} E_i \\ k_i \end{pmatrix}$	$\begin{pmatrix} E_f \\ k_f \end{pmatrix}$
1	0.235556	0.2364039	0.24212731.8	0.2425034	0.2489544	0.2490834
	7.2848E-04	0.2054310	0377E-03	0.2055647	2.34763E-03	0.20332668
2	0.9382145	0.9424164	0.965702	0.9675424	0.99394000.2	0.99456111.5
	0.2062123	5.30852E-04	0.2062408	8.21971E-04	062622	9119E-03
3	2.0937767	2.1074745	2.1611691	2.1670218	2.2287803	2.23069830.2
	2.5140E-04	0.2067477	5.02789E-04	0.20651016	4.58020E-04	060107
4	3.6679031	3.71017349	3.8073799	3.8247546	3.94088639	3.9463107
	0.2067133	2.84084E-05	0.2065818	1.66407E-04	0.2067576	4.83406E-04

Table 3-7. Continued

n	Co		Rh		Ir	
	$V_0 = 10.13\ eV$		$V_0 = 12.24\ eV$		$V_0 = 14.99\ eV$	
	$\begin{pmatrix} E_i \\ k_i \end{pmatrix}$	$\begin{pmatrix} E_f \\ k_f \end{pmatrix}$	$\begin{pmatrix} E_i \\ k_i \end{pmatrix}$	$\begin{pmatrix} E_f \\ k_f \end{pmatrix}$	$\begin{pmatrix} E_i \\ k_i \end{pmatrix}$	$\begin{pmatrix} E_f \\ k_f \end{pmatrix}$
1	0.2436704	0.2439725	0.2481935	0.2483409	0.252672	0.2527354
	2.3513E-03	0.205617436	2.61444E-03	0.2043150	3.81447E-3	0.2062334
2	0.9721112	0.973583	0.990806	0.9915178	1.0092037	1.0095059
	0.206654	2.9730E-04	0.205454	6.85913E-04	0.2057000	8.959737E-4
3	2.1766427	2.1812983	2.2213464	2.2235495	2.2647887	2.2657052
	3.0596E-04	0.2063318	1.38146E-04	0.206173821	1.321987E-3	0.2065381
4	3.838440	3.852119	3.9264674	3.9327337	4.0099824	4.0125010
	0.206664	2.20172E-04	0.20663695	1.20503E-04	0.2060871	3.563559E-4

The results presented in Table 3-6 show small variations in the allowed energy bands and k points as a function of the gap energy barrier. As the gap energy barrier of the film increases the values of the allowed energy bands increase. In these results, we did not consider the quantization of the film thickness with respect to the films chemical nature which results from the fact that every element has a different lattice constant making possible to have variations in the film thickness for different film chemical nature.

Since the allowed energy bands and k points have a small variation as a function of the gap energy barrier of each film, it is expected, as shown in Figure 3-8, that the probability distributions to find an electron at specific energy and k point as a function of film chemical nature are similar to each other. In Figure 3-8, the probability distributions

for Co, Rh, and Ir correspond to the lowest energy and its k point for the fourth allowed
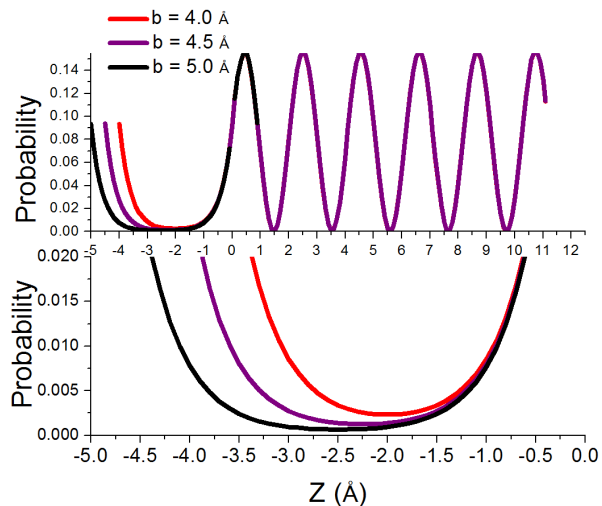
energy band, see Table 3-7.
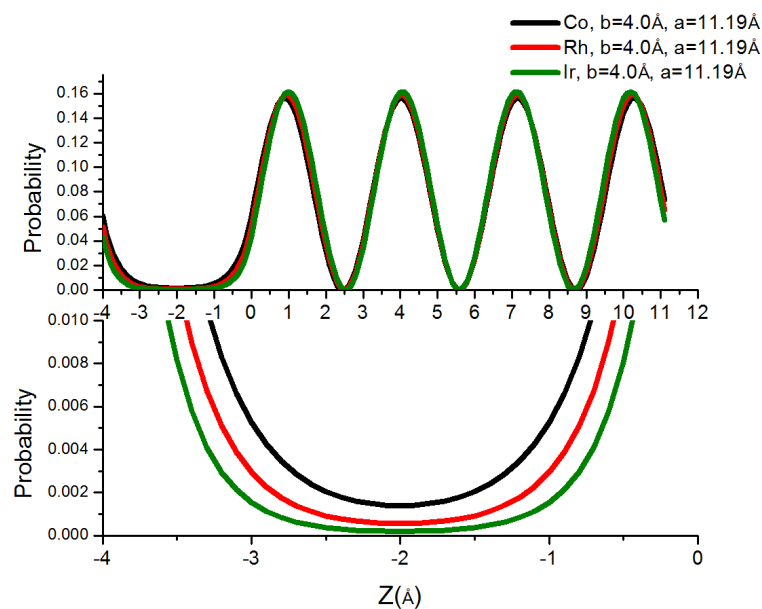
Figure 3-8. The top graph is the probability distribution to find an electron with specific

energy and k point in both regions of the system, inside the material and in the gap

between films for three different thin film elements. The bottom graph is the probability

distribution to find an electron with specific energy and k point in the gap between films.

Each element that composes the films has different Fermi energy level and gap energy

barrier; this is reflected in different probability distribution in the systems.

Table 3-8 shows the total probability to find an electron inside the gap between

the films and inside the material at the energies and k points used in the probability

distributions depicted above. It is observed that the total probability to find an electron in the gap between films increases as the gap energy barrier decreases. In order to have a more complete analysis, it is necessary to point out that specific film chemical nature has specific Fermi energy levels, which implies that the number of allowed energy bands changes with the chemical nature of the film; in the results just presented only four allowed energy bands for each system are studied.

Table 3-8. Total probabilities inside the thin film and in the gap between films calculated using the Kronig-Penney model. The probabilities correspond to the lowest energy and its k point for the fourth allowed energy band.

System a=11.19Å, b= 4.0Å	Total probability inside the thin film: $\int_0^a \psi\psi^* dz$	Total probability in the gap between thin films: $\int_{-b}^0 \psi\psi^* dz$
Cu $V_0 = 8.23\ eV$	0.929	0.070
Ag $V_0 = 7.36\ eV$	0.913	0.087
Au $V_0 = 9.74\ eV$	0.947	0.052
Ni $V_0 = 7.47 eV$	0.915	0.084
Pd $V_0 = 9.53\ eV$	0.945	0.054
Pt $V_0 = 12.65\ eV$	0.966	0.034
Co $V_0 = 10.13\ eV$	0.951	0.049

Table 3-8. Continued.

System a=11.19Å, b= 4.0Å	Total probability inside the thin film: $\int_0^a \psi\psi^* dz$	Total probability in the gap between thin films: $\int_{-b}^0 \psi\psi^* dz$
Rh $V_0 = 12.24\ eV$	0.964	0.035
Ir $V_0 = 14.99\ eV$	0.974	0.026

Table 3-9 shows the DFT results of several systems with different film chemical nature, 5 layers of thickness, and separation between films of 4.0Å. Despite the film thickness is always 5 layers, the film thickness changes due to the lattice constant differences between elements. The results show some general trends taking into account the location of each element in the periodic table. The percentage of charge in the gap per total valence charge in the system increases in a same group of the periodic table as the atomic number increases, with the exception of Ag in the eleventh group; and the percentage of charge in the gap per total valence charge in the system increases in a same period of the periodic table as the atomic number decreases. In these results, there are many variables changing; the thickness, Fermi energy, energy barrier between films, and total valence charge for each system.

Table 3-9. Total valence charge in the system and in the gap between films calculated using DFT. The total charges change as function of film chemical nature.

System b=4.0Å	Total valence charge in the system	Total charge in the gap between films	Total charge in the gap per total valence charge in the system
Cu, a=10.50Å	220	1.92	0.87%
Ag, a=11.99Å	220	1.84	0.84%
Au, a=12.05Å	220	2.14	0.97%
Ni, a=10.18Å	200	1.73	0.87%
Pd, a=11.42Å	200	2.11	1.06%
Pt, a=11.48Å	200	2.66	1.33%
Co, a=10.15Å	180	2.27	1.26%
Rh, a=11.07Å	180	2.55	1.42%
Ir, a=11.19Å	180	3.07	1.71%

3.4.4 Potential applications

Technological applications can be envisioned in the areas of catalysis, sensors, and nano-electronics. In catalysis, the gap between metallic surfaces filled with electrons may act as a chemical reactor where the equilibrium electronic and geometric structure of molecules may differ than that of the free molecule. Under these conditions, the energy barriers for occurrence of chemical reactions may be modified thus resulting in new or more efficient chemical processes. It is important to point out that when a molecule is inside the gap between metallic surfaces, the electronic confinement effects described above depend on the relative size of the molecule and on the distance between metallic surfaces; thus, the confinement phenomena are not restricted to 4 Å-10 Å of separation between surfaces. We have previously suggested that molecular oxygen

dissociation [37, 38] and the polymerization of ethylene[39] can be favorable when the molecules are inside the gap between specific metallic surfaces. Experimentally, the results presented above may explain the enhancement of reactivity of metal porous systems formed after dealloying metal nanoparticles in acid medium, [1-4] the high activity of platinum nanotubes as fuel cell electrodes where the chemical reactions may occur both outside and inside the tube, and the polymerization using an STM tip[5, 6] resembling two metallic surfaces separated by a short distance (the tip surface and the substrate surface) that form a gap where an anion radical initiates the polymerization that continues as a chain reaction.

In nano-electronics, the interaction between metallic surfaces separated by a short distance plays a role in the energetic competition between the electron-electron exchange and the kinetic energy of electrons that defines the magnetic properties. This is the case of Pt/Ti systems where the magnetic moment changes with the gap size. [40] This magnetic moment behavior could be used for magnetic storage of information. Other applications are in the formation of metallic p-n junctions. As suggested by this work, it is possible to modify the density of electrons in the gap between metallic surfaces, and especial devices such as the junction of two systems with different density of electrons inside the gap may be arranged resembling a p-n junction. These junctions can be the building blocks for many electronic devices. We are currently working in this application.

To finalize, it is worth to mention that a great deal of efforts are currently focused on the related area of plasmonics.[41] Applications in this field include a wide

range of optical and sensing devices that take advantage of the changes in electromagnetic properties occurring when metallic nanoparticles are in close mutual proximity. Besides the well-known phenomena of spectroscopic enhancements, the use of induced electron current on confined molecules may allow molecular excitations that could result in new spectroscopic and sensing applications.[41]

3.5. Conclusions

It was demonstrated using two physical models with different degrees of complexity that there is a region between thin films separated by short distances in the order of 4-10 Å that is characterized by the interaction between the surfaces, and can be fully described by the electronic distribution resulting from that interaction in the films and in the gap separating them. The features of that electronic distribution in the gap between films, such as its energy, momentum, and number of electrons, are determined by thin film properties: thickness, separation between films, and film chemical nature. More specifically, by changing the thin film thickness, the allowed energy bands for electrons, electrons energy and momentum, and the probability of having electrons at specific energy and momentum in the gap between films change. In addition, the number of electrons in the gap between films is practically constant regardless of the film thickness which implies that systems with smaller thickness are more affected by migration of electrons to the gap. This may be reflected in its physical behavior in comparison with systems with thicker thicknesses.

By changing the separation between films, the allowed energy bands, the electrons energy and momentum, and the total probabilities to find an electron at specific energy and k point in the gap between films is practically constant. This implies that as the separation between films decreases, the charge in the gap is constant but occupies a smaller volume, leading to an increase of the electronic density.

And finally, by changing the film chemical nature, the electrons energy and momentum as well as the total probability to find an electron at specific energy and k point are practically the same; but each film with different chemical nature has different number of allowed energy bands since each element has its own Fermi energy level. In addition, each element has different number of valence electrons, and gap energy barrier. All these variables play an important role in the charge distribution existent in the gap between films. The charge distribution is reflected in the number of total electrons in the gap, which correlates with the location of each element in the periodic table. These results are the basis on which possible technological applications may rest, since desirable physical properties can be tuned as suggested by the analyses given by this work.

4. EFFECTS OF CONFINEMENT ON OXYGEN ADSORBED BETWEEN Pt(111) SURFACES*

4.1 Summary

Density functional theory is used to investigate the interaction between Pt (111) surfaces, clean and in the presence of atomic and molecular oxygen, as a function of the distance between the two surfaces. It is found that the confinement effect produces a series of new physico-chemical phenomena, including changes in the surface-subsurface distance between the approaching surfaces, variations in the adsorption energy of O and O_2, and dissociation of molecular oxygen when the separation between surfaces becomes lower than particular threshold distances. It is suggested that these findings may be useful for designing novel devices for catalysis and sensors, and to elucidate the role of cracks in surface degradation behavior.

4.2 Introduction

Surface phenomena usually involve only a few layers below the top exposed surface.[42] It is well known that depending on the structure of the materials, a variety of surface defects such as fractures, dislocations, low-coordination sites, steps, kinks, and others may play a significant role on surface reactions, adsorption and desorption of impurities, and interactions with the environment [43, 44]. Cracks and dislocations

characterized by mismatched solid-solid interfaces may induce mechanical or chemical degradation because small atoms (hydrogen, oxygen, carbon) from the surroundings may penetrate these surface defects starting oxidation or other corrosion processes.[45] Thus, an atomistic study of cracks in presence of impurities, such as molecular or atomic oxygen, may help to understand their role on degradation behavior.

Moreover, in the nanotechnology era, understanding chemical and physical properties of surfaces separated by small distances may offer the possibility of using the distance between surfaces as a control variable for tuning specific catalytic or sensor properties. Here we present a novel density functional theory (DFT) study of the interactions between Pt(111) surfaces, clean and with atomic and molecular oxygen as a function of the separation distance. A similar computational approach has been used by Dholabhai et. al.[46] to investigate the adsorption and dissociation of molecular oxygen on americium surfaces. The results of our study suggest that new physico-chemical phenomena may arise between metal surfaces at small separations. Surface-surface distance influences surface geometry and electronic structure determining changes in the magnitude of surface adsorption energies. These changes are reflected in surface adsorbate distance and electronic density which in turns affect phenomena such as adsorption, absorption and dissociative process of adsorbates.

4.3 Computational and system details

Calculations were performed within the DFT framework using the Vienna ab initio simulation package (VASP) [33-36], which is a DFT code based on plane wave

basis sets. Electron-ion interaction is described using the projector-augmented wave (PAW) method [47], which was expanded within a plane wave basis setting up a cutoff energy of 350 eV. Electron exchange and correlation effects were described by the Perdew-Burke-Ernzerhof (PBE) [11] generalized gradient approximation (GGA) type exchange correlation functional. Spin polarization was included in every simulation. The system is a slab model, infinite in the x and y directions and finite in z direction, and it consists of a periodically repeated fcc Pt slab composed by six-layers modeled using 2×2 supercells. The first top two layers are allowed to relax, the two in the middle are fixed and the bottom two layers again are allowed to relax. In order to represent a crack defined by two separated surfaces of Pt, a vacuum space was used to build the system separating the slabs of the upper and lower cells. Because of the periodic boundary conditions used in the three spatial directions, the top (111) surface is separated a distance H from another (111) surface, the bottom layer of the slab in the top neighboring cell (Figure 4-1). Such H distance is varied from 3.13 to 6.07 Å to evaluate specific properties as discussed below. The optimum bulk lattice constant of Pt was determined as 3.98 Å, a value 1.45% higher than the experimental (3.92 Å).[48] Brillouin zone integration was performed using a 9×9×9 Monkhorst Pack grid [12] and a Methfessel-Paxton[13] smearing of 0.2 eV.
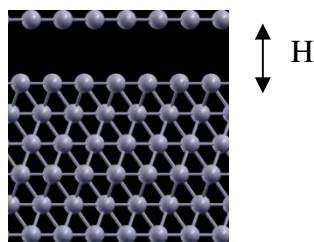
Figure 4-1. Slab system representing a crack defined by two Pt surfaces separated by a distance H in a range from 3.13 to 6.07 Å. Six layers of fcc (111) Pt form the slab, the two at the top and the two at the bottom are allowed to relax, the two central ones are fixed.

Two other systems were built in similar manner but additionally, an adsorbate was introduced into the vacuum space. As illustrated in Figure 4-2, in one set of simulations, atomic oxygen was adsorbed in the fcc hollow site of one of the surfaces; and in another set of simulations, molecular oxygen was initially located in the middle of the vacuum space in vertical direction. Two different initial positions of molecular oxygen were studied: 1) O_2 is located above one surface and beneath the other one with each oxygen atom pointing to an hcp hollow site of the bottom and top surfaces respectively (Figure 4-2b), and 4-2) O_2 is located above one of the surfaces pointing to an fcc hollow site and beneath the other surface pointing to a top site (Figure 4-2 c). In each simulation the initial O-O distance in molecular oxygen was the gas phase value of 1.23 Å. This distance was also obtained by DFT calculations.
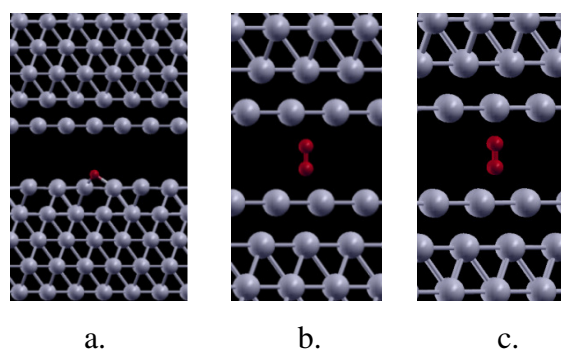
Figure 4-2. (a) Atomic oxygen was adsorbed in fcc position on one of the surfaces. (b).

O$_2$ initial position, in the middle of the vacuum space in vertical direction above one

surface and beneath the other one pointing to hcp hollow sites. (c). O$_2$ initial position, in

the middle of the vacuum space in vertical direction above one surface pointing to the

fcc hollow site and beneath the other surface pointing to a top site. In all cases the initial

O-O distance was 1.23 Å, which corresponds to the equilibrium gas phase distance of

O$_2$.

The adsorption energy of molecular and atomic oxygen, E_{ad}, was calculated by

the following relation:

$$E_{ad} = \frac{(E_{clean\ slab} + N \cdot E_{Oxygen}) - E_{slab\ w/adsorbed\ O}}{N} \qquad (4-1)$$

$E_{slab\ w/adsorbed\ O}$ stands for   the total energy of the interacting Pt surfaces and the

adsorbed O atoms; N is the number of Oxygen atoms on the surface; $E_{clean\ slab}$ is the

total energy of the bare Pt slab, and E_{Oxygen} is the energy of one Oxygen atom in vacuum. Positive E_{ad} values indicate favorable (exothermic) adsorption.

To calculate the total electronic charge of an atom we used the Bader analysis.[49, 50] This analysis defines an atom based on the electronic charge density using zero flux surfaces to divide atoms; the total electronic charge of an atom is approximately the charge enclosed within the Bader volume defined by zero flux surfaces.

4.4 Results and discussion

In this section we discuss changes observed in adsorption energy, as well as in surface-subsurface and in oxygen-surface distances as a result of varying the distance H between both surfaces (Figure 4-1) in a range of 3.13 to 6.07 Å.

4.4.1 Effect of surface-surface separation on slab geometry

To verify the accuracy of our computational model and to have a reference for further results, the adsorption of atomic oxygen on Pt(111) surface at 0.25 ML surface coverage as well as the surface-subsurface separation and oxygen-surface separation were calculated. These calculations were performed in the slab described above with a vacuum space of 12 Å to avoid interaction between consecutive labs. The calculated adsorption energy of atomic oxygen in fcc hollow site was 4.24 eV which agrees with experimental results: Gland et al.[51] determined an initial desorption energy of 4.77 eV for the O/Pt(111) system at 700K, and Yeo et al.[52] reported a binding energy of 4.32

eV on a clean Pt(111) surface. The calculated surface-oxygen distance for fcc adsorption, 1.16 Å, is in agreement with the experimental value of 1.21 ±0.03 Å.[53] The calculated surface-subsurface separations in presence of oxygen, 2.35 Å, and without oxygen, 2.34 Å, are also in good agreement with previous calculations.[54]

However, when the two surfaces are separated by a small distance, the above data change considerably. Figure 4-3 illustrates how the effect of separation between surfaces, H, affects the surface-subsurface distance: at long values of H (> 4.5 Å) no effect is observed on the surface-subsurface distance; at intermediate values (~4.3 Å), the surface-subsurface distance starts to become elongated and at smaller distances the effect is more notorious. This effect can be interpreted as an attractive interaction between the approaching surfaces, where each surface layer tends to separate from its corresponding substrate.
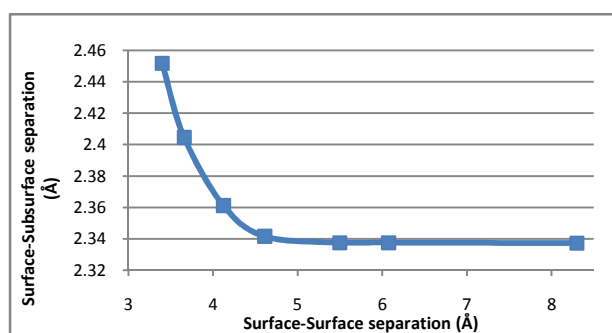
Figure 4-3. Surface-subsurface separation distance vs. surface-surface separation (H) between two Pt(111) surfaces. The separation between surfaces H significantly affects the surface-subsurface distance at values of H < 4.5 Å.

4.4.2 Atomic oxygen adsorption between surfaces

For large H separations (> 5.5 Å), the O adsorption energy tends to a constant value which results from the O adsorption in an fcc hollow site of one of the surfaces, 4.24 eV at 0.25 ML coverage. When H is < 5.5 Å, the atomic adsorption energy starts to decrease steadily (Figure 4-4). An electron density analysis helps to understand the atomic oxygen adsorption energy variation as a function of surface-surface separation.
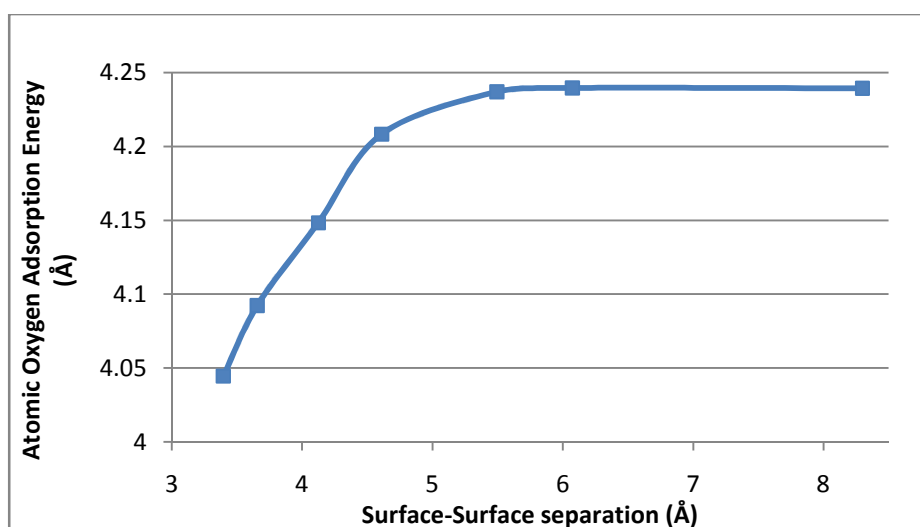
Figure 4-4. O adsorption energy vs. separation distance between surfaces (H). The O adsorption in fcc hollow site of one of the surfaces starts to decrease steadily when H is < 5.5 Å.

When the two surfaces are separated by small distances (Figure 4-5a), the electron density plot shows sharing of electrons among both surfaces and the atomic

oxygen; this interaction weakens the adsorption strength of O with just one of the surfaces, because the adsorbate becomes shared by both surfaces. The effect disappears as soon as the distance goes beyond a certain threshold (Figure 4-5b).
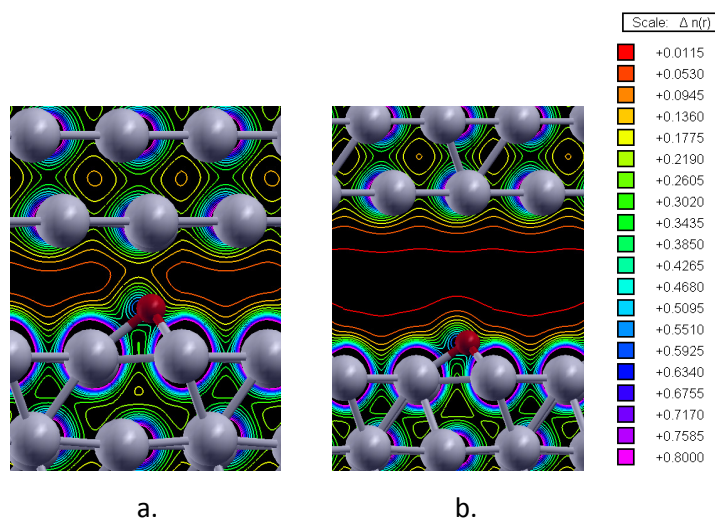
Figure 4-5. Isoelectronic density contours (a). The two surfaces are separated by a small distance (4.12 Å), the electron density plot shows a sharing of electrons among both surfaces and the atomic oxygen. (b). As soon as the distance goes beyond a certain treshold (5.5 Å) the sharing phenomena disappear, and the system is similar to one Pt(111) surface alone with an O adsorbed in the fcc hollow site.

As expected, in the presence of the adsorbate, the system geometry also changes as a function of H. In the range of H= 3 to 5.5 Å surface-surface separation, the clean surface attracts the other metal surface and the oxygen atom, increasing both surface-

subsurface and oxygen-surface separation. This attraction is strong at small H and becomes weaker as H increases (Figure 4-6). Note that the threshold described in relation to Figure 4-4 is also in agreement with those found in Figure 4-6 for the surface-subsurface distance and for the O-surface distance.
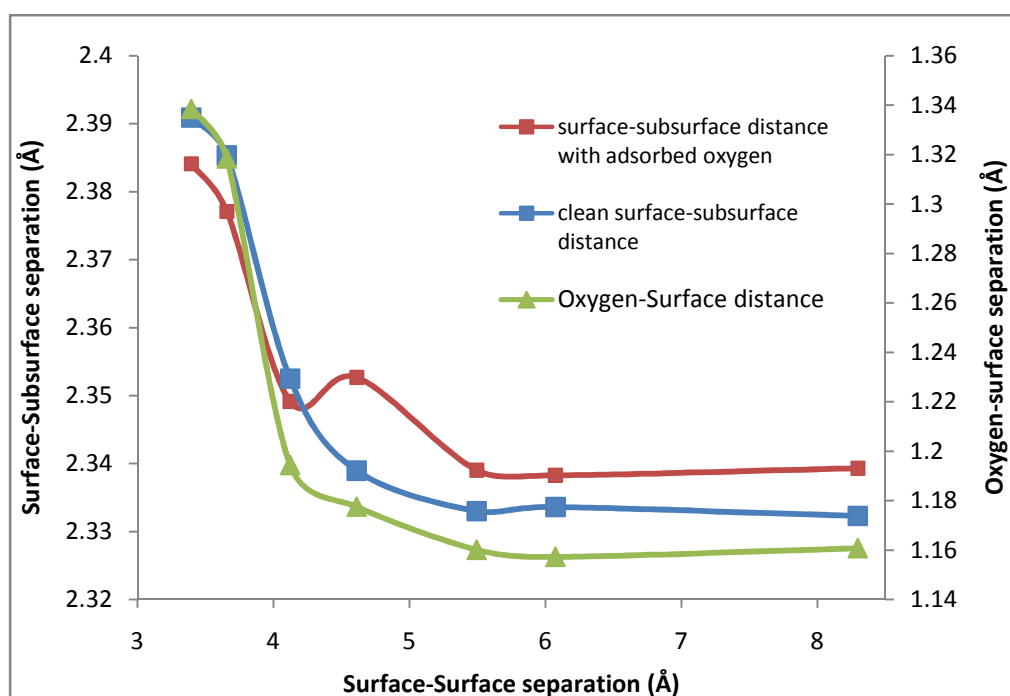
Figure 4-6. Surface-subsurface separation (left) and Oxygen-surface separation (right) vs. surface-surface separation H between two Pt(111) surfaces.

Thus, at some critical surface-surface separation H, the interaction between the clean surface and the O-covered surface becomes negligible and the system behaves similar as a single surface. This critical surface-surface separation is 5.5 Å for the

studied Pt system; after this point the adsorption energy, the surface-subsurface and Oxygen-surface separations become constant and equal to the values calculated for the single surface.

4.4.3 O_2 adsorption

Molecular oxygen adsorption was studied when the surfaces are separated by small distances H in a range of 4 to 6.5 Å. The initial system configuration had O_2 located in the middle of the vacuum space in vertical direction (as shown in Figure 4-2b and 4-2c) with an O-O separation of 1.23 Å corresponding to an equilibrium separation of molecular oxygen in gas phase.

As discussed above, new interactions arise when the surfaces are separated by small distances. When each of the O atoms are located above and beneath the surfaces respectively pointing to hcp hollow sites (Figure 4-2b), our results indicate that a spontaneous molecular oxygen dissociation occurs in the range from H = 4 to 4.8 Å surface-surface separation distances, as a consequence of the additional surface interactions; the electron density analysis in Figure 4-7 shows that both surface and oxygen share a high density of electrons indicating strong interactions.

H= 4.405 Å   H= 4.856 Å   H= 4.930 Å

H= 5.096 Å   H= 5.969 Å
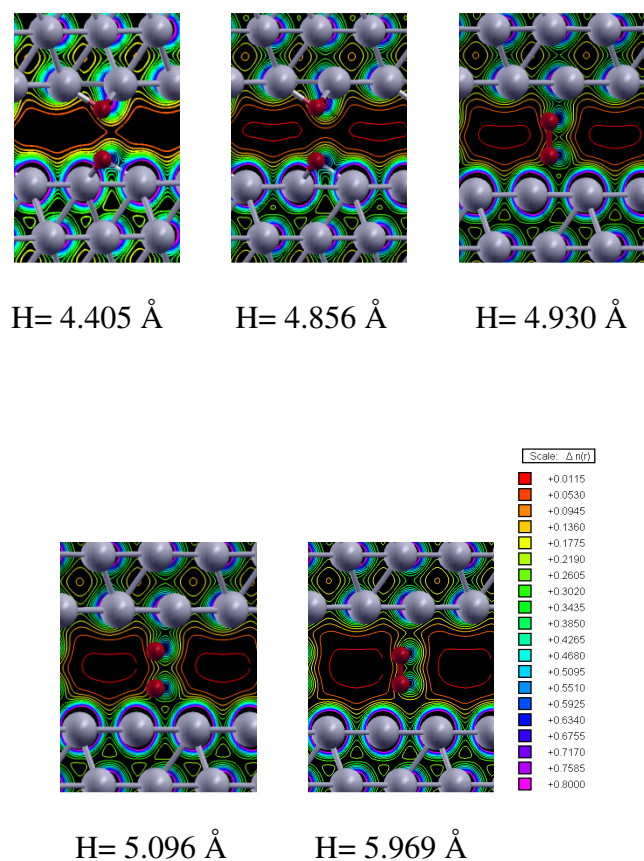
Figure 4-7.   Isoelectronic density contours for an O_2 molecule confined between two surfaces separated by various values of H. In each case, O_2 was initially located in the middle of the vacuum space between the two surfaces in vertical direction, with each oxygen atom pointing to an hcp hollow site as shown in Figure 4-2b. Note the O_2 dissociation at the two smallest inter-surface distances.

In addition, the Bader atomic charges shown in Table 4-1 reveal that at small H values < ~4.8 Å, both oxygen atoms bear high negative charges (~-0.6) indicating that the already separated O atoms are adsorbed and receive electrons from their respective

surfaces. Note that at 4.8 Å there is a sharp drop in the O-O distance from 2.43 Å to 1.48

Å as shown in Figure 4-8. Thus, between 4.8 and 5.1 Å, when the O-O separation is

approximately 1.48-1.58 Å, the charges on each atom are significantly reduced (Table 4-

1), such charges are reminiscent of the peroxo and superoxo molecular precursor states

of O_2 adsorbed on bridge sites of Pt (111) surfaces.[55, 56] Finally at H= 5.1 Å the O-O

distance changes again abruptly from 1.58 to 1.32 Å (Figure 4-8), and the respective

charges in Table 4-1 become lower indicating the decrease of the molecule-surface

interaction. For even larger inter-surface separations H, the O-O distance decreases as H

increases until the O-O distance recovers the O_2 bond length close to 1.23 Å.
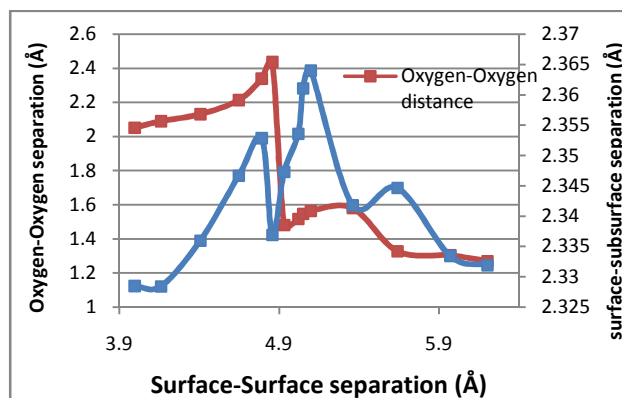
Figure 4-8. O-O distance (left) and surface-subsurface separation (right) vs. surface-surface separation distance H; the initial system was O_2 located in the middle of the vacuum space in vertical direction with each oxygen pointing to hcp hollow sites (as shown in Figure 4-2b). Changes reported in surface-subsurface separation distance are found similar for both surfaces.

In summary, the oscillatory behavior of the surface-subsurface distance that correlates with the variation of the O-O bond length reveals the large flexibility of the surface layer under these conditions, which facilitates the almost spontaneous breaking of the O-O bond, a process that has an activation barrier on a single Pt(111) surface of about 0.7-0.9 eV.[57]

Table 4-1. Bader atomic charges. The electronic charge of each O atom as a function of the surface-surface separation; O_2 was initially located in the middle of the vacuum space in vertical direction with each oxygen pointing to hcp hollow sites in each of the surfaces (Figure 4-2b).

Surface-surface separation (Å)	Electronic charge of top Oxygen atom	Electronic charge of bottom Oxygen atom
3.996	-0.652	-0.614
4.159	-0.619	-0.641
4.405	-0.629	-0.630
4.646	-0.618	-0.639
4.790	-0.635	-0.635
4.856	-0.362	-0.402
4.930	-0.460	-0.322
5.018	-0.397	-0.398
5.048	-0.371	-0.429
5.096	-0.345	-0.465
5.358	-0.242	-0.272
5.638	-0.194	-0.229
5.969	-0.106	-0.176
6.201	-0.122	-0.201

Figure 4-9 indicates that the calculated adsorption energy of the two oxygen atoms in the confined system referred to the energy of two separated oxygen atoms is in accordance with the above results; it increases when H is in the range from 4 to 4.8 Å

surface-surface separation distances, until a maximum value of 3.70 eV, then there is an abrupt change in the adsorption energy from 3.70 eV to 3.03 eV.
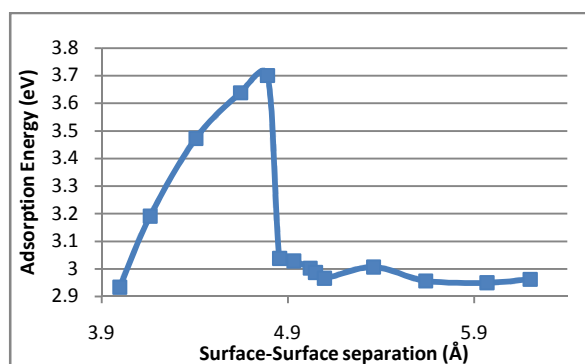
Figure 4-9. Adsorption energy vs. surface-surface separation distance H. O_2 was initially located in the middle of the vacuum space in vertical direction with each oxygen pointing to hcp hollow sites in each of the surfaces (Figure 4-2b).

The O-O separation changes described above are also accompanied by surface-subsurface changes (Figure 4-8). For example, a maximum O-O separation of 2.43 Å corresponds to a maximum surface-subsurface separation of 2.35 Å and to maximum adsorption energy of 3.70 eV; in such cases it could be interpreted that the O atom is interacting with an almost isolated monolayer of Pt. Then, a decrease of O-O separation from 2.43 Å to 1.48 Å is accompanied by reductions in adsorption energy and surface-subsurface separation, 3.70 eV to 3.03eV and 2.35 to 2.33 Å respectively, corresponding to the adsorption of an O_2 molecule.

The trends of adsorption energy and oxygen-oxygen distance for a system with O_2 initial configuration having its O atoms located above and beneath the surfaces pointing to top and fcc sites (Figure 4-2c), are qualitatively similar to those with oxygen atoms pointing to hcp sites; however, the values are quite different, as shown in Figure 4-10 that can be compared to those in Figure 4-9. The maximum adsorption energy and oxygen-oxygen distance for initial configuration with oxygen atoms pointing top and fcc sites are lower; 3.197 eV and 2.097 Å at 4.943 Å (Figure 4-10) in comparison with 3.7 eV and 2.44 Å at 4.79 Å (Figure 4-9).
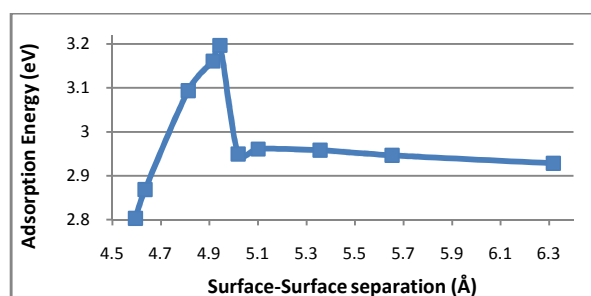
Figure 4-10.   Adsorption energy vs. surface-surface separation H. O_2 was initially located in the middle of the vacuum space in vertical direction with one oxygen pointing to an fcc hollow site and the other oxygen to a top site (as shown in Figure 4-2c).

Different trends were also observed in the variation of the surface-subsurface distances (Figure 4-11). In presence of O_2 with O atoms pointing to top and fcc sites at small surface-surface distances H (from 5.0 Å to 4.59 Å) the surface-subsurface distance

becomes shortened (2.33 Å to 2.26 Å). This state of surface-subsurface compression is caused by the presence of molecular oxygen and may be related with the fact that one oxygen atom is on top of a Pt atom. The O-O distance in this range of surface-subsurface compression varies from 1.44 Å to 2.09 Å indicating molecular oxygen dissociation at the compressed state. It is also observed that the surface-subsurface distance reaches a maximum value of 2.34 Å at H= 5.36 Å; this maximum elongation is shorter than that shown in Figure 4-8 (2.36 Å at H= 5.1 Å) and it does not show an oscillatory behavior as a function of H. The smoother behavior of the O-O and surface-subsurface separation distances is attributed to different nature of the O_2 adsorbed states.
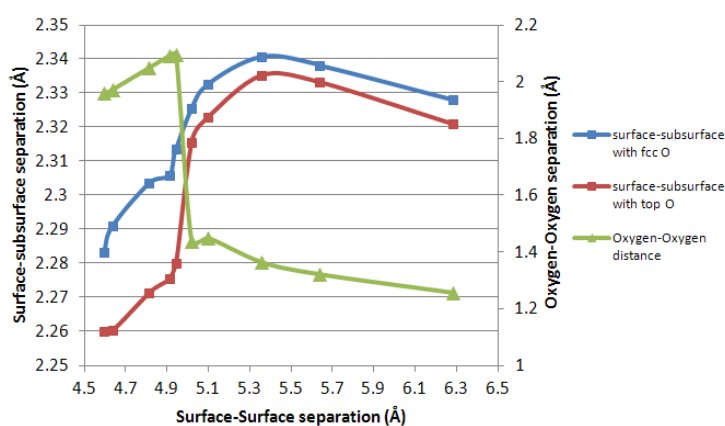
Figure 4-11. O-O separation (right) and surface-subsurface separation (left) vs. surface-surface separation H. O_2 was initially located in the middle of the vacuum space in vertical direction with one oxygen pointing to an fcc hollow site and the other oxygen to a top site (as shown in Figure 4-2c).

As in the previous molecular oxygen adsorption case, Bader atomic charges shown in Table 4-2 indicate that at small H values < ~5.0 Å, both oxygen atoms bear high negative charges (~-0.6) reflecting the dissociation of molecular oxygen and the electron donation from their respective surfaces. As the surface separation H become longer, the Bader charges of each oxygen decrease due to reduction of the interaction between each oxygen atom and the surface, and stronger oxygen-oxygen interaction reflected also in smaller oxygen-oxygen separations shown in Figure 4-11.

Table 4-2. Bader atomic charges. The electronic charge of each O atom as a function of the surface-surface separation; O_2 was initially located in the middle of the vacuum space in vertical direction with one oxygen pointing to fcc hollow site and the other oxygen to top site (Figure 4-2c).

Surface-surface separation (Å)	Electronic charge of top Oxygen atom	Electronic charge of bottom Oxygen atom
4.595	-0.513	-0.590
4.635	-0.513	-0.595
4.812	-0.554	-0.598
4.914	-0.483	-0.620
4.943	-0.494	-0.625
5.018	-0.424	-0.329
5.100	-0.352	-0.412
5.357	-0.355	-0.222
5.653	-0.149	-0.369
6.317	-0.166	-0.033

4.5 Conclusions

This study suggests that the presence of cracks in a solid bulk or nanoparticle, allowing two surfaces to be at relatively close distances results in enhanced interactions between the exposed surfaces, and may induce new chemical phenomena. Our DFT analysis shows that the top layer of each of the two clean surfaces separated by a small gap tends to take apart from its corresponding subsurface layers. Moreover, in presence of an impurity (such atomic and molecular oxygen), the two surfaces exert a strong interaction over the atom or molecule, facilitating bond dissociation in the case of molecular oxygen. The flexibility of the top surface layers is revealed by oscillations of the surface-subsurface distance in presence of molecular oxygen, which evolves from chemisorbed precursor states to a dissociated state where each O atom is strongly adsorbed on one of the surfaces.

We note that these phenomena should be dependent on the nature of the exposed surfaces. For example, here we expose two fcc slabs that are arranged in ABC sequence, therefore the two approaching surfaces belong to "A" and "C" layers; however other combinations and/or different crystallographic planes are also possible and may give rise to different interactions. However, such rich behavior may be used for tuning the desired effects for sensing or catalytic applications among others.

5. CONFINEMENT EFFECTS ON ALLOY REACTIVITY*

5.1 Summary

Density functional theory is used to characterize reactivity in systems confined between alloy surfaces separated by a gap from three to 10 Å. It is found that the proximity of a second surface alters the geometric and electronic properties of the first one, and the changes are related to the nature of the interacting surfaces. These phenomena are explored by analysis of the dissociation of molecular oxygen and that of water in the confined systems. The results suggest that such confinement effects may be further designed for specific applications by tuning the alloy composition.

5.2 Introduction

The proximity of two transition-metal surfaces separated by a gap of molecular dimensions gives rise to strong interactions that could be potentially useful for enhanced reactivity in catalysis, separations, and sensing processes.[58, 59] Depending on the nature of the interacting surfaces, confined adsorbates may be strongly adsorbed, dissociated, or reacted with other species.[60] Separation of mixed gases or liquids could be obtained by appropriately tuning the composition of the alloy surfaces and the gap geometry.[61] Furthermore, the importance of local atomic disorder on reactivity has pointed out recently based on X-Ray absorption spectroscopy experiments.[4]

In previous work[37] we presented a study of the confinement effect on the dissociation of molecular oxygen between two Pt (111) surfaces. From our density functional theory (DFT) analysis, we concluded that enhanced interactions between the exposed surfaces might induce new chemical phenomena. The flexibility of the interacting surface layers revealed by oscillations of the surface-subsurface distance, determines the evolution of molecular oxygen from chemisorbed precursor states to a dissociated state where each O atom is strongly adsorbed on one of the surfaces.

Here we further investigate the effect of the nature of the interacting surfaces by testing the interaction of two surfaces each having a monolayer of a metal M (M= Ag, Au, Co, Cu, Fe, Ir, Ni, Pd, Re, and Ti) deposited over a core of platinum. Reactivity is tested by introduction of molecular oxygen in the confined space at different separations between surfaces ranging between three to 10 Å. Finally, we explore the effect of tuning surface composition on the adsorption and dissociation of a water molecule in the confined space.

5.3 Computational and system details

Calculations were performed within the DFT framework using the Vienna ab initio simulation package (VASP) [33-36], which is a DFT code based on plane wave basis sets. Electron-ion interaction is described using the projector-augmented wave (PAW) method [47], expanded within a plane wave basis setting up a cutoff energy of 350 eV. Electron exchange and correlation effects were described by the Perdew-Burke-Ernzerhof (PBE) [11] generalized gradient approximation (GGA) type exchange

correlation functional. Spin polarization was included in every simulation. The system is a slab model, infinite in the x and y directions and finite in z direction, and it consists of a periodically repeated fcc Pt slab covered by a monolayer of a metal X, (X = Ag, Au, Co, Cu, Fe, Ir, Ni, Pd, Re, and Ti); the slab is composed by six-layers modeled using 2×2 supercells. The first top two layers are allowed to relax, the two in the middle are fixed, and the bottom two layers again are allowed to relax; the first top layer and the last bottom layer are of metal X. In order to represent a crack defined by two separated surfaces, a vacuum space was used to build the system separating the slabs of the upper and lower cells. Because of the periodic boundary conditions used in the three spatial directions, the top (111) surface is separated a distance H from another (111) surface, the bottom layer of the slab in the top neighboring cell. Such H distance is varied to evaluate specific properties as discussed below. The optimum bulk lattice constant of Pt was determined as 3.98 Å, a value 1.45% higher than the experimental (3.92 Å).[48] Brillouin zone integration was performed using a 9×9×9 Monkhorst Pack grid [12] and a Methfessel-Paxton[13] smearing of 0.2 eV. The convergence criteria for the electronic self-consistent iteration and the ionic relaxation loop were set to 10^{-4} eV and 10^{-3} eV, respectively.

Figure 5-1. Left: Slab system representing a crack defined by fcc Pt bulk covered by a monolayer of metal M, (M = Ag, Au, Co, Cu, Fe, Ir, Ni, Pd, Re, and Ti); the skin surfaces are separated by a distance H. The slab is formed by four central layers of fcc (111) Pt (grey) between monolayers of metal M (blue), the M monolayers and the Pt layers in contact with it are allowed to relax, the two central Pt layers are fixed. Right: O_2 initial position, pointing to hcp hollow sites of each surface. In all cases the initial O-O distance was 1.23 Å, which corresponds to the equilibrium O-O gas phase distance in O_2.

Other simulations were done by adding an adsorbate into the vacuum space. As illustrated in Figure 5-1, molecular oxygen was initially located in the middle of the vacuum space in vertical direction, above one surface and beneath the other one with each oxygen atom pointing to an hcp hollow site of the bottom and top surfaces respectively. In each simulation the initial O-O distance was the gas phase value of 1.23 Å. This distance was also obtained by DFT calculations.

The adsorption energy, E_{ad}, defined as the energy gain or lost by taking both O atoms from the surface and forming O_2 in the gas phase was calculated by the following relation:

$$E_{ad} = E_{2O/surf} - E_{O_2(g)} - E_{surf} \tag{5-1}$$

where $E_{2O/surf}$ stands for the total energy of the interacting skin surfaces and the adsorbed O atoms, E_{surf} is the total energy of the bare slab, and $E_{O_2(g)}$ is the molecular oxygen energy in gas phase. In a similar way was calculated the adsorption energy of water:

$$E_{ad} = E_{2H/O/surf} - E_{H_2O(g)} - E_{surf} \tag{5-2}$$

To calculate the total electronic charge of an atom we used the Bader analysis,[49, 50] where the total electronic charge of an atom is approximately the charge enclosed within the Bader volume defined by zero flux surfaces. The d-band and p-band centers are referenced to the Fermi level; they were calculated from the site-projected electronic density of states using a k-point mesh of 16×16×1.

5.4 Results and discussion

5.4.1 Study of clean surfaces as a function of their separation

In this section we discuss the effects produced by two M surfaces (M= Ag, Au, Co, Cu, Fe, Ir, Ni, Pd, Re, and Ti) separated by a distance H as depicted in Figure 5-1.

5.4.1.1 Geometrical effects

The geometrical structure is affected in each system due to the lattice constant mismatch between Pt and the transition metal M used as overlayer. The metal-metal surface bond distances are determined by the lattice constant of Pt and they are always equal to 2.80 Å regardless of the overlayer metal; therefore, the overlayer metal experiences a compression or expansion that may significantly change its electronic properties. In addition, as H changes, the interaction between the two M surfaces induces changes in the interlayer distances, adding other variable that may play a role in surface activity.

Figure 5-2 shows the changes of surface-subsurface distance upon relaxation expressed as a percentage of bulk Pt layer separation, which is the layer spacing between the two central fixed layers. The percent of layer spacing is positive for an expansion and negative for a compression. In all cases surface-subsurface distance decreases as H increases. However, with respect to bulk Pt layer spacing, the surface-subsurface separations of Ag and Au skin surfaces are always expanded, whereas for Pd skin surface at small H it expands but it contracts at larger values of H, and for Co, Cu, Fe, Ir,

Ni, Re, and Ti skin surfaces the surface-subsurface separation is always contracted. The expanded and contracted surface-subsurface distances change considerably according to the nature of the skin surface. In most cases, the trend follows the size difference between Pt and M, the most expanded surface-subsurface corresponds to the Au skin surface with values around 8% and 6%, and the most contracted to the Co skin surface with values around -12% and -14% with respect to the bulk Pt spacing.
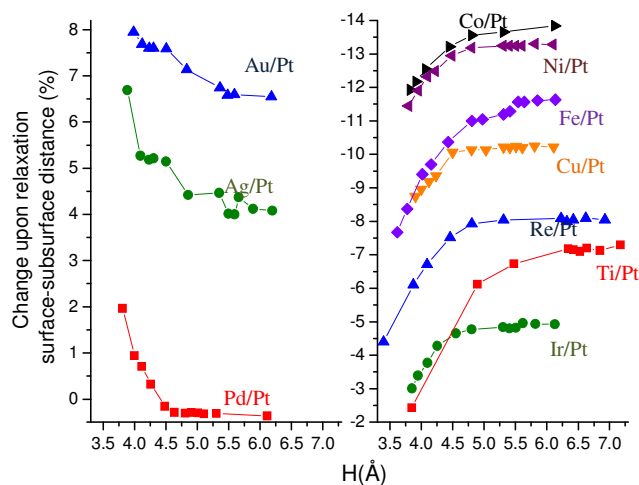
Figure 5-2. Change upon relaxation of the surface-subsurface distance expressed as a percentage of a bulk Pt layer spacing. Positive numbers mean expansion and negative numbers contraction.

Figure 5-3 shows a similar analysis done with respect to the distance between the subsurface and third layer. In all cases, except for Ir at long H values, the distance between second and third layer expands with respect to bulk Pt layer spacing. Figures 5-2 and 5-3 also show that at short surface-surface separations H (approximately between 3.7 and 4.2 Å), there is a strong surface-surface interaction significantly modifying interlayer distances.
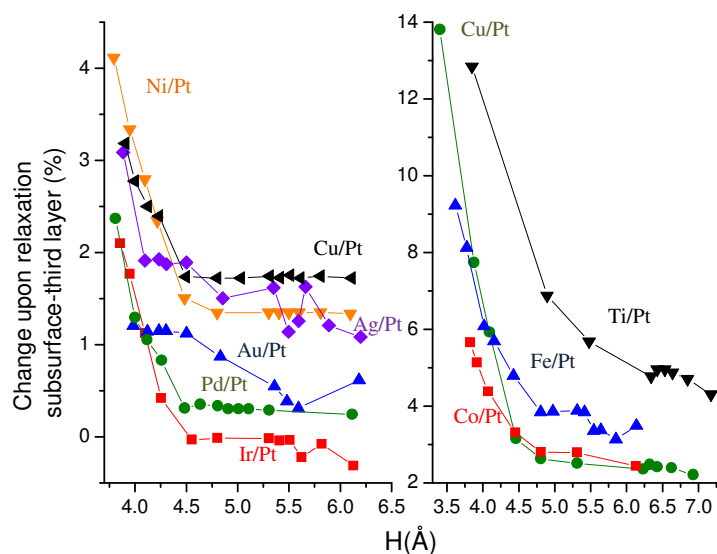
Figure 5-3. Change upon relaxation of the subsurface-third layer distance expressed as a percentage of a bulk Pt layer spacing. Positive numbers mean expansion and negative numbers contraction.

5.4.1.2. Electronic effects

In conjunction with geometric changes, electronic changes are found as functions of surface-surface separation H and of the nature of the overlayer metal. At any given separation H, the strongest effect is the tendency of Pt atoms to withdraw electrons oxidizing the M overlayer that is not affected by changes in H. The surface charge for most systems is positive, with the exception of Au/Pt and Ir/Pt where the charge per atom is negligible; the surface oxidation trend clearly relates with the chemistry of each overlayer element. For instance, the overlayer elements that belong to the period 4th of the periodic table follow the oxidation trend: Ti > Fe > Co> Ni = Cu, with Ti the most oxidized atom. Similarly, the oxidation trends: Pd > Ag, and Re > Ir > Au are found for period 5th and period 6th of the periodic table. A similar analysis can be made with respect to overlayer elements belonging to a given =group in the periodic table: the oxidizing trends are: Co > Ir; Ni > Pd; and Cu > Ag > Au. The results are summarized in Table S-1 provided as Supplemental Information.

Figure 5-4 shows changes in the d-band center of the overlayer atoms as a function of H observed for the most notorious cases: Pd/Pt, Co/Pt and Ti/Pt. The d-band center evolves from -1.716 to -1.539 eV for Pd/Pt, from -1.44 eV to -1.207 for Co/Pt and from 0.036 to 0.743 eV for Ti/Pt respectively as H decreases. For overlayers of Au, Cu, Ir, Pd, Fe and Co the d-band center moves closer to the Fermi level, whereas for Re and Ti, the d-band center moves further to the Fermi level when H decreases; and in Ag and Ni the d-band center changes are negligible. These electronic changes definitely

affect reactivity of species confined between the overlayers, as shown in the next sections.
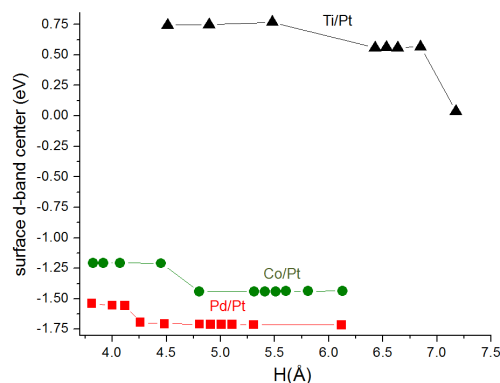
Figure 5-4. Surface d-band center (in eV, referred to the Fermi level) as a function of surface-surface separation for Ti/Pt, Co/Pt and Pd/Pt systems.

5.4.2 O_2 adsorption and dissociation

Adsorption energies defined as in equation (1) were calculated in a range of H values from 4 to 7 Å, always with the same initial O_2 location as shown in Figure 5-1. It is found that the interaction between the two M surfaces in most cases causes O_2 dissociation for a given value of H. The exceptions are the surfaces of Au and Ag that are not able to dissociate O_2 although there is a significant maximum elongation of the O-O distance of 1.83 Å for Ag and 1.91 Å for Au at H values of 5.23 Å and 4.97 Å respectively. The O_2 dissociation regions shown in Figure 5-5, as well as the adsorption energies, vary depending on the nature of the overlayer. At sufficiently high values of H,

the O-O distances recover the gas phase values of 1.23 Å. The molecular dissociation occurs at different H separations depending on M; the values shown in Table 5-1 indicate the order Ti > Re > Co > Fe > Ir > Cu > Ni > Pd> Pt.

Table 5-1. Surface-surface separations H (in Å) where O_2 dissociates for each overlayer metal M, and their adsorption energies, in eV.

Overlayer	Ag	Au	Pt	Pd	Cu	Ir	Ni	Co	Fe	Re	Ti
H (Å)	-	-	4.79	4.93	5.47	5.40	5.23	5.78	5.64	6.12	6.35
E_{ad} O_2	0.25	1.16	-1.32	-2.00	-3.33	-4.11	-5.28	-5.90	-6.90	-7.27	-11.5
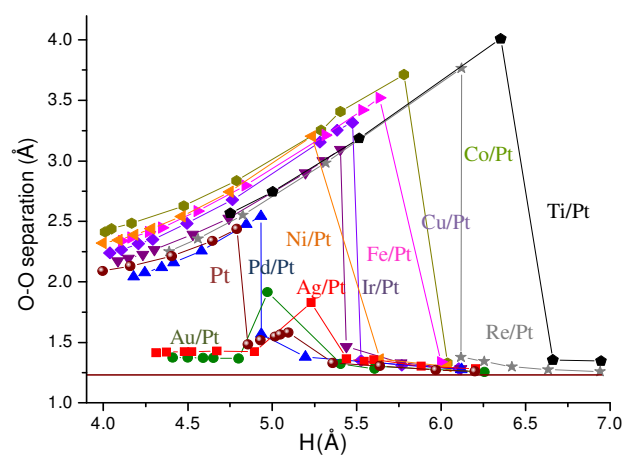
Figure 5-5. O-O separation distance (in Å) vs. surface-surface separation H (in Å). The transition indicates the separation at which molecular dissociation takes place. The horizontal line at 1.23 Å is the gas phase O-O bond length.
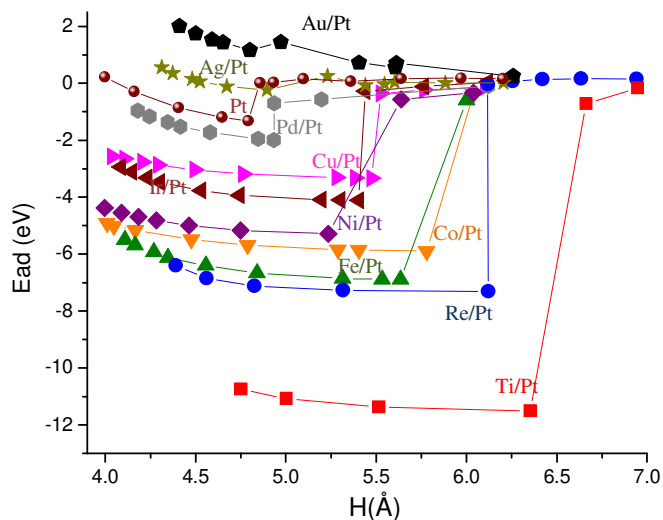
Figure 5-6. The energy gained or lost by taking both O atoms from the surface to form O$_2$ in the gas phase.

O$_2$ adsorption energies follow a similar behavior as a function of H, as depicted in Figure 5-6. At long separations, there is no adsorption due to the location of the O$_2$ molecule in the middle of the space between the surfaces, independent of the nature of the overlayer. As H decreases and the two M surfaces become closer to each other, a slight increase in adsorption strength denotes O$_2$ physisorption that is followed by an abrupt change corresponding to O$_2$ dissociation. The strongest adsorption energies for each skin system are shown in Table 5-1. With the exception of Ag and Au, all the metal overlayers resulted in stronger adsorption energies and larger regions of O$_2$ dissociation in comparison with pure Pt.

Table 5-2 summarizes the adsorption energy and representative electronic properties at different H separations for each skin surface. In the region of direct molecular oxygen dissociation, there is a clear correlation between the oxygen p-band center and the adsorption energy; for each system, there is a shift in the oxygen p-band center toward the Fermi level reflected in stronger adsorption energies as H increases (Figure 5-7). Once H reaches a certain value, shown in Table 5-1 for each system, there is an abrupt change in the oxygen p-band center, surface d-band center, and surface charge, which explain the sudden decrease in the adsorption energies described above.

Table 5-2. For each system six H separations (in Å) were selected to show changes in the oxygen charge (Q, in e), the oxygen p-band center (in eV, relative to the Fermi level), and surface d-band center (in eV, relative to the Fermi level).

System	H	E_{ad}	Q (O)	p-band center for O	d-band surface center	System	H	E_{ad}	Q (O)	p-band center for O	d-band surface center
Ag/Pt	4.31	0.56	-0.53	-8.67	-2.13	Ir/Pt	4.09	-2.94	-0.71	-7.44	-2.45
	4.48	0.15	-0.54	-8.40	-2.11		4.23	-3.31	-0.74	-7.28	-2.44
	4.67	-0.12	-0.54	-8.12	-2.08		4.53	-3.77	-0.73	-6.98	-2.42
	5.23	0.25	-0.60	-1.28	-1.99		5.40	-4.11	-0.73	-6.52	-2.40
	5.88	0.014	-0.27	-5.61	-2.04		5.76	-0.12	-0.25	-5.61	-2.65
	6.21	0.020	-0.19	-7.15	-2.04		6.12	-0.04	-0.19	-6.61	-2.67
Au/Pt	4.41	2.01	-0.42	-6.84	-2.17	Ni/Pt	4.00	-4.38	-0.83	-5.74	-2.54
	4.59	1.54	-0.43	-9.07	-2.15		4.18	-4.70	-0.82	-5.65	-2.54
	4.80	1.16	-0.43	-8.74	-2.12		4.46	-5.00	-0.81	-5.52	-2.53
	4.97	1.45	-0.57	-1.46	-2.08		5.23	-5.28	-0.84	-5.30	-2.52
	5.61	0.70	-0.17	-5.79	-2.04		5.64	-0.57	-0.43	-5.58	-2.55
	6.26	0.26	-0.08	-7.60	-2.05		6.04	-0.34	-0.16	-6.51	-2.59
Co/Pt	4.01	-4.91	-0.95	-5.22	-2.55	Pd/Pt	4.18	-0.96	-0.61	-6.17	-2.16
	4.17	-5.16	-0.93	-5.18	-2.56		4.34	-1.37	-0.60	-5.99	-2.15
	4.48	-5.48	-0.94	-5.10	-2.57		4.58	-1.73	-0.61	-5.71	-2.14
	5.40	-5.86	-0.96	-4.97	-2.58		4.93	-2.00	-0.65	-5.59	-2.11
	5.78	-5.90	-0.96	-4.98	-2.57		5.20	-0.56	-0.29	-5.59	-2.06
	6.04	-0.39	-0.23	-5.91	-2.67		6.12	-0.10	-0.06	-7.05	-2.10

Table 5-2. Continued

System	H	E_{ad}	Q (O)	p-band center for O	d-band surface center	System	H	E_{ad}	Q (O)	p-band center for O	d-band surface center
Cu/Pt	4.04	-2.57	-0.87	-4.88	-2.18	Re/Pt	4.39	-6.40	-0.89	-6.19	-2.89
	4.21	-2.77	-0.88	-4.78	-2.39		4.56	-6.85	-0.92	-5.97	-2.88
	4.49	-3.03	-0.86	-4.65	-2.39		5.32	-7.27	-0.92	-5.72	-2.87
	5.47	-3.33	-0.90	-4.46	-2.38		6.12	-7.30	-0.93	-5.67	-2.87
	5.77	-0.23	-0.38	-5.46	-2.13		6.63	0.17	-0.13	-6.96	-3.04
	6.10	-0.13	-0.29	-7.09	-2.14		6.94	0.15	-0.01	-7.32	-3.05
Fe/Pt	4.11	-5.50	-0.98	-5.45	-2.56	Ti/Pt	4.75	-10.7	-1.07	-5.40	-2.66
	4.27	-5.93	-1.00	-5.27	-2.56		5.00	-11.1	-1.06	-5.34	-2.66
	4.56	-6.40	-1.00	-5.23	-2.55		5.51	-11.4	-1.08	-5.25	-2.65
	5.31	-6.86	-1.01	-5.03	-2.54		6.35	-11.5	-1.09	-5.23	-2.66
	5.64	-6.90	-1.02	-5.02	-2.55		6.66	-0.72	-0.36	-5.62	-2.70
	6.00	-0.60	-0.41	-5.90	-2.50		6.95	-0.17	-0.27	-5.87	-2.70
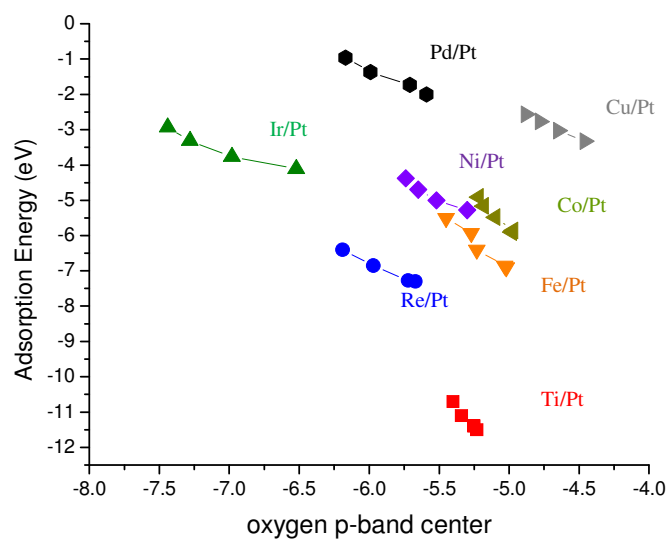
Figure 5-7. Oxygen p-band center as a function of adsorption energy defined as the energy gain or lost by taking both O atoms from the surface and forming O_2 in the gas phase.

A similar trend is observed in the surface d-band center as a function of adsorption energy, with the exception of Co/Pt which has an opposite trend, the surface d-band center shift toward the Fermi level as the adsorption energy is stronger (see Figure 5-8).
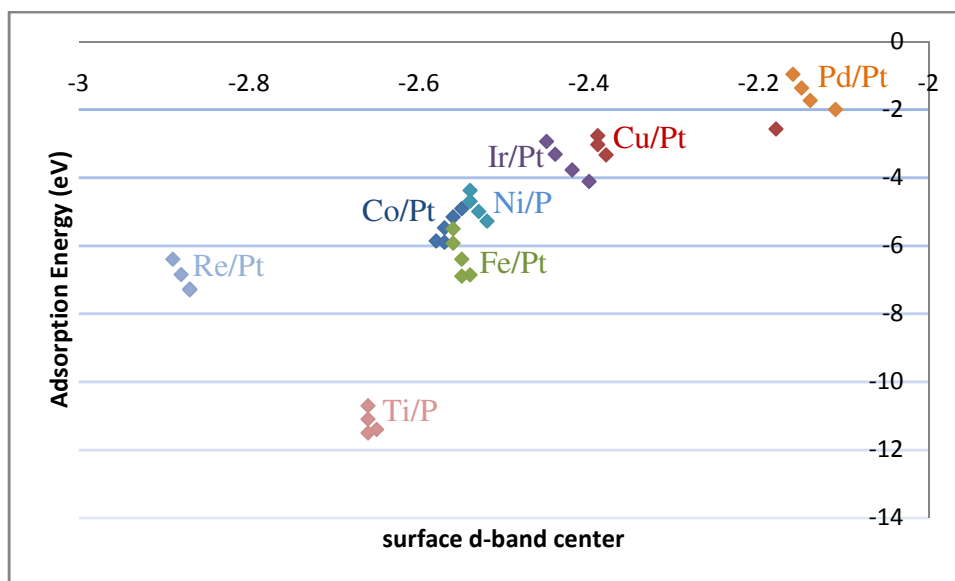
Figure 5-8. Surface d-band center as a function of adsorption energy defined as the energy gain or lost by taking both Oxygen atoms from the surface and forming molecular Oxygen in the gas phase.

From the results presented in Figure 5-8, it is observed that the trend of adsorption energy correlates with the location of the overlayer element in the periodic table, for example: the trend of adsorption for elements of period 4th is Ti > Fe > Co > Ni > Cu; similar correlations hold for Pd and Ag (5th period), and Re, Ir, Pt, Au (6th period).

These trends suggest that electronic effects may explain adsorption values in the region where O_2 dissociates. Table 5-3 summarizes the charge surface and d-band surface at a certain values of H in the region of O_2 dissociation for systems without molecular oxygen (Table 5-2 has more complete data for different surface-surface separation). From the data can be concluded that the adsorption energies depend on both the surface d-band center and charge; for example: overlayer elements of period 4th bear large surface charges with considerable differences of surface charge between them; thus, the trend of Adsorption energies correlates with the surface charge. The exceptions are Ni/Pt and Cu/Pt, which have the same surface charge, 0.16; in this case, the surface d-band center is the parameter that determines the adsorption energy; the system with the d-band center closer to the Fermi level has the greater adsorption energy, which is Ni/Pt with a d band center of -1.17 eV compared to Cu/Pt with d-band center of -1.79 eV. For overlayer elements of period 5th, the surface charge is too small and the difference between them negligible; thus, the surface d-band center determines the adsorption energy being greater for the system with surface d-band center closer to the Fermi level, which is Pd with d-band center of -1.56 eV compared to Ag with surface d-band center of -3.84 eV. A similar situation happens for the overlayer elements of period 6th, with the exception of Re that has a large surface charge and the d-band center closer to the Fermi level of the period, the surface charge of the overlayer elements is negligible; therefore, in these systems the adsorption energies is influenced by the surface d-band center. This reasoning may explain also why Ag and Au are the only overlayer elements that do not have greater adsorption energy than pure Pt; Ag, Au and Pt have negligible

charge, thus, the d-band center defined the values of adsorption energy, being greater for

pure Pt since it has the d-band center closer to the Fermi level, -2.006 eV, in comparison

with Ag and Au, -3.84 and -3.24 eV respectively.

Table 5-3. Surface charge and surface d-band center for each skin-surface.

System	Charge surface	d-band surface	System	Charge surface	d-band surface
Ti	0.48	0.77 (5.48Å)	Fe	0.28	0.85 (4.02Å)
Co	0.23	-1.21 (4.07Å)	Ni	0.16	-1.17 (4.10Å)
Cu	0.16	-1.79 (4.12Å)			
Pd	0.014	-1.56 (4.12Å)	Ag	0.079	-3.84 (4.23Å)
Re	0.20	-0.22 (5.31Å)	Ir	-0.00065	-1.54 (4.10Å)
Pt	-0.045	-2.006 (4.79Å)	Au	-0.0068	-3.24 (4.23Å)

5.4.3 H$_2$O adsorption

The above results showing enhanced interactions between the exposed surfaces

suggest the possibility of controlling those enhanced interactions by either manipulating

the electronic surface effects through changes in the nature of the surface and

subsurface, or in the surface-surface separation. In this section we explore the chemical

behavior of a more complex molecule: water. We used two different systems, both with

the same slab model used for O$_2$ adsorption, but changing the composition of the

surface-subsurface layers. One system has a Ti surface and Rh subsurface for both

exposed surfaces (Figure 5-9a and b) with the surface-surface separation H = 4.55 Å.

The other system has a Ti surface/Rh subsurface for one exposed surface and a Re

surface/Mn subsurface for the other exposed surface (Figure 5-9c and d) with H= 4.04 Å. A water molecule was initially located in the middle of both surfaces with its O atom pointing a hcp location as shown in Figures 5-9 a and c.

Pt				Pt
Rh				Rh
Ti				Ti
Ti				Re
Rh				Mn
Pt				Ti

a   *b*   *c*   *d*
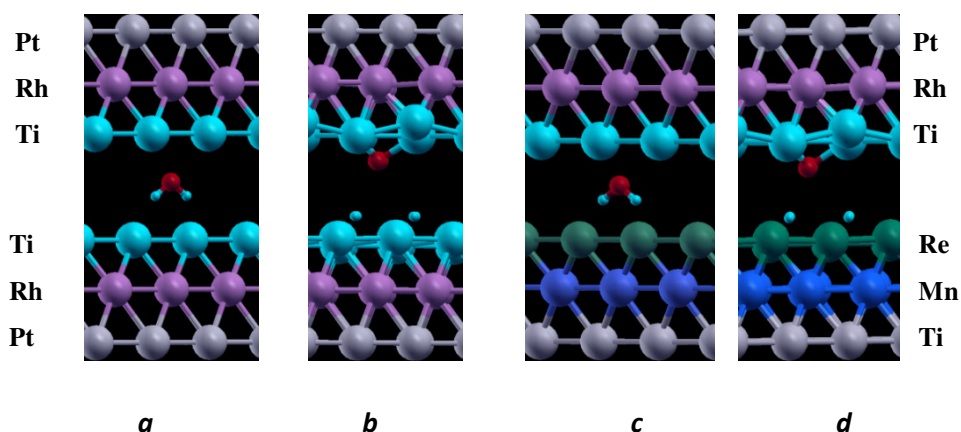
Figure 5-9. H_2O initial location, in the middle of both exposed surfaces with oxygen pointing a hcp position. Two different systems were studied: a. both exposed surfaces are of Ti and the subsurface of Rh, surface-surface separation of 4.55 Å, and b. the top exposed surface is of Ti with subsurface Rh and the bottom exposed surface is of Re with a subsurface of Mn, surface-surface separation of 4.04 Å.

Interestingly, spontaneous water dissociation arises in both systems; the O atom chemisorbs on the top surface in hcp position, and the H atoms in fcc positions on the bottom surface as shown in Figures 5-9 b and d. Note the deformation of the Ti surfaces. The calculated adsorption energy of the system with respect to the water molecule is -

5.35 eV for the system with both exposed surfaces of Ti; and -4.27 eV for the system with one exposed surface of Ti and the other of Re.

As mentioned in the previous sections, these systems have geometrical and electronic features that affect the activity. The geometrical effects are due to the lattice constant mismatch between the surface, subsurface and the "bulk" elements, which in this case is also Pt. The electronic effects are due to the reduction or oxidation of the surface, which has the subsurface as the reducing or oxidizing agent. This reduction-oxidation reaction between layers defines the surface charge and surface d-band center, which may describe the activity behavior of the surfaces. For the specific case shown in Figure 5-9a, both exposed surfaces have a Ti/Rh surface/subsurface; the surface Ti is oxidized bearing positive charges of 0.47 e and the subsurface Rh is reduced bearing negative charges of -0.39 e. The electronic density of this system, shown in Figure 5-10a, illustrates the presence of electrons in the region that separates both surfaces resulting in a unique situation characteristic of confined systems; this electronic phenomena gives rise to new chemical behavior described in this work. The system shown in Figure 5-9b has two different surfaces: one is the same Ti/Rh and the other Rh/Mn. In the second surface (Figure 5-10c), Re is reduced bearing negative charges of -0.20 e and the Mn subsurface is oxidized bearing positive charges of 0.41 e. The electronic density near the Re surface is denser in comparison with that of the Ti surface due to its reduction.
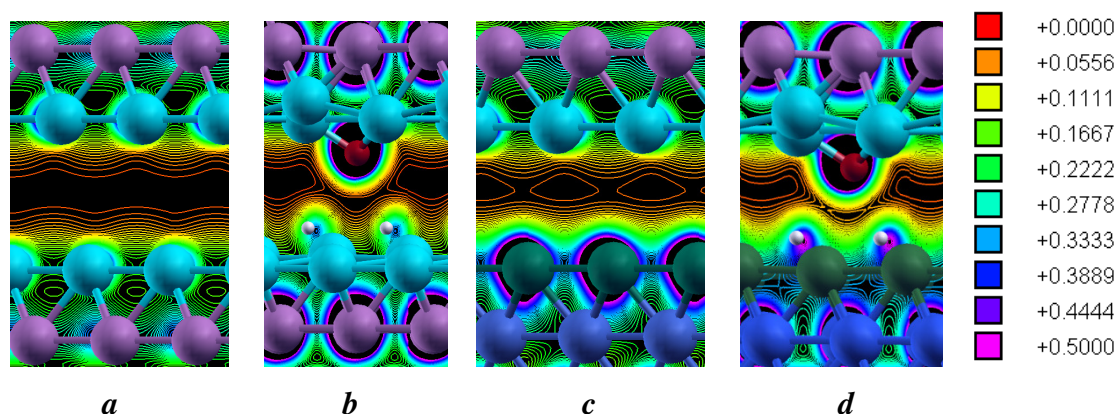
Figure 5-10. Electronic density for the systems described in Figure 5-9. There are electrons in the region that separates both surfaces, which is a unique situation of confined systems. From *a* to *b* the system shows oxidation of the Ti surface atoms. In *c* and *d* the system is characterized by the oxidation of Ti atoms in the top surface and the reduction of Re atoms in the bottom surface, that is evidenced by the increase of the electronic density surrounding the Re atoms (extended green regions compared to those near the surface atoms in *a*).

Figures 5-10b and d show the dissociated water molecule in each of the systems. The calculated difference of the average surface charge between the clean surface and that after water dissociation is -2.28 eV for Figure 5-10 a/b and -1.74 eV for Figure 5-10 c/d. In both systems there is a clear electron transfer from the surface to the water molecule that causes its dissociation into an adsorbed O and two adsorbed H atoms. The smaller charge transfer in the case of Figure 5-10 c/d may explain its weaker adsorption energy (-4.27 eV) with respect to the other system with both surfaces of Ti (-5.35 eV).

5.5 Conclusions

Strong interactions between transition metal surfaces determine the existence of a high-electronic density region where new chemical phenomena can be induced. We show this behavior for molecular oxygen confined between two slab systems having a monolayer of a metal M (M= Ag, Au, Co, Cu, Fe, Ir, Ni, Pd, Re, and Ti) deposited on a Pt core. Further, we illustrate that tuning the surface/subsurface composition of the interacting surfaces may also be used to control reactivity of species in the confined region. We are currently initiating a series of proof of concept experiments to validate our theoretical predictions. Fabrication of thin overlayers is now possible due to advances in experimental techniques such as atomic layer deposition and electrochemical deposition methods. Based on the results presented here, we expect that alloy overlayer systems with proper compositional tuning show especial promise for catalysis and sensing devices and processes.

6. CONFINEMENT-INDUCED POLYMERIZATION OF ETHYLENE*

6.1 Summary

Density functional theory calculations show changes in geometric and electronic properties of an ethylene molecule confined between two metal surfaces, and its conversion into a radical anion monomer ready to react forming a polymer chain. Here we demonstrate the evolution of the molecular properties under confinement, as well as that of the metal surfaces, and the optimum range of surface-surface separation that allows the production of the radical anion and the dimerization reaction. The effect of an electron donor surface on the already known confinement effect on reactivity is useful not only in many applications where a controlled polymerization is desired, but also where specific chemical reactions are sought.

6.2 Introduction

Let us imagine water molecules having a different geometry, for example an H-O-H angle of 180^0. For sure the world as we know it would be totally different. This hypothetical situation can become real when molecules are under geometric and electronic confinement. Due to these effects molecules may change their geometry and

electronic distribution making possible new reaction mechanisms and unusual chemical reactions [25, 26, 37, 38].

There are several studies about confinement effects in atoms and molecules. The first confined hydrogen atom model was introduced in 1937.[62] Since then, more accurate solutions have been reported for the confined hydrogen atom problem,[63, 64] as well as studies of the effect of confinement in other elements such as helium,[65] and changes have been predicted and observed in molecular orbitals of more complex molecules, such as ethylene, [25] anthracene[26] and toluene[66] inside of zeolites. There are many fields interested on the properties of confinement systems such as semiconductors,[67] thermodynamics of systems under extreme pressure [62] and catalysis [25]. The interest is driven by the fact that specific properties and/or reactions can be facilitated by varying the degree or nature of confinement. In our recent work we showed that electronic and geometric properties of metallic surfaces interacting through a gap of 0.4 to about 1 nm change significantly as a function of the surface-surface separation. These confinement-induced electronic and geometrical surface variations were explored for the dissociation of molecular oxygen[37] and water[38] and it was concluded that devices based on the underlying concept can be designed for specific applications by tuning alloy composition and surface separation.[37]

In this Section, we address a question similar to that in Corma's group earlier work: [25] Can ethylene confined be electronically and geometrically modified favoring the formation of polyethylene? However, at difference with previous works, [68] the geometric confinement arises from electron-donor (transition metal) surfaces that play a

vital role on the observed molecular changes. Thus, to induce electronic confinement, we examine a gap created between parallel slabs each exposing a monolayer of Ti over a Pt core (Ti/Pt). An ethylene molecule was located in the middle of the gap defined by the Ti/Pt surfaces and relaxed at different surface-surface separations, starting from two different initial configurations. Our findings provide a theoretical demonstration that the ethylene molecule under electronic and geometric confinement is converted into a radical anion and can initiate the polymerization chain without the need of an initiator. This concept is useful in a variety of applications ranging from a controlled polymerization,[69, 70] surface coating, and more generally to produce specific radicals and/or unusual chemical reactions by appropriate tuning of the surface properties.

6.3 Computational methods

Calculations were performed within the DFT framework using the Vienna ab initio simulation package (VASP) [33-36]. Electron-ion interactions are described using the projector-augmented wave (PAW) method [47], expanded within a plane wave basis setting up a cutoff energy of 400 eV. Electron exchange and correlation effects were described by the Perdew-Burke-Ernzerhof (PBE) [11] generalized gradient approximation (GGA) type exchange correlation functional. Spin polarization was included in every simulation. Figure 6-1 illustrates the system, taken as infinite in the x and y directions and finite in z direction. It consists of a periodically repeated fcc Pt slab covered in the top and in the bottom surfaces by a monolayer of a Ti metal; the systems were modeled using 4×4 supercells. The slabs are composed by 6 layers; the top and

bottom layers are allowed to relax, whereas the two layers in the middle are fixed, on the assumption that they represent a "bulk". Because of the periodic boundary conditions used in the three spatial directions, the top (111) surface is separated a distance H from another (111) surface, the bottom layer of the slab in the top neighboring cell. Such H distance is varied to evaluate specific properties as discussed below. The optimum bulk lattice constant of Pt was determined as 3.98 Å, a value 1.45% higher than the experimental (3.92 Å).[48] Brillouin zone integration for the surface system was performed using a 4×4×1 Monkhorst Pack grid [12] and a Methfessel-Paxton[13] smearing of 0.2 eV, whereas for the molecules in gas phase a 1×1×1 Monkhorst Pack grid was employed. The convergence criteria for the electronic self-consistent iteration and the ionic relaxation loop were set to 10^{-4} eV and 10^{-3} eV, respectively.

After relaxing the Ti/Pt surface at a given H surface-surface separation without any adsorbate and the ethylene molecule in gas phase, both optimized systems were combined. The ethylene molecule was located in the middle of the gap between surfaces. Two cases were studied, with ethylene in horizontal and in vertical position as shown in Figure 6-1.
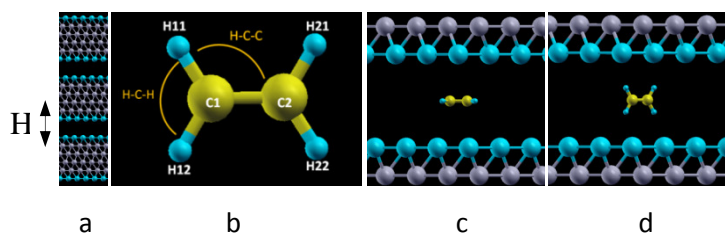
Figure 6-1. a. A gap of dimension H is defined every two slabs. Each slab has four central layers of fcc Pt (grey) covered on top and bottom by a monolayer of Ti (blue). Each of the Ti monolayers and the Pt subsurface layers are allowed to relax, the two central Pt layers are fixed. b. Ethylene molecule with labels of atoms and angles used for description of Figure 6-2 and Tables 6-1 and 6-2. The relaxed gas phase ethylene molecule has the following bond distances and angles: C-C = 1.33 Å, H-C = 1.09 Å, H-C-C = 121.78°, H-C-H = 116.44°. Initial locations for confined C_2H_4: horizontal (c) and vertical position (d). In both cases, the initial C-C and C-H distances and angles correspond to the equilibrium C_2H_4 gas phase geometry.

The total electronic charge of an atom was obtained using Bader analysis,[49, 50] where the atomic charge is approximated by the charge enclosed within the Bader volume defined by zero flux surfaces. The d-band centers are referenced to the Fermi level; they were calculated from the site-projected electronic density of states using a k-point mesh of 16×16×1.

6.4 Results and discussion.

6.4.1 Geometric and electronic effects of ethylene under confinement.

Figure 6-2 shows the distances and angles of the ethylene molecule after relaxation for each initial configuration at various values of surface-surface separation H. For ethylene initially located in horizontal position, H < 6.5 Å induces a significant change in the molecular geometry that, as discussed below, goes along with significant electronic changes. In contrast, little changes are observed in the geometry of ethylene initially in vertical position relative to gas phase ethylene.
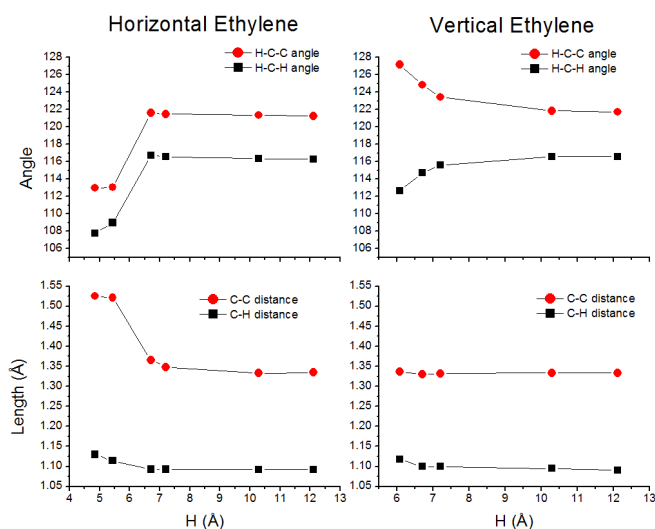
Figure 6-2. Geometric evolution of the confined ethylene molecule as a function of surface-surface separation (H) between Ti/Pt surfaces. The vertical axes correspond to angles and interatomic distances at different H values.

The final geometries in each case are shown in Figure 6-3. The ethylene molecule (initially in horizontal location) under the confinement of Ti/Pt surfaces is converted into a radical. The electronic charges shown in Table 6-1 reveal that electrons are transferred from the surface to the confined space and localized on the carbon atoms. As confinement increases, the total charges show the extra electrons on the ethylene molecule when is converted into a radical anion.
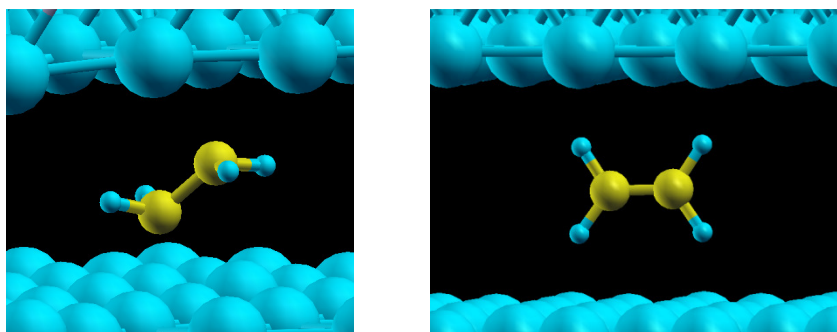
Figure 6-3. Relaxed ethylene molecules under confinement. Left: molecule initially located in horizontal position at H = 5.43 Å. The final geometry is similar to a monomer in the polyethylene chain. Right: Final geometry of the molecule initially located in vertical position at H = 6.08 Å. Very small changes are observed in this case with respect to the gas phase geometry.

Table 6-1. Electronic charges (e) of carbon and hydrogen atoms belonging to the ethylene molecule after relaxation as a function of the surface-surface separation H between Ti/Pt surfaces. The bottom row corresponds to the total charge of ethylene, and it is the total extra electrons that the surfaces have transferred to the molecule transferred. The values correspond to relaxed ethylene initially located in horizontal position (Figure 6-1c).

Atoms	H= 4.85 Å	H= 5.43 Å	H= 6.70 Å	H= 7.21 Å	H= 10.29 Å	H= 12.11 Å
C1	-0.91	-0.44	-0.26	-0.25	-0.19	-0.19
C2	-0.61	-0.65	-0.06	0.00	0.12	0.13
H11	0.15	-0.06	0.11	0.12	0.11	0.11
H12	0.10	0.02	0.00	0.01	0.00	0.00
H21	-0.02	0.02	0.04	0.04	-0.07	-0.06
H22	0.00	0.02	0.00	0.00	0.00	0.00
Total	-1.29	-1.10	-0.17	-0.10	-0.02	0.00

In contrast, the atomic charges of the molecule initially located in vertical location (Table 6-2) are much smaller, although some electron localization is also observed at the lowest values of H. However, as confinement increases (H < 6.08 Å) the H atoms become attached to each of the surfaces and eventually they could be separated from the original molecule. We do not discuss here such reaction that could also have other interesting consequences.

Table 6-2. Electronic charges (e) of carbon and hydrogen atoms belonging to the ethylene molecule after relaxation as a function of surface-surface separation H between Ti/Pt surfaces. The bottom row correspond to the total charge of ethylene. The values correspond to relaxed ethylene initially located in vertical position (Figure 6-1d).

Atoms	H= 6.08 Å	H= 6.70 Å	H= 7.21 Å	H= 10.29 Å	H= 12.11 Å
C1	-0.26	-0.30	-0.25	-0.27	-0.28
C2	-0.22	-0.08	-0.20	-0.17	-0.13
H11	0.03	0.10	0.08	0.16	0.13
H12	0.05	0.07	0.08	0.09	0.15
H21	0.04	0.01	0.06	0.07	0.04
H22	0.03	-0.02	0.06	0.07	0.07
Sum	-0.32	-0.23	-0.18	-0.04	-0.02

To understand the electronic changes in the ethylene molecule we analyze the frontier molecular orbitals for the gas phase and confined molecules. The results are shown in Figure 6-4. This diagram shows that the energy gap, defined as the difference between the energies of the highest occupied molecular orbital (HOMO) and that of the lowest unoccupied molecular orbital (LUMO) is 7.45 eV in the gas phase molecule, and is reduced to 5.33 eV for the confined ethylene started in horizontal position. Thus, the energy of the π^* antibonding orbital of the confined molecule becomes much closer to the corresponding π bonding orbital. On the other hand, the energy gap of confined ethylene in vertical location remains very similar (7.37 eV) to that of the gas phase molecule. Essentially, our findings are in agreement with those of the simpler model proposed by Corma et al. [25] The reduction of the HOMO-LUMO gap suggests the enhanced reactivity of the confined molecule.
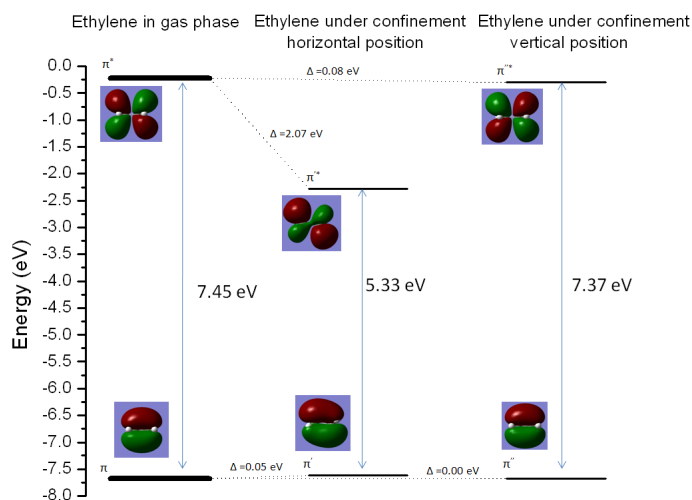
Figure 6-4. Molecular orbital diagrams showing energies of HOMO and LUMO for ethylene (left), horizontal confined ethylene, H = 4.85 Å (center), and vertical confined ethylene, H = 6.08 Å (right). The energy difference (Δ) between the π orbital (HOMO) of confined ethylene relative to the free molecule, and that between the π∗ orbital (LUMO) of confined ethylene relative to the free molecule are shown, as well as the HOMO-LUMO gaps in each case.

In contrast, the work of Borgoo et al [71] finds exactly the opposite trend, with the HOMO-LUMO gap increasing as confinement increases. However, as remarked by the authors, their study does not include the interaction between the molecule and the confinement medium. Thus, in our complex system including molecule + confinement medium the analysis has three components: one is the effect of confinement on the molecule (as given by Borgoo et al's work), another is the electronic effect of the two clean interacting surfaces; the third is the interaction of the confined molecule with the

interacting surfaces; this last one yields the HOMO-LUMO trend as reported in our work and in Refs. 1 and 9.

Therefore, the described molecular properties are induced not only by geometric confinement but by the strong electron-donor character of the surfaces. As reported recently, the electronic structure of the metallic skin-surface is affected by electronic confinement.[37, 38] To investigate this, we look at the density of states of the surface atoms (first exposed layer of Ti atoms).
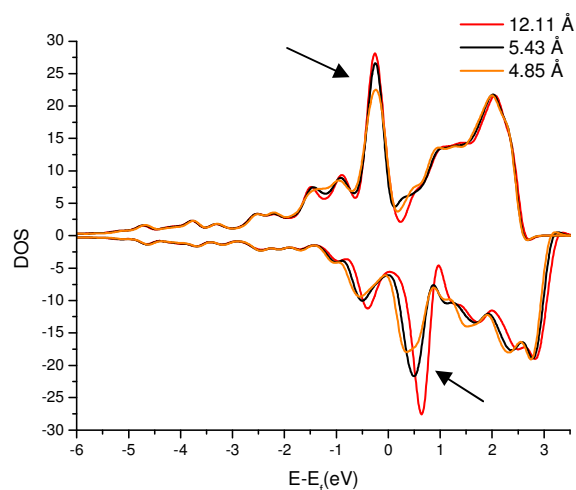
Figure 6-5. Density of states of clean Ti/Pt surfaces separated by a gap of 12.11 Å, 5.43 Å and 4.85 Å. Their respective d-band centers are 0.029, 0.766, and 0.756 eV; they are all located at the right of the Fermi level located at 0 eV. Arrows point to the majority and minority DOS peaks where the largest changes are observed as the surface-surface separation varies.

Figure 6-5 shows the d-band density of states (DOS) for the clean surface atoms at various values of the surface-surface separation H. Note that when H becomes small enough, the two surfaces collapse (avalanche effect) [23] and the system becomes a "bulk" metal. Thus, changes in the electronic distribution observed in Figure 6-5 are due to a transition between a system consisting of two interacting surfaces and a bulk. Two major changes are observed in the DOS as a function of surface-surface separation: the values of the density of states corresponding to the peaks of the majority and minority d states (see arrows in Figure 6-5), and the exchange splitting (energy difference between DOS maxima of the spin-up and spin-down peaks at each side of the Fermi level); they both diminish as the surface-surface separation gets shorter. The first change represents the broadening of the d-band as the two surfaces become closer to each other; the difference in exchange splitting is directly related to the magnetic properties of the thin Ti film due to its interactions with Pt.[72-75] The net result is an enhancement of surface activity and the modification of other surface physical properties such as the magnetic moment. For the Ti/Pt clean surfaces, we observed charge transfer from Ti to Pt. The interaction of the Ti monolayer over the Pt core produces a strong polarization of the film, with positive charges of the order of 0.47 e on the Ti layer, and an average of -0.43 e in the Pt layer in contact with the surface Ti layer. This surface polarization effect has been detected previously by experiments and computations.[76-78] However, there is very little change in the charge distribution as the surface-surface separation varies, indicating that the observed modifications in the DOS and exchange splitting do not translate in higher polarization, but rather in a broadening of the d-states and a

decrease of the number of electrons available at the Fermi level, due to the enhanced interactions of the two surfaces.
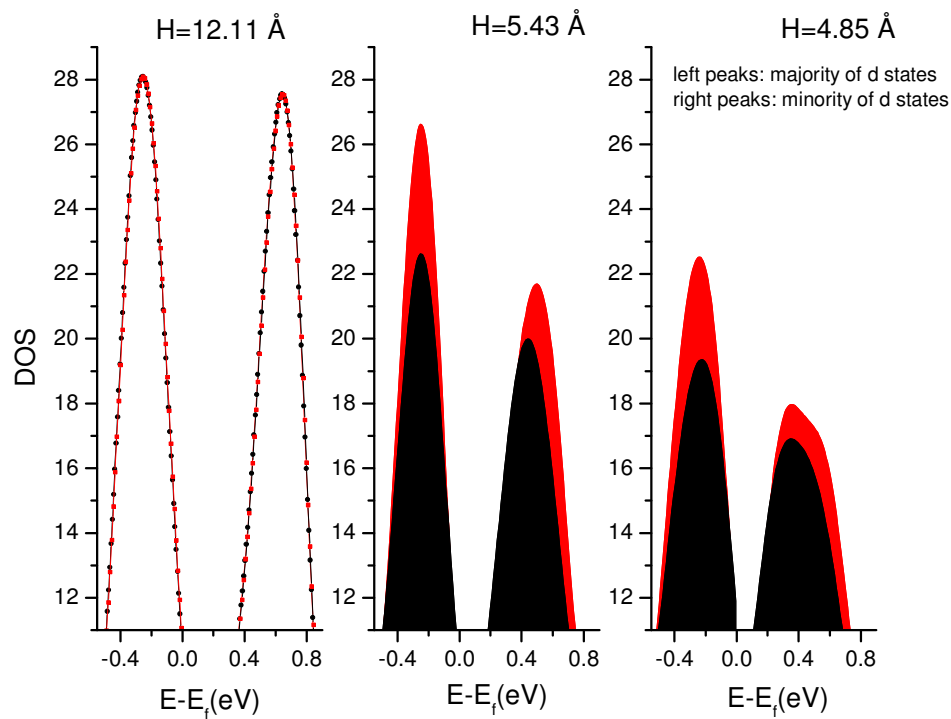
Figure 6-6. Prominent peaks from the DOS of the clean surface (red peaks) and in presence of ethylene (black peaks) at different surface-surface separations. The left peaks are from the majority of d states, and the right peaks from the minority of d states. Changes in the peak density of states and exchange splitting are due to the electronic interaction between both surfaces and also between the Ti/Pt surface and ethylene.

The same phenomena are analyzed in presence of ethylene. As shown in Figure 6-6, similarly to the clean surface features, the main effects at a given surface-surface separation are the reduction of the density of states at the prominent peaks in the majority and minority d states, and that of the exchange splitting. Figure 6-6 shows this ethylene "finger print" at various surface-surface separations. At H=12.11 Å the surfaces practically do not interact with the ethylene molecule so no changes are detected between the clean surface DOS and that in presence of ethylene. On the other hand, at H=5.43 Å and H=4.85 Å the DOS at the peaks in the majority d states (left peaks) diminish from 26.62 to 22.62, and from 22.52 to 19.35, respectively; the peaks in the minority d states (right peaks) diminish from 21.69 to 19.99, and from 17.96 to 16.90 at H=5.43 Å and H=4.85 Å respectively. Following similar trends, the exchange splitting diminishes from 0.75 eV to 0.69 eV, and from 0.61 eV to 0.58 eV H=5.43 Å and H=4.85 Å respectively. These modifications in the surface DOS are due to the surface/ethylene electronic interaction; thus, they are expected to be unique for a specific surface-molecule interaction, suggesting that this phenomenon may be suited for sensor applications.

Investigation of the charge distribution indicates that a similar polarization effect as the one detected in the clean surfaces is observed in the presence of ethylene. The average charges of the metal surface and subsurface layers are approximately 0.50 e and -0.43 e respectively, whereas the average net charge in the molecule is -0.22 e at H= 4.85 Å, whereas at 12.11 Å the charge distribution in the surface layers resembles that of the clean surfaces and the net molecular charge is zero. Thus, again we can conclude that

the surface polarization is less affected by the change in the surface-surface separation while the charge transfer to the molecule is enhanced due to the increased availability of surface electrons in the gap when the two surfaces become closer to each other.

6.4.2 Dimerization.

As discussed above, analyses of the results of the relaxed geometry and charge density suggest that the horizontal ethylene under confinement becomes an anionic radical suited for polymerization, since its geometry and electronic properties are similar to the unit of a polyethylene chain. Figure 6-7 shows two anionic radicals with the geometry obtained under confinement. Rotating the radical it is possible to find a favorable location for reaction since carbon-carbon interaction can occur without the interference of H-H repulsion to favor the dimer formation.

a   b
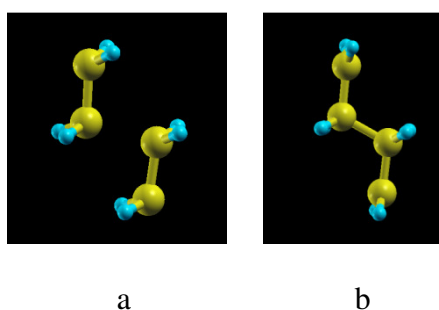
Figure 6-7. a) Two anion radicals obtained from exposing ethylene molecules to electronic and geometric confinement. b) Dimer obtained after relaxation of the initial geometries.

After relaxing both radicals initially located as shown in Figure 6-7, a dimer is formed, which may react with another radical to increase the chain length. The same reaction mechanism was evaluated under confinement. Two ethylene molecules with the geometry obtained after confined relaxation were located as shown in Figure 6-8 at H = 5.43 Å , 5.77 Å and 6.08 Å between Ti/Pt surfaces. After relaxation, the dimer chain is formed indicating the feasibility of polymerization under confinement (Figure 6-8).

H= 5.43 Å   H=5.77 Å   H=6.08 Å
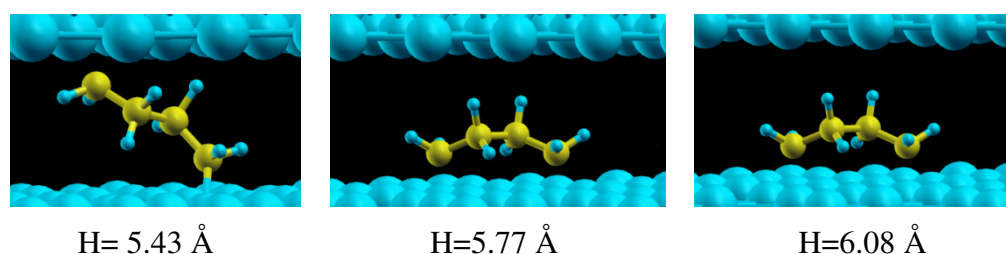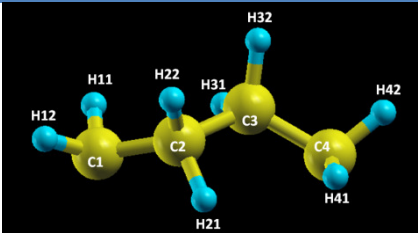
Figure 6-8. Relaxed polyethylene dimer molecules under various extents of confinement.

The charge analysis of polyethylene dimer under confinement supports its feasibility for continuous growth. The carbon atoms located in the extremes of the dimer bear a considerable excess of electrons in comparison with the other carbon and hydrogen atoms (Table 6-3). The sum of charges of all atoms reported in Table 6-3 shows the extra electrons on the dimer anion radical transferred from the Ti/Pt surfaces.

Table 6-3. Atomic charges on polyethylene dimer molecule relaxed under confinement. The extreme carbon atoms of the molecule bear an excess of electrons favoring continuum growth. The bottom row is the amount of electrons transferred from the metal surface to the molecule.

Atoms	H= 5.43 Å	H= 5.77 Å	H= 6.08 Å
C1	-0.69	-0.61	-0.64
C2	-0.20	-0.24	-0.17
C3	-0.23	-0.21	-0.19
C4	-0.67	-0.62	-0.75
H11	0.04	-0.02	-0.01
H12	0.07	0.05	0.04
H21	0.06	-0.04	-0.03
H22	-0.05	0.09	0.09
H31	0.08	-0.03	-0.02
H32	-0.08	0.05	0.06
H41	0.06	-0.02	0.13
H42	-0.02	0.07	0.07
Sum	-1.64	-1.54	-1.42

6.5 Conclusions

Our density functional theory studies have shown that the confinement effect produced by the proximity of two metal surfaces induces a reactive environment which converts ethylene in an anion radical that adopts the geometry of the monomer in a polyethylene chain and is ready to react initiating the polymerization chain. The reactive environment is caused by electron transfer from the two surfaces when they are separated by sufficiently short distances in the order of 0.6 to 0.4 nm.

We remark that whereas the extensively studied adsorption of ethylene on a single transition metal surface[79-81] is mainly driven by bonding of the π electrons to the metal sites, in this work we report a different phenomenon that is the conversion of ethylene into a radical anion, and this is exclusively caused by the interaction of the two surfaces, which we prove by taking the system to the limit of non-interacting surfaces. We have explained in Figures 6-5 and 6-6 what are the electronic changes caused by confinement on the clean system formed by the two interacting surfaces, and how it induces changes on the molecule located in the gap. Besides controlled polymerization, we suggest that this enhanced reactivity may be useful for promoting many other chemical reactions with much lower barriers than those needed to be overcome on single catalytic surfaces.

7. CONFINEMENT-INDUCED CHANGES IN MAGNETIC BEHAVIOR OF A Ti MONOLAYER ON Pt*

7.1 Summary

Density functional theory is used to examine the magnetic properties of a Ti monolayer over Pt when is brought in contact with a Pt surface, at distances of 4 to 12 Å. The average magnetic moment of the Ti film decreases sharply as the surface-surface separation decreases, coincident with migration of surface electrons towards the gap, surface d-band broadening, and decrease of the density of states at the Fermi level. The phenomenon is analyzed using the Stoner criterion that correlates the ferromagnetic behavior with exchange splitting and density of states at the Fermi level obtained from a paramagnetic calculation.

7.2 Introduction

There is a growing necessity to understand the magnetic behavior of nanoscale materials due to their potential for many technological applications. The advent of giant magnetoresistance phenomenon and its applications to commercial magnetic hard disk systems have made popular the development of novel materials such as epitaxially grown ultrathin transition metal films on other transition metal substrates. The effect of

the substrate on the thin-film materials gives rise to physical properties very different from bulk systems.[82]. For example, it has been reported that thin films of many magnetic elements when deposited on non-magnetic substrates change considerably their magnetic ground state from that of the bulk.[83, 84] More surprisingly, nonmagnetic 4d-metal monolayers on nonmagnetic substrates favor ferromagnetic states. These phenomena has been explained applying Stoner theory,[85-87] arguing that due to the reduced number of nearest-neighbor atoms within the overlayer, the balance between the competing electron-electron exchange and kinetic energies determine changes in magnetic behavior. On the other hand, significant interest has been given to monolayer 3d films deposited on platinum cores for catalysis applications.[88]

In this work we show that the magnetic moment of thin films may be changed by controlling the surface-surface separation of specific metallic surfaces. As a consequence of confinement effects in metallic systems, we report the formation of an electron gas in the gap between two surfaces of Ti/Pt and pure Pt at short surface-surface separations. Consequently, we observe a reduction in the magnetic moment of the system that depends on the gap size. This theoretical result is explained applying Stoner theory.[87] In recent work we have shown that similar confinement-driven phenomenon also results in new physico-chemical surface properties giving rise to dissociation of molecular oxygen and water, and inducing ethylene polymerization [37-39].

Our computational results illustrate the magnetic moment variation of ultrathin transition metal films as a function of separation between Ti/Pt and Pt surfaces. The magnetic moment variation occurs when both surfaces are separated by less than 6 Å, in

a range of surface-surface separation that corresponds to a transition zone between the bulk state and the formation of two surfaces. The structure of this paper is: first, a description of the computational methods used to obtain the magnetic moment results; second, analysis of magnetic moment variation as a function of surface separation of Ti/Pt and Pt surfaces; and third, interpretation and discussion of the computational results.

7.3 Computational methods

Calculations were performed within the density functional theory (DFT) framework using the Vienna ab initio simulation package (VASP) [33-36]. Electron-ion interactions are described using the projector-augmented wave (PAW) method [47], expanded within a plane wave basis setting up a cutoff energy of 350 eV. Electron exchange and correlation effects were described by the Perdew-Burke-Ernzerhof (PBE) [11] generalized gradient approximation (GGA) type exchange correlation functional. Spin polarization was included in every simulation, except when explicitly indicated. Figure 7-1 illustrates the system, taken as infinite in the x and y directions and finite in z direction. It consists of a periodically repeated fcc Pt slab covered in the top by a monolayer of a Ti metal; the systems were modeled using 2×2 supercells. Two slabs were used, one composed by 6 layers and another with 12 layers; the top and bottom layers are allowed to relax, whereas the two layers in the middle are fixed, on the assumption that they represent a "bulk". Because of the periodic boundary conditions used in the three spatial directions, the top (111) surface is separated a distance H from

another (111) surface, the bottom layer of the slab in the top neighboring cell. The surface-surface separation H distance is varied to evaluate specific properties as discussed below. The optimum bulk lattice constant of Pt was determined as 3.98 Å, a value 1.45% higher than the experimental (3.92 Å).[48] Brillouin zone integration for the surface system was performed using a 9×9×1 Monkhorst Pack grid [12] and a Methfessel-Paxton[13] smearing of 0.2 eV. The convergence criteria for the electronic self-consistent iteration and the ionic relaxation loop were set to 10^{-4} eV and 10^{-3} eV, respectively. The d-band electronic density of states is referenced to the Fermi level; and it is calculated from the site-projected electronic density of states using a k-point mesh of 16×16×1.

All the results presented in the following section were obtained without adding a dipole correction to the calculations. However, the calculations were repeated for the 6-layer system using 9x9x1 k-points and a dipole correction. Compared with the results without dipole correction, only negligible changes were found in the values of the magnetic moment per Ti atom and in the total energies for the various surface-surface separations. In addition, to explore the basis set effect, we performed calculations at various energy cutoffs between 240 and 500 eV. The results indicate practically no variation of the magnetic moment, and variations in energy showing convergence at the largest cutoff.
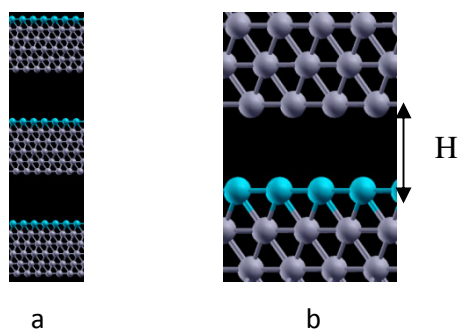
Figure 7-1. a) A gap of dimension H is defined every two slabs. This figure illustrates a slab with four central layers of fcc Pt (grey) covered on top by a Ti monolayer (blue) and on the bottom by a Pt monolayer. Another slab (not shown) was built with ten central layers of fcc Pt covered on top by a Ti monolayer and on the bottom by a Pt monolayer. Only the two central Pt layers in each slab system were fixed whereas the rest of the layers were allowed to relax. b) Gap between the Ti and Pt surfaces.

Since the calculations give only local minima, several initial spin ordering were examined in order to be sure that the results of magnetic moment represent a good approximation to a global minimum. For the Ti atoms we tested the following initial magnetic moments: 1.14, 1.37, 1.65, 1.98, 2.38, and 4 μ_B per Ti atom. It was found that the magnetic moment changes in the systems were small and the initial magnetic moment that resulted with the lowest system energy was 1.98 μ_B per Ti atom.

7.4 Results and discussion

Although both Ti and Pt are non-magnetic a thin layer of Ti over Pt generates a ferromagnetic state as has been found for Ti/Ag and other systems [72-75]. However, the magnetic moment of Ti/Pt surfaces changes as a function of surface-surface separation, as illustrated in Figure 7-2. At large surface-surface separations (12 to 6 Å), we find a magnetic moment of 1.03 μ_B per Ti atom, which corresponds to the limit of non-interacting surfaces. As the surfaces start to interact, at surface-surface separations H smaller than 6 Å, the magnetic moment decreases as shown in Figure 7-2. Calculations done with systems containing 6 and 12 layers showed only a slight variation in the magnetic moment values, thus indicating that the magnetic moments are independent on the amount of Pt in the system.

The Ti overlayer on Pt substrate has a Ti-Ti bond distance of 2.8 Å, which is the same Pt-Pt distance of a pure Pt (111) surface; here it was assumed that the Ti overlayer adopts the Pt substrate geometry. Comparing the Ti-Ti distance of 2.8 Å in (111) surface on a Pt substrate with the lattice constant of pure hcp Ti (a =2.95 Å) found experimentally [89], the mismatch is of 5.08%; thus the experimental realization of this system would be feasible.
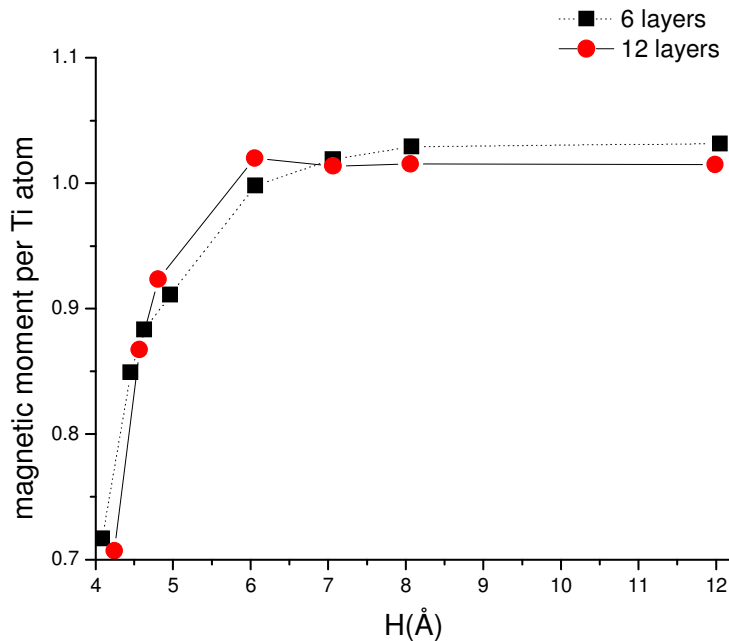
Figure 7-2. Magnetic moment of Ti/Pt system in μ_B (Bohr's magneton per Ti atom) as a function of surface-surface separation (H, in Å) between Ti/Pt and Pt surfaces. At H values shorter than 6 Å the magnetic moment of the system decreases. The calculations were done with a system composed by 6 layers and 12 layers, in both cases only the overlayer of the system was composed by Ti atoms; thus the magnetic moment is independent of the number of Pt atoms in the system.

At surface-surface separations shorter than 6 Å, the system is in a transition zone between a surface and a bulk. The bulk state of this system corresponding to bulk platinum having Ti planes intercalated every 6-12 layers would result when the two surfaces become sufficiently close to each other, causing an "avalanche" effect to take

place [23]. Thus, the surface-bulk transition zone is characterized by a gradual change in the electronic density existent in the gap between two surfaces, as illustrated in Figure 7-3. It is interesting to determine how the electronic properties of the gap change as the surface-surface separation decreases. When the Ti/Pt and Pt surfaces are separated by a distance where the surface-surface interaction is negligible, the electronic density in the gap is almost zero, as shown in Figure 7-3 for H= 8.07 Å.
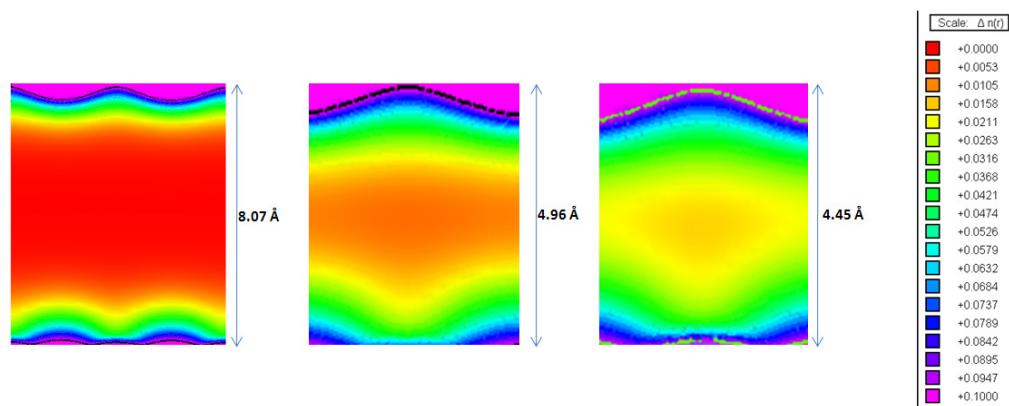
Figure 7-3. Electronic density in the gap between the Ti/Pt and Pt surfaces as a function of surface-surface separation. At surface-surface separation of 8.07 Å the red color in the gap between surfaces indicates the absence of electrons; whereas for surface-surface separations of 4.96 Å and 4.45 Å, the orange and yellow color indicate that electrons have migrated to the gap between surfaces. The scale at the right shows that the electronic density in the gap between surfaces increases as the surface-surface separation decreases.

In contrast, at shorter surface-surface separations, in the transition zone between surface and bulk, the electronic density in the gap between surfaces gradually increases as H decreases (see Figure 7-3, at H = 4.96 and 4.45 Å). The electron delocalization that takes place at short values of H gives rise to a series of interesting physicochemical phenomena when molecules are confined in the gap, [37-39] and also induces a sudden change in the magnetic moment shown in Figure 7-2. At short values of H, the interactive metallic Ti/Pt and Pt surfaces are in the surface/bulk transition zone, and the electron gas formed in the gap between surfaces brings along modifications in the electronic density of the valence band of the surfaces. These modifications are the cause of magnetic moment variation as we describe next.

As the surface-surface separation decreases, the gradual increase of the electronic density in the gap between surfaces shown in Figure 7-3 is reflected in a broader d-band and lower DOS at the Fermi level of the Ti surface atoms. Figure 7-4 shows the broadening of density of states obtained from paramagnetic calculations of the Ti/Pt system as H decreases. Based on the Stoner model,[87] the density of states at the Fermi level obtained from paramagnetic calculations may be an indicator of the ferromagnetic behavior. Figure 7-4 shows that the value of the DOS at the Fermi level decreases gradually as the surface-surface separation H becomes shorter, and according to the Stoner criterion, this would suggest a reduction of the ferromagnetic behavior as observed in Figure 7-2. Indeed, the DOS of the bulk material-defined by platinum bulk having Ti planes intercalated every 6 layers- has 1.9 states/eV at the Fermi level, which

is considerably lower than those where the surfaces are separated by H values ranging between 4 to 12 Å.
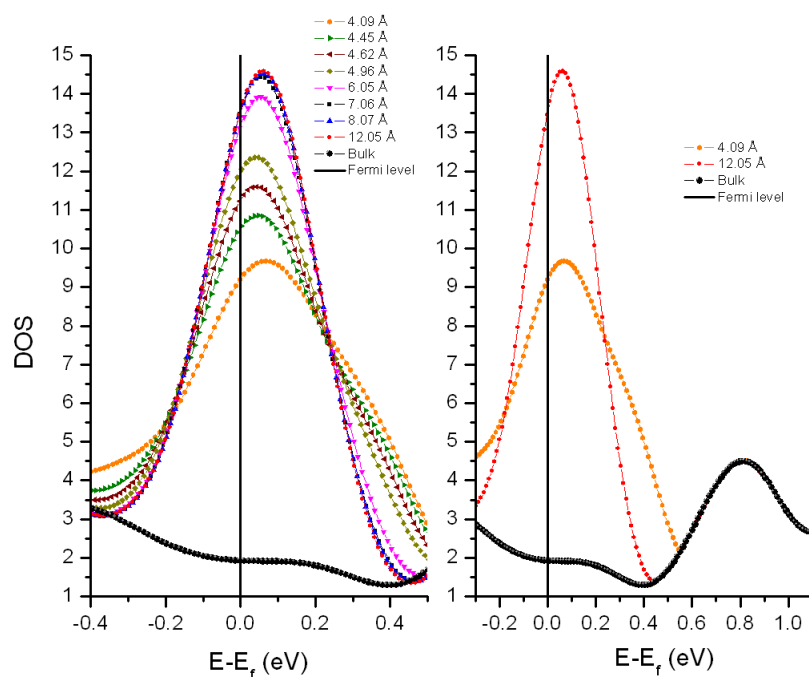
Figure 7-4. Paramagnetic density of states (DOS) of Ti overlayer surface as a function of surface-surface separation H in Å. As the separation between surfaces decreases, the density of states becomes broader decreasing the electron density at the Fermi level, $n^0(E_f)$.

This low bulk DOS at the Fermi level makes the system paramagnetic, since the necessary condition for a ferromagnetic system according to the Stoner criterion: $n^0(E_F)I > 1$, the product of the number of states at the Fermi level ($n^0(E_F)$) times the exchange

integral Stoner parameter I (0.34 eV for Ti, [90]), is not satisfied. Since I is a constant characteristic of each metal,[87, 90] the variation of $n(E_F)$ can be directly related to the ferromagnetic behavior. Therefore, according to Figure 6-4, the Ti film is clearly ferromagnetic at large surface-surface separations (limit of a single surface), and the ferromagnetic character decreases as the second surface becomes closer, although at 4.09 Å the product $n^0(E_F)I$ can be estimated as 3.06, still satisfying the Stoner criterion.

Spin polarized DFT calculations yield the DOS shown in Figure 7-5. The DOS shapes corresponding to both spin directions at a given surface-surface separation (Figure 7-5a) are similar, except that they are shifted with respect to each other by the exchange splitting, $\Delta = Im$, that is the product of the Stoner parameter I and the magnetic moment m. The exchange splitting is constant (0.88 eV) at longer surface-surface separations: 12.05 Å, 8.07 Å, 7.06 Å, and 6.05 Å as a result of electron localization on the surface due to the interactions of the Ti overlayer over the Pt core.

On the other hand, the exchange splitting decreases at shorter H values of 4.96 Å, 4.62 Å, 4.45 Å, and 4.08 Å, becoming 0.82 eV, 0.81 eV, 0.81 eV, and 0.73 eV respectively (Figure 7-5b) reflecting the electron delocalization produced when the two surfaces approach each other. Since the exchange integral I is an element-specific quantity,[87] which is approximately independent of the local environment, a decrease in the exchange splitting Δ implies a decrease in the magnetic moment m. Thus, the ferromagnetic behavior of the Ti/Pt system at long surface-surface separations is favored by large values of both, the exchange splitting, Δ , and the density of states at the Fermi level energy $n^0(E_f)$ (obtained in paramagnetic calculations); whereas, at shorter surface-

surface separations these two parameters decrease disfavoring the ferromagnetic behavior of the system. In summary, the results shown in Figure 7-2 are well explained by the Stoner model.
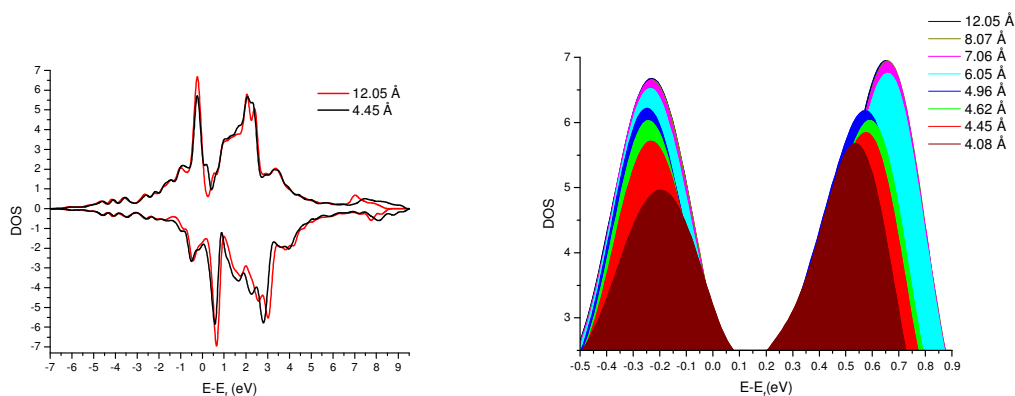
Figure 7-5. Spin-polarized density of states of the d-band of Ti overlayer surface as a function of surface-surface separation. a) Reduction of the density of states and of the exchange splitting are the main changes found in the d-band of the system. These electronic changes explain the magnetic moment variation. b) Spin-polarized peaks of the density of states; the left peak corresponds to the majority of states and the right peak to the minority of states. The shapes of both spin directions at certain surface-surface separation are similar only shifted with respect to each other by the exchange splitting, $\Delta = Im$.

7.5 Conclusions

We have shown the variation of the magnetic properties of a Ti monolayer over Pt when interacting with a Pt surface at distances shorter than 6 Å. The phenomenon is explained in terms of the changes observed in the number of electronic states at the Fermi level and in the exchange splitting, as a function of surface-surface separation.

Based on the Stoner theory, it is possible to infer that other metallic systems with the geometry presented in this work, can increase instead of decrease the magnetic moment as the gap is reduced. As reported above, the decrease of the surface-surface separation modifies the density of states obtained from paramagnetic calculations. The non-magnetic density of states becomes broader. In the current case involving Ti/Pt and Pt surfaces, the broadening of the non-magnetic density of states causes a reduction in the density of states at the Fermi level disfavoring the system magnetic moment. However, it is possible that the opposite effect may be obtained by other systems, as reported in a study of magnetic 4d monoatomic rows on Ag [91].

Another variable that can play an important role in magnetic moment variations and in confinement effects in general is the structure of the metal interfaces that form the gap. Depending on the structure of the interfaces, the atomic surface density will increase or decrease. The atomic surface density may change the amount of electrons in the gap between surfaces and alter the magnetic moment accordingly.

8. P-N JUNCTION AT THE INTERFACE BETWEEN METALLIC SYSTEMS

8.1 Summary

Density functional theory (DFT) is used to propose a metallic device that resembles a semiconductor p-n junction. It consists of two metallic thin films separated by 4 to 10 Å gap. In the gap between the metallic thin films is formed a built in potential. The proposed system is the combination of two parts forming an interface, The first part is a skin-metal M/Pt system composed of a core of Pt atoms and a single overlayer of a different metal, M, forming a skin. The second part is composed only of Pt atoms. The Electron density in the gap between thin films, the work function of the system and the built in potential in the gap at the interface are calculated for various metal skins. The results are discussed in order to present a possible explanation of the process of forming a built-in potential characteristic of a p-n junction. The proposed device has two characteristics that may play an important role in the continuous race for downscaling of solid state devices; one refers to the basic physical phenomena occurring in the material, quantum tunneling, and the second refers to the specific materials that compose the system, metals.

8.2 Introduction

Engineering materials usually refers to tailoring of synthetic materials with specific or novel physical, mechanical and chemical properties. Most of the devices based on semiconductor nanostructures are engineered materials. Among them, p-n

junctions, play an important role as elementary building blocks. Several semiconductor devices such as transistors, diodes, LEDs, integrated circuits, and solar cells are based on p-n junctions. The physical properties of p-n junctions are based on the formation of a potential barrier across the junction in an equilibrium state of the material. In this work, a composite metallic system is proposed having at equilibrium a potential barrier that resembles a semiconductor p-n junction.

The composite metallic system is the combination of two parts; each part consists of two thin films arranged in parallel and separated by a 4 to 10 Å gap. The first part is a skin-metal M/Pt system composed of a core of Pt atoms and a single overlayer of a different metal, M, forming a skin. The second part is composed only of Pt atoms. The two parts join in the y direction to form the composite material that is claimed to resemble a p-n junction, see Figure 8-1.

Density functional theory is used to theoretically model and calculate phenomena occurring when the described system is built. Electron density in the gap, work function of the system and potential barrier at the junction interface are calculated for various metal skins. The dependence of these variables on the nature of the metal skin is correlated with the location of the metal skin in the periodic table. The results are discussed in order to present a possible explanation of the process of forming a built-in potential characteristic of a p-n junction.
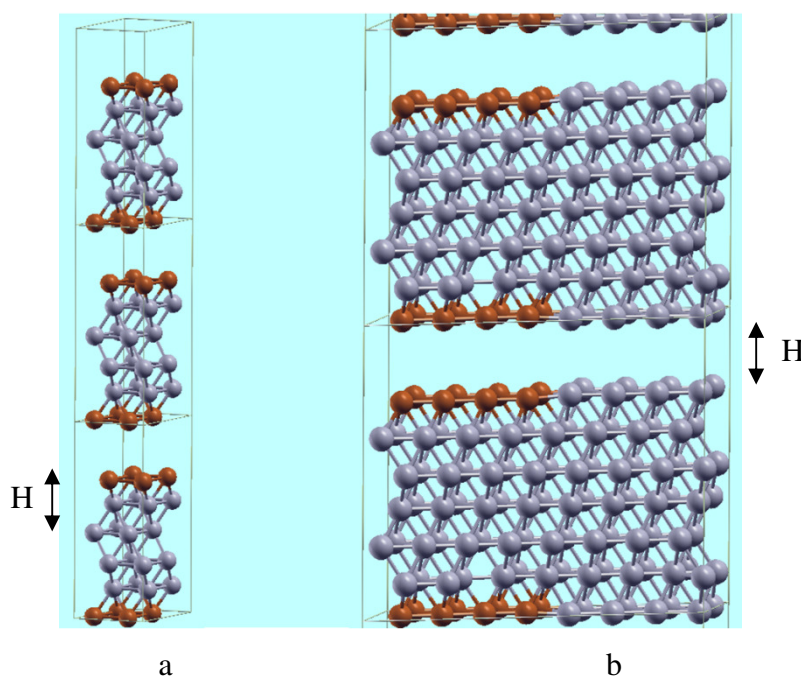
Figure 8-1. a. Slab model used as skin surface system that consists in monolayer metal M, (M = Ti, V, Fe, Co, Ni, Cu, Tc, Ru, Rh, Pd, Ag, Ta, W, Re, Os, Ir, and Au) sitting on a substrate of different chemical nature in this case pure Pt. The periodicity of the slab model in the z directions allows the separation between slabs, in this case of 5Å, and formation of a gap between films. b) Interface formed by the junction of M/Pt slab to a Pt slab.

The proposed system has two characteristics that may play an important role in the continuous race for downscaling of solid state devices; one refers to the basic physical phenomena occurring in the material and the second refers to the specific materials that compose the system. The physical phenomena are associated with

quantum tunneling, only explained by quantum mechanics; the material used is a metal composite, instead of silicon. The phenomenon of quantum tunneling may result in disadvantage or advantage for downscaling of electronic devices. Disadvantage in applications in which electron leakage is deleterious may occur as in the case of complementary metal-oxide semiconductor (CMOS) transistors where at the limit of 5-layer thick oxide results in a high leakage gate current due to tunneling effects from the gate into the film. Advantages in downscaling are expected for devices such as tunnel diode, and single electron transistors where quantum tunneling is the electron transfer mechanism. Since the scale at which quantum tunneling occurs is in the order of a few Angstroms, it seems like quantum tunneling is a key phenomenon of electron transfer mechanism suitable for the downscale of integrated circuits [92]. In the same downscale paradigm, the electronic devices will approach fundamental limits with the present pattern transfer technique, photolithography [93]. This fundamental limitation urges the development of devices based on new materials. Metals can be an alternative, since in general, they outperform the silicon based materials in terms of integration density, parasitic resistances, and fabrication costs due to the significantly higher conductivities, less short channel restrictions, and single step lithography process.

The literature and the technological application of the concept of electron tunneling are abundant and it is an active field in today's research activity. An early start was the idea of using Coulomb charging effects that appears due to the localization of individual electrons in islands between tunnel junctions for performing electronic functions at immensely higher densities. Likharev proposed transistors by controlling the

tunneling of electrons across double junction series by an applied bias [94], which was soon demonstrated by Dolan et al. [95]. This finding motivated the design of digital logic circuits in double-junctions using the Coulomb blockade effect which is the block of all tunnel events near zero bias voltage in series arrays of junctions[96]. This kind of transistor is called single electron transistor SET, the most studied device in the field of single charge electronics. In the fabrication of SET, metals are used to form the two small tunnel junctions connected in series that composed the transistor [97]. In addition to SET, other kind of metallic transistor has been proposed that uses the electric field effects on metallic nanotubes and planar metallic nanowire structures [98, 99].

8.3 Computational methods

Calculations were performed within the density functional theory (DFT) framework using the Vienna ab initio simulation package (VASP) [33-36]. Electron-ion interactions are described using the projector-augmented wave (PAW) method [47], expanded within a plane wave basis setting up a cutoff energy of 350 eV. Electron exchange and correlation effects were described by the Perdew-Burke-Ernzerhof (PBE) [11] generalized gradient approximation (GGA) type exchange correlation functional. Spin polarization was included in every simulation.

Two different systems were studied; both are represented as slab models infinite in the x and y directions and finite in z direction. One system consists of a periodically repeated fcc Pt slab covered by a monolayer of a metal M, (M = Ti, V, Fe, Co, Ni, Cu, Tc, Ru, Rh, Pd, Ag, Ta, W, Re, Os, Ir, Pt and Au); the system was modeled using 6

layers in 2×2 supercells. The other system consists of a periodically repeated fcc Pt slab where half of the system is covered by a monolayer of the same metals described before and the other half is pure Pt. This system was modeled using 7 layers in 2×8 supercells. Because of the periodic boundary conditions used in the three spatial directions, in the systems just described, the top (111) surface is separated a distance H from another (111) surface, the bottom layer of the slab in the top neighboring cell. Both kind of systems were relaxed at H = 12 Å, the top and bottom layers were allowed to relax, whereas the two layers in the middle for the case of 2×2 supercells and three layers in the middle for the case of 2×8 supercells were fixed, on the assumption that they represent a "bulk". After relaxation, the resultant atomic positions were fixed and the slab models were simulated at a slab separation of 5 Å where the surfaces interact; under these conditions and slab separation, the charge transfer in the interface and the charge in the gap between slabs were calculated. In order to calculate the amount of electrons in the gap between the slabs and the built-in potential along the gap between the slabs it is necessary to define the limits of the gap. Figure 8-2 shows the average potential along the direction perpendicular to the surfaces in the slab. The gap between slabs is defined starting at a distance Δz from the surface layer of one slab and ending at a distance Δz from the other slab surface as shown in the figure. The Δz distance is always half of the distance between the surface and subsurface of the slab model relaxed at 12 Å of slab separation.
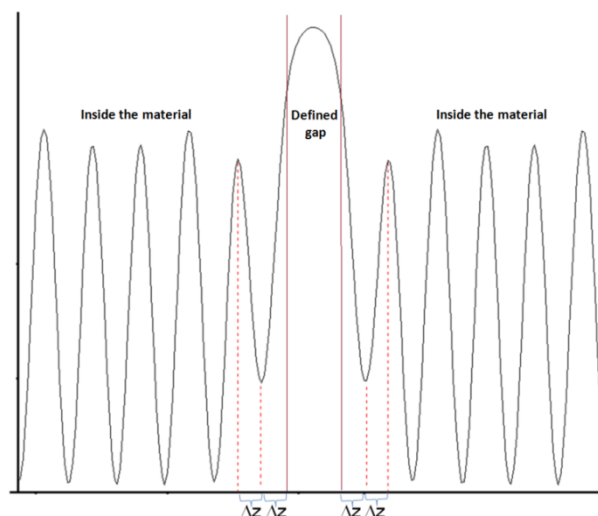
Figure 8-2. Average potential along the direction perpendicular to the surfaces. The gap that separates the metallic thin films is defined in this work starting at a distance Δz from the surface layer of one slab and ending at a distance Δz from the other slab surface. The Δz distance is always half of the distance between the surface and subsurface of the slab model relaxed at 12 Å of slab separation.

The optimum bulk lattice constant of Pt was determined as 3.98 Å, a value 1.45% higher than the experimental (3.92 Å).[48] Brillouin zone integration for the surface system was performed using a Monkhorst Pack grid [12] of 9×9×1 for the case of 2×2 supercells and 8×2×1 for the case of 2×8 supercells, and a Methfessel-Paxton[13] smearing of 0.2 eV. The convergence criteria for the electronic self-consistent iteration and the ionic relaxation loop were set to 10^{-4} eV and forces smaller than 0.01 eV/Å, respectively.

To calculate the total electronic charge of an atom we used the Bader analysis.[49, 50] This analysis defines an atom based on the electronic charge density using zero flux surfaces to divide atoms; the total electronic charge of an atom is approximately the charge enclosed within the Bader volume defined by zero flux surfaces.

8.4 Results and discussion

8.4.1 Electron density in the gap

Figure 8-3 represents a composite system, formed by a Ti/Pt skin slab joint in the y direction to a second region of pure Pt slab. Surface separation in both regions is 5Å. It was found that the electron density generated in the gap between the surfaces is different in each region of the system: there is a higher electron density in the region of Ti/Pt than in the pure Pt region. This difference in electron density between the two regions is expected to generate electrostatic and energetic phenomena that can be calculated. We illustrate this point by evaluation of electron density in the gap, work function of the system, electrostatic potential, and net charge transference in the junction. On the other hand, different skin metals are expected to generate different electron densities in each region, therefore different values of the above named phenomena.
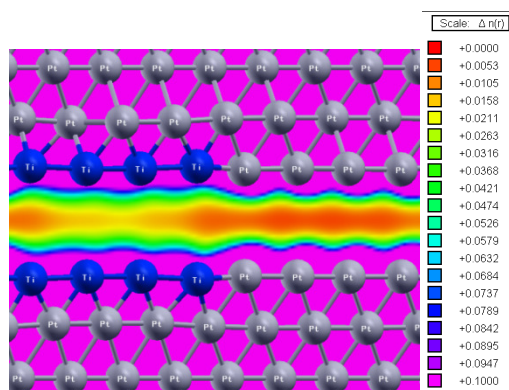
Figure 8-3. Non-uniform distribution of the electron density along the gap between metallic thin film surfaces; the separation between the thin films is 5Å. The non-uniform electron density distribution is due to the interfacial structure composed by a region delimited by Ti/Pt skin surfaces in contact with another region defined by pure Pt surfaces.

8.4.2 Reduction-oxidation reaction

Figure 8-4 shows the net charge change in the surface atoms for three systems: Ti/Pt; pure Pt and for the composite Ti/Pt joint to pure Pt.

The monolayer metal sitting on different core metal results in a reduction-oxidation reaction between the surface monolayer and the sub-surface layer from the core, which is reflected in the Ti/Pt skin system, case a, as a positive charge (0.48) indicating that Ti atoms lost electrons gained by Pt atoms, that is, a reduction-oxidation reaction occurred between the skin and the sub layer. In the case of pure Pt, case b, a negative electron density is shown indicating that the last layer atoms gain electrons as a

consequence of their low coordination number with respect to the bulk atoms. At the junction of the two systems, in case c, the net charge change in the surface atoms is significantly different indicating much higher electron transfer between Ti that loses electrons to Pt that gains electrons.

| a. | b. | c. |
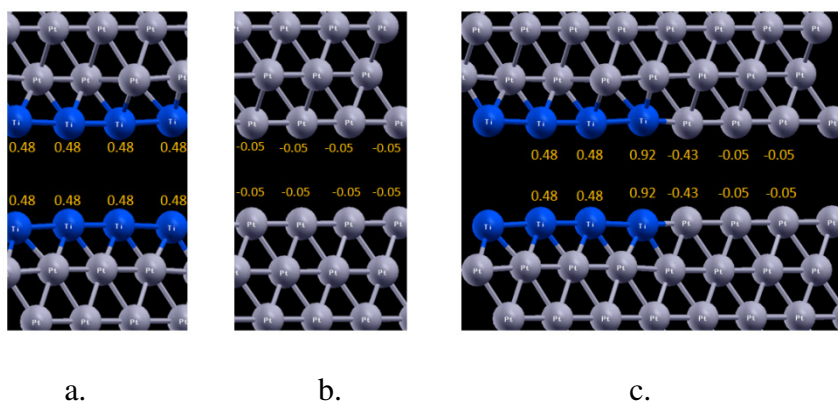
Figure 8-4. Sketch of systems: a. Ti/Pt; b. pure Pt and c. composite Ti/Pt joint to pure Pt. The net charge in each surface atom is shown. The net charge in the surface atoms forming the junction indicates a charge transfer at the interface as illustrated in case c. The Change of charge of the other atoms after forming the interface is negligible with the exception of the Pt atoms just below the junction with transfer charge of -012.

8.4.3 Metallic skin-surfaces of the type M/Pt:

Different metal skin-surfaces (M/Pt) were studied to determine the equilibrium amount of electrons in the gap between thin films and the minimum energy needed to

remove an electron from the material or work function of the system, as shown in Table 8-1.

Table 8-1. Amount of electrons in the gap and work function for various M/Pt skin systems

Metallic skin-surfaces	Amount of electrons in the gap	Work function of the system (eV)
Cu/Pt	1.93	4.71
Ag/Pt	1.82	4.74
Au/Pt	2.04	5.33
Ni/Pt	2.21	4.83
Pd/Pt	2.04	5.21
Pt	2.64	5.71
Co/Pt	2.41	4.66
Rh/Pt	2.64	5.17
Ir/Pt	3.28	5.65
Fe/Pt	2.46	4.45
Ru/Pt	3.13	5.22
Os/Pt	3.75	5.55
Tc/Pt	3.44	5.26
Re/Pt	3.92	5.47
W/Pt	3.97	5.45
V/Pt	3.04	4.49
Ta/Pt	3.70	5.10
Ti/Pt	2.75	4.37

The results show that the amount of electrons in the gap between metallic thin films and the work function of the system can be tuned by having a different metallic skin layer. With respect to pure Pt, the amount of electrons in the gap can increase or decrease by changing the surface chemical nature of the overlayer. On the other hand, the work function of each skin-surface system is always smaller than that of pure Pt.

The results of amount of electrons in the gap could be rearranged with respect to the position of the skin-metal in different periods of the atomic table, namely periods,

$4^{th}, 5^{th}$ and 6th as is shown in Figure 8-5. The trends indicate that the amount of electrons in the gap increases as the atomic number decreases in the same period. The average charge in the gap for metal skin systems of skin atoms pertaining to the same period in the periodic table was found to be a function of the period: 2.46 for n = 4; 2.61 for n = 5 and 3.32 for n =6. These results suggest that there is also a trend with respect to the period in the periodic table: the amount of electrons in the gap increases as the period n increases.
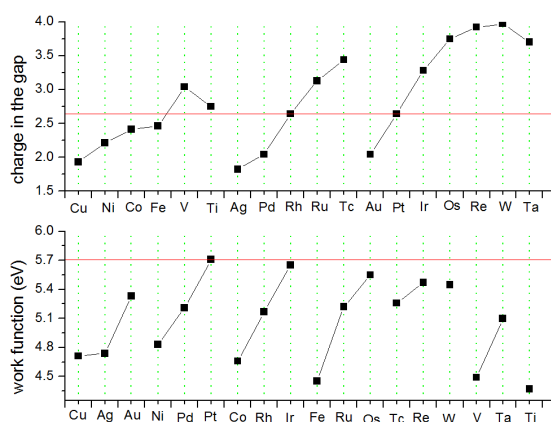
Figure 8-5. Top figure: amount of electrons in gap as a function of the overlayer element located in the same period in the periodic table;bottom figure: the work function in the same group in the periodic table. Red lines represent the amount of electrons in the gap and the work function of pure Pt.

In the framework of the periodic dependence of the results it appears reasonable to test a correlation between the amount of electrons in the gap and a property such as electronegativity. That is, a correlation may exist between the number of electrons separated from the surface to fill the gap and a chemical property that describes the tendency of an atom to attract electrons or electron density. It would be expected that the higher the electronegativity the smaller the number of electrons in the gap. In fact, for a given period of the periodic table, as the atomic number increases (Z increases) the electronegativity increases whereas the amount of electrons in the gap decreases. On the other hand, for a given group in the periodic table, as n increases, electronegativity decreases whereas the average number of electrons in the gap increases.

Furthermore, the number of electrons in the gap could be related with the number of unpaired electrons in the most external orbitals: the higher the number of unpaired electrons, the higher the mobility of electrons, the easier the electrons to separate from the surface to fill the gap, the higher the number of electrons in the gap. This was the case, for a given period, the number of unpaired electrons increases as Z decreases inasmuch as the number of electrons in the gap increases.

8.4.4 Composite M/Pt -Pt slab systems

By putting together a M/Pt slab and a Pt slab, the electrons in the system flow to new locations until an equilibrium is reached in which the Fermi energy, therefore the chemical potential, is equal in both slab regions. Most of the transference of electrons necessary to reach the equilibrium in the system occurs between the atoms located at the

interface; in the case shown in Figure 8-4c large part of the charge transfer occurs between Ti and Pt surface atoms at the interface.

At equilibrium, the electronic density in the gap is different in each region and, as a consequence, a potential barrier is formed in the gap, at the junction point, between the metal thin films in contact, as shown in Figure 8-6.
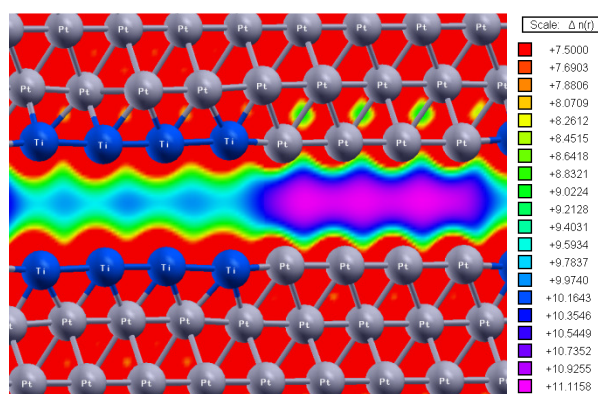
Figure 8-6. Electrostatic potential along the gap formed by the contact of a Ti/Pt skin surface system with an equivalent system made of pure Pt; the separation between the metallic thin films is 5 Å. Two regions with different electrostatic potential are clearly identified.

In the gap between metallic thin films, at the junction point, a built-in potential results in the y direction. Figure 8-7 shows an illustration of the electrostatic potential and the calculated planar average of the potential along the gap between the metallic thin

films at equilibrium for the case of a Ti/Pt system in contact with pure Pt. Two regions with different electrostatic potential are formed, and at the interface, there is a potential barrier or built-in potential, in this case of 0.257 eV, calculated as the difference between the average potential along the gap in the region of pure Pt surfaces and the average potential along the gap in the region of Ti/Pt surfaces.
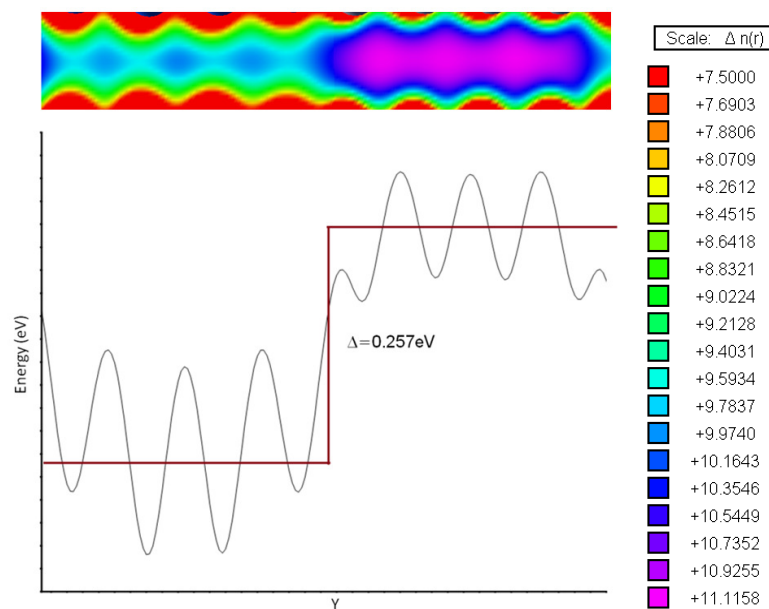
Figure 8-7. Electrostatic potential along the gap between metallic thin films and average electrostatic potential calculated along the gap defined as shown in Figure 8-2 for the Ti/Pt skin surface system in contact with pure Pt. A built-in potential of 0.257eV was calculated as the difference between the average potential along the gap in the region of pure Pt surfaces and the average potential along the gap in the region of Ti/Pt surfaces.

Table 8-2 lists the values of the built-in potential for several skin surfaces in contact with pure Pt; as well as the work function of the systems and the charge gained by the Pt atom at the interface. The built-in potential and the transference of charge may change up to one order of magnitude by varying the skin-metal. The work function of the system varies with the type of skin-metal M between the corresponding values for pure Pt and M/Pt system before contact.

Table 8-2. Built-in potential, work function of the system, and charge (in e) gained by Pt at the interface for various metal-skins.

Metallic skin-surfaces	Built-in Potential (eV)	Work function of the system (eV)	Charge gained by the Pt atom in the interface (ΔQ, in e)
Cu/Pt	0.052	5.27	0.14
Ag/Pt	0.17	5.19	0.12
Au/Pt	0.12	5.55	0.12
Ni/Pt	0.021	5.35	0.15
Pd/Pt	0.041	5.47	0.083
Pt	0	5.71	0.05
Co/Pt	0.059	5.24	0.18
Rh/Pt	0.027	5.49	0.094
Ir/Pt	-0.025	5.69	0.081
Fe/Pt	0.11	5.13	0.23
Ru/Pt	0.004	5.49	0.13
Os/Pt	0.012	5.63	0.13
Tc/Pt	0.067	5.46	0.19
Re/Pt	0.047	5.58	0.20
W/Pt	0.11	5.51	0.30
V/Pt	0.15	5.12	0.33
Ta/Pt	0.22	5.29	0.40
Ti/Pt	0.26	4.92	0.43

Data could be rearranged in search of a periodic tendency. In fact, if the atomic number is used as a key to reorder data, Figure 8-8 is obtained. It appears that both, the

built-in potential and the transferred charge, decrease in a given period of the atomic table as the atomic number, Z, decreases.

The tendencies of both values: the built-in potential and the charge gained by the Pt atom at the interface, with respect to the location in the periodic table are similar since the built-in potential in the gap is related with the transfer of charge at the interface necessary to reach the system equilibrium.
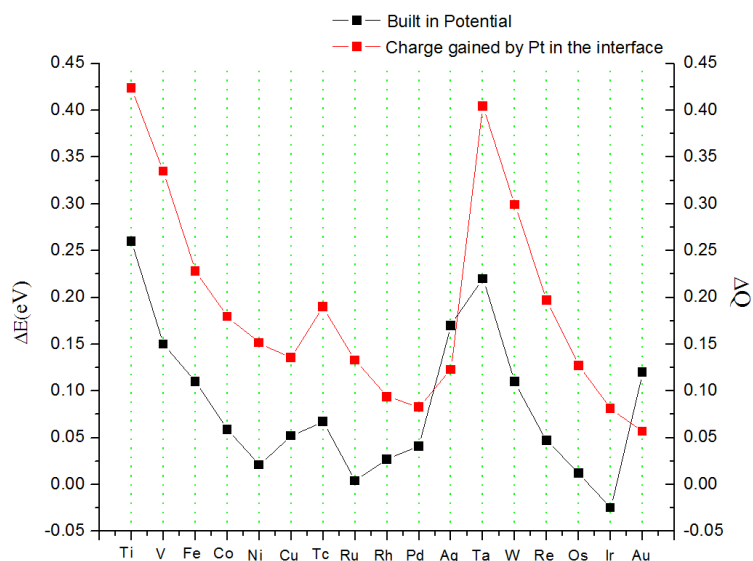
Figure 8-8. Built-in potential and charge gained by Pt atoms at the interface as a function of the overlayer element that form the interface with pure Pt organized in ascendant way with respect to the atomic number. Both trends are similar since the built-in potential in the gap is related with the transfer of charge at the interface necessary to reach the system equilibrium.

8.5 Conclusions

Reduction-oxidation reaction occurs between metallic atoms located in the skin and in the sub surface layer in a skin-metal system. An electron density appears in the gap if the thin films are separated in the range of 4 to 10Å.

By connecting M/Pt to pure Pt slabs in the y direction, a two-region system is formed in which electron transfer occurs at the junction point until the Fermi energy level, i.e., the chemical potentials are equal in both regions of the system. At equilibrium, the two regions have different electron density; therefore, also different electrostatic potential that generate a potential barrier or built-in potential at the junction. The built-in potential in the gap between metallic thin films, at the junction point, depends on the chemical nature of the overlayers forming the interface.

Values of electron density, work function of the system, and potential barrier seem to follow a tendency that can be ordered according to the periodic table and could be correlated to properties such as electronegativity and number of unpaired electrons in the most external orbitals.

The electrostatic barrier formed at the interface between the M/Pt and pure Pt systems, resembles a p-n junction and therefore opens a great opportunity for electronic applications of this kind of a system.

9. CONCLUSIONS AND RECOMENDATIONS

Descriptive and analytical models of the physical state of systems composed by thin metallic films of various chemical composition separated at distance in the order of 4 to 12 Angstroms were developed by solving a many body time independent Schrödinger equation applied to these systems using Density Functional Theory and also by a simplified quantum mechanics analysis.

It was concluded that at certain intermediate distance, in the mentioned distance range, interaction occurs between surfaces due to electron tunneling through the energy barrier that separates both metallic thin film surfaces. The correspondent electron density and electronic, energy and momentum distributions were calculated by DFT and basic quantum mechanics.

Those features of the modeled systems may be tuned through film parameters such as thickness, separation between films, and chemical nature of the surface and subsurface. Those features of the modeled systems induce changes in the mechanical and chemical environment in the gap between surfaces, completely different from those of the films at large distances, therefore generating a potential for technological applications.

The study of the effect of the electronic environment on different molecules present inside the gap between thin films, leads to the conclusion that the electron density in the gap modifies the normal geometrical and electronic structure of molecules placed in the gap. These distortions can be tuned with the variables described above:

thin film thickness, separation between thin films and chemical nature. In particular, the effect of having molecular oxygen, water and ethylene inside the gap between metallic thin films was studied. In the case of molecular oxygen, it was found that dissociation energy can be tuned by changing the separation between thin films and changing the chemical nature of both, the surface and overlayer of the thin film. In the case of water, it was found that by tuning the chemical nature of the surface and sub-surface of both metallic thin films, water dissociation can be propitiated. In the case of an ethylene molecule located in the gap between Ti/Pt thin films, the molecule is distorted into an anion radical adopting the geometry and structure of an active monomer sufficient to initiate polymerization towards a polyethylene chain. All of these results support the idea of using two metallic thin films separated by short distances as a novel catalyst for technological applications.

It was demonstrated that the interaction between metallic thin films separated by short distances plays a role in the energetic competition between the electron-electron exchange and the kinetic energy of electrons that defines the magnetic properties. The case studied was Ti/Pt thin film interacting with a Pt thin film. In this system, the magnetic moment decreases as the separation between thin films decreases. The phenomenon was explained by the changes observed in the number of electronic states at the Fermi level and in the exchange splitting as a function of separation between films. These changes resulted from the interaction between both metallic thin film surfaces.

It was proposed a system that resembles a p-n junction consisting in a junction of two metallic thin films having different chemical nature by having different metal atoms

in the overlayer surface. The system generates different electronic density in the gap between surfaces. The result is a two-region system in the same gap between metallic thin films with different electrostatic potential. This proposed system can be the building blocks for many electronic applications.

It is also concluded that even though there are uncertainties due to the approximations used to solve the Schrödinger equation, related with the unknown exchange correlation potential and the numerical methods implemented, and also simplifications of the systems, the results, obtained and reported in this work, are consistent with quantum mechanics theories and with some experimental results found by others.

For a theoretical work, the first recommendation may be to confront the results by physical experiments. A second recommendation is to revise and improve the theoretical analysis. A third recommendation would be to include variations in the systems or in the condition variables such as temperature and external potentials for further research to test general conclusions and to study limit cases.

With this guide, future work is proposed:

- To look for better results by using the continuous improvements of DFT calculations accuracy in order to eventually provide more reliable information to compare with experimental data. New corrected DFT functionals that includes more physical information $(n, \nabla n, \nabla^2 n)$ or the exact exchange (i.e, hybrid functionals) should be tested to decide if it is worthy to use them always taking into account the competing demands

between numerical and physical accuracy with increased computational time. These corrected functionals should describe better the band gaps and Van der Waals interactions.

- How stable are the systems proposed as catalysts and nanoelectronic devices? Phenomena such as segregation, dissolution, delamination, fracture, and film buckling may alter and or destroy the physical predictions in the proposed systems. Almost all of these phenomena can be studied theoretically; in fact, similar questions for catalysts used to improve the Oxygen reduction reaction for fuel cells have been answered with computational methods similar to those used in this work [100-103].

- How temperature will affect the physical predictions presented in this work? It is expected that the atomic vibration at temperatures greater than zero will affect the stability of the systems; especially, because the proposed systems are in a transition zone. It is hypothesized that temperature will change the separation range between the thin films at which the surfaces interact but not the basic physical predictions derived from this work. In addition, the kinetics of the chemical reactions described in this work will depend on temperature. It is recommended to explore possible answers for this question using ab initio molecular dynamics since the temperature dynamical trajectories of atoms are generated by using forces computed by DFT electronic calculations.

- What happens if an external potential is applied to the system? In order to have a real electronic device, external potential or bias must be applied. The proposed devices resemble physical properties of real devices just in equilibrium without external potential. It is recommended to study the effect of external potential by adding an electric field in the system; this can be implemented in VASP calculations. In addition, it will be interesting to explore the effect of an external potential on the physical properties of electrons and molecules located in the gap between thin films in search of possible control of tunneling of electrons in junctions.

- How defects can affect the physical properties of the proposed systems? It is well known that defects such as impurities, vacancies, dislocations, etc, change the physical properties of materials, for instance, the activity of catalysts. It is recommended to study with more detail the effect of defects in the proposed systems.

REFERENCES

1.   S. Chen, H. A. Gasteiger, K. Hayakawa, T. Tada and Y. Shao-Horn, Platinum-alloy cathode catalyst degradation in proton exchange membrane fuel cells: nanometer-scale compositional and morphological changes, *Journal of the Electrochemical Society*, 2010, **157**, A82-A97.

2.   P. Mani, R. Srivastava and P. Strasser, Dealloyed binary PtM3 (M = Cu, Co, Ni) and ternary PtNi3M (M = Cu, Co, Fe, Cr) electrocatalysts for the Oxygen reduction reaction: performance in polymer electrolyte membrane fuel cells, *Journal of Power Sources*, 2011, **196**, 666-673.

3.   M. H. Shao, K. Shoemaker, A. Peles, K. Kaneko and L. Protsailo, Pt mono layer on porous Pd-Cu alloys as Oxygen reduction electrocatalysts, *Journal of the American Chemical Society*, 2010, **132**, 9253-9255.

4.   E. Principi, A. Witkowska, S. Dsoke, R. Marassi and A. D. Cicco, An XAS experimental approach to study low Pt content electrocatalysts operating in PEM fuel cells, *Physical Chemistry Chemical Physics*, 2009, **11**, 9987-9995.

5.   Y. Okawa, S. K. Mandal, C. Hu, Y. Tateyama, S. Goedecker, S. Tsukamoto, T. Hasegawa, J. K. Gimzewski and M. Aono, Chemical wiring and soldering toward all-molecule electronic circuitry, *Journal of the American Chemical Society*, 2011, **133**, 8227-8233.

6.   S. K. Mandal, Y. Okawa, T. Hasegawa and M. Aono, Rate-determining factors in the chain polymerization of molecules initiated by local single-molecule excitation, *ACS Nano*, 2011, **5**, 2779-2786.

7.   M. A. Mahmoud, F. Saira and M. A. El-Sayed, Experimental evidence for the nanocage effect in catalysis with hollow nanoparticles, *Nano Letters*, 2010, **10**, 3764-3769.

8.   S. M. Morton, D. W. Silverstein, and L. Jensen, Theoretical studies of plasmonics using electronic structure methods, *Chemical Reviews*, 2011, **111**, 3962-3994.

9.   P. Hohenberg and W. Kohn, Inhomogeneous electron gas, *Physical Review*, 1964, **136**, B864.

10. W. Kohn and L. J. Sham, Self-consistent equations including exchange and correlation effects, *Physical Review*, 1965, **140**, A1133.

11. J. P. Perdew, K. Burke and M. Ernzerhof, Generalized gradient approximation made simple, *Physical Review Letters*, 1996, **77**, 3865.

12. H. J. Monkhorst, and J. D. Pack, Special points for Brillouin-zone integrations, *Physical Review B*, 1976, **13**, 5188-5192.

13. M. Methfessel, and A. T. Paxton, High-precision sampling for Brillouin-zone integration in metals, *Physical Review B*, 1989, **40**, 3616-3621.

14. A. E. Mattsson, R. Armiento, J. Pair, G. Kresse, J. M. Wills and T. R. Mattsson, The AM05 density functional applied to solids, *Journal of chemical physics,* 2008, **128**, 084714.

15. J. P. Perdew, A. Ruzsinszky, G. I. Csonka, O. A. Vydrov, G. E. Scuseria, L. A. Constantin, X. Zhou and K. Burke, Restoring the density-gradient expansion for exchange in solids and surfaces, *Physical Review Letters*, 2008, **100**, 136406.

16. J. Paier, R. Hirschl, M. Marsman and G. Kresse, The Perdew-Burke-Ernzerhof exchange-correlation functional applied to the G2-1 test set using a plane-wave basis set, *Journal of chemical physics,* 2005, **122**, 234102.

17. J. Paier, M. Marsman, K. Hummer, G. Kresse, I. C. Gerber and J. G. Angyan, Screened hybrid density functionals applied to solids, *Journal of chemical physics,* 2006, **124**, 154709.

18. C. M. Mate, G. M. McClelland, R. Erlandsson and S. Chiang, Atomic-scale friction of a tungsten tip on a graphite surface, *Physical Review Letters*, 1987, **59**, 1942.

19. S. C. Langford, D. L. Doering and J. T. Dickinson, Production of free charge carriers during fracture of single-crystal silicon, *Physical Review Letters*, 1987, **59**, 2795.

20. J. H. Rose, J. Ferrante and J. R. Smith, Universal binding energy curves for metals and bimetallic interfaces, *Physical Review Letters*, 1981, **47**, 675.

21. J. H. Rose, J. R. Smith and J. Ferrante, Universal features of bonding in metals, *Physical Review B*, 1983, **28**, 1835.

22. A. Banerjea and J. R. Smith, Origins of the universal binding-energy relation, *Physical Review B*, 1988, **37**, 6632.

23. J. R. Smith, G. Bozzolo, A. Banerjea and J. Ferrante, Avalanche in adhesion, *Physical Review Letters*, 1989, **63**, 1269.

24. P. A. Taylor, J. S. Nelson and B. W. Dodson, Adhesion between atomically flat metallic surfaces, *Physical Review B*, 1991, **44**, 5834.

25. C. M. Zicovich-Wilson, A. Corma and P. Viruela, Electronic confinement of molecules in microscopic pores. A new concept which contributes to the explanation of the catalytic activity of zeolites, *Journal of Physical Chemistry*, 1994, **98**, 10863-10870.

26. F. Marquez, H. Garcia, E. Palomarez, L. Fernandez and A. Corma, Spectroscopic evidence in support of the molecular orbital confinement concept: case of Anthracene incorporated in zeolites, J*ournal of the American Chemical Society*, 2000, **122**, 6520-6521.

27. E. A. A. Jarvis, R. L. Hayes, and E. A. Carter, Effects of Oxidation on the nanoscale mechanisms of crack formation in Aluminum, *ChemPhysChem*, 2001, **2**, 55-59.

28. P. Lazar and R. Podloucky, Cleavage fracture of a crystal: Density functional theory calculations based on a model which includes structural relaxations, *Physical Review B*, 2008, **78**, 104114.

29. T. Atay, J.-H. Song and A. V. Nurmikko, Strongly interacting plasmon nanoparticle pairs: from dipole−dipole interaction to conductively coupled regime, *Nano Letters*, 2004, **4**, 1627-1631.

30. J. Zuloaga, E. Prodan and P. Nordlander, Quantum description of the plasmon resonances of a nanoparticle dimer, *Nano Letters*, 2009, **9**, 887-891.

31. R. de L. Kronig and W. G. Penney, Quantum mechanics of electrons in crystal lattices, *Proceedings of the Royal Society*, 1931, **A130**, 499.

32. P. -f. Yuh and K. L. Wang, Formalism of the Kronig-Penney model for superlattices of variable basis, *Physical Review B*, 1988, **38**, 13307.

33. G. Kresse and J. Furthmüller, Efficient iterative schemes for ab initio total-energy calculations using a plane-wave basis set, *Physical Review. B*, 1996, **54**, 11169-11186.

34. G. Kresse and J. Furthmüller, Efficiency of ab-initio total energy calculations for metals and semiconductors using a plane-wave basis set, *Computational Materials Science*, 1996, **6**, 15-50.

35. G. Kresse and J. Hafner, Ab initio molecular dynamics for liquid metals, *Physical Review B*, 1993, **47**, 558-561.

36. G. Kresse and J. Hafner, Ab initio molecular-dynamics simulation of the liquid-metal–amorphous-semiconductor transition in germanium, *Physical Review B*, 1994, **49**, 14251-14269.

37. G. E. Ramirez-Caballero and P.B. Balbuena, Effect of confinement on oxygen adsorbed between Pt(111) surfaces, *Journal of Physical Chemistry C*, 2009, **113**, 7851-7856.

38. G. E. Ramirez-Caballero and P.B. Balbuena, Confinement effects on alloy reactivity, *Physical Chemistry Chemical Physics*, 2010, **12**, 12466-12471.

39. G. E. Ramirez-Caballero, A. Mathkari and P. B. Balbuena, Confinement-induced polymerization of ethylene, *Journal of Physical Chemistry C*, 2011, **115**, 2134-2139.

40. G. E. Ramirez-Caballero and P. B. Balbuena, Confinement-induced changes in magnetic behavior of a Ti monolayer on Pt, *Chemical Physics Letters*, 2010, **507**, 117-121.

41. N. J. Halas, S. Lal, W. S. Chang, S. Link and P. Nordlander, Plasmons in strongly coupled metallic nanostructures, *Chemical Reviews*, 2011, **111**, 3913-3961.

42. *Introduction to Surface Chemistry and Catalysis*, G. A. Somorjai, John Wiley & Sons, Inc, New York ,1994.

43. N. Tian, Z. Y. Zhou and S. G. Sun, Platinum metal catalysts of high-index surfaces: from single-crystal planes to electrochemically shape-controlled nanoparticles, *Journal of Physical Chemistry C*, 2008, **112**, 19801-19817.

44. S. Chen, W. Sheng, N. Yabuuchi, P. J. Ferreira, L. F. Allard and Y. Shao-Horn, Origin of Oxygen reduction reaction activity on "Pt3Co" nanoparticles: atomically resolved chemical compositions and structures, *Journal of Physical Chemistry C*, 2008. **113,** 1109-1125.

45. C. Stampfl, M. V. Ganduglia-Pirovano, K. Reuter and M. Scheffler, Catalysis and corrosion: the theoretical surface-science context, *Surface Science*, 2002, **500**, 368-394.

46. P. P. Dholabhai, R. Atta-Fynn and A. K. Ray, An ab initio study of the adsorption and dissociation of molecular oxygen on the (0001) surface of double hexagonal close-packed americium, *Physica B*, 2008, **403**, 4269-4280.

47. P. E. Blochl, Projector augmented-wave method, *Physical Review B*, 1994, **50**, 17953-17979.

48. *Handbook of Chemistry and Physics*, ed. D. R. E. Lide, CRC Press, Boca Raton, 1997.

49. G. Henkelman, A. Arnaldsson and H. Jónsson, A fast and robust algorithm for Bader decomposition of charge density, *Computational Materials Science*, 2006, **36**, 354-360.

50. E. Sanville, S. D. Kenny, R. Smith and G. Henkelman, Improved grid-based algorithm for Bader charge allocation, *Journal of Computational Chemistry*, 2007, **28**, 899-908.

51. J. L. Gland, B. A. Sexton and G. B. Fisher, Oxygen interactions with the Pt (111) surface, *Surface Science*, 1980, **95**, 587-602.

52. Y. T. Yeo, L. Vattuone and D. A. King, Calorimetric heats for CO and Oxygen adsorption and for the catalytic CO oxidation reaction on Pt(111), *Journal Chemical Physics*, 1997, **106**, 392-401.

53. D. H. Parker, M. E. Bartram and B. E. Koel, Study of high coverages of atomic Oxygen on the Pt(111) surface, *Surface Science*, 1989, **217**, 489.

54. Y. Ma and P. B. Balbuena, Surface properties and dissolution trends of Pt_3M alloys in the presence of adsorbates, *Journal of Physical Chemistry C*, 2008, **112**, 14520-14528.

55. A. Eichler, F. Mittendorfer and J. Hafner, Precursor-mediated adsorption of oxygen on the (111) surfaces of platinum-group metals, *Physical Review B*, 2000, **62**, 4744-4755.

56. T. Li and P.B. Balbuena, Computational studies of the interactions of oxygen with platinum clusters, *Journal of Physical Chemistry B*, 2001, **105**, 9943-9952.

57. P. Gambardella, Z. Sljivancanin, B. Hammer, M. Blanc, K. Kuhnke and K. Kern, Oxygen dissociation at Pt steps, *Physical Review Letters*, 2001, **87**, 056103.

58. L. Aballe, A. Barinov, N. Stojic, N. Binggeli, T. O. Mentes, A. Locatelli and M. Kiskinova, The electron density decay length effect on surface reactivity, *Journal of Physics-Condensed Matter*, 2010, **22**, 015001.

59. Q. X. Li and S. L. Simon, Surface chemistry effects on the reactivity and properties of nanoconfined Bisphenol M Dicyanate ester in controlled pore glass, *Macromolecules*, 2009, **42**, 3573-3579.

60. A. Borgoo, D. J. Tozer, P. Geerlings and F. D. Proft, Confinement effects on excitation energies and regioselectivity as probed by the Fukui function and the molecular electrostatic potential, *Physical Chemistry Chemical Physics*, 2009, **11**, 2862-2868.

61. L. Aballe, A. Barinow, A. Locatelli, S. Heun and M. Kiskinova, Tuning surface reactivity via electron quantum confinement, *Physical Review Letters*, 2004, **93**, 196103.

62. A. Michels, J. D. Boer and A. Bijl, Remarks concerning molecular interaction and their influence on the polarisability, *Physica*, 1937, **4**, 981-994.

63. N. A. Aquino, Accurate energy eigenvalues for enclosed hydrogen atom within spherical impenetrable boxes, *International Journal of Quantum Chemistry*, 1995, **54**, 107-115.

64. N. Aquino, G. Campoy and H. E. Montgomery Jr., Highly accurate solutions for the confined hydrogen atom, *International Journal of Quantum Chemistry*, 2007, **107**, 1548-1558.

65. N. Aquino, J. Garza, A. Flores-Riveros, J. F. Rivas-Silva and K. D. Sen, Confined helium atom low-lying S states analyzed through correlated Hylleraas wave functions and the Kohn-Sham model, *The Journal of Chemical Physics*, 2006, **124**, 054311.

66. A. Corma, H. Garcia, G. Sastre and P. M. Viruela, Activation of molecules in confined spaces: an approach to zeolite-guest supramolecular systems, *The Journal of Physical Chemistry B*, 1997, **101**, 4575-4582.

67. A. F. Kovalenko, E. N. Sovyak and M. F. Holovko, On the quantum properties of adsorbed particles within the model of a hydrogen atom near a hard wall, *International Journal of Quantum Chemistry*, 1992, **42**, 321-337.

68. J. Planelles, C. Zicovich-Wilson, W. Jaskolski and A. Corma, Semiempirical Hamiltonians for spatially confined pi-electron systems, *International Journal of Quantum Chemistry*, 1996, **60**, 971-981.

69. J. M. Lenhardt, M. T. Ong, R. Choe, C. R. Evenhuis, T. J. Martinez and S. L. Craig, Trapping a diradical transition state by mechanochemical polymer extension, *Science*, 2010, **329**, 1057-1060.

70. J. A. Lipton-Duffin, J. A. Miwa, M. Kondratenko, F. Cicoira, B. G. Sumpter, V. Meunier, D. F. Perepichka and F. Rosei, Step-by-step growth of epitaxially aligned polythiophene by surface-confined reaction, *Proceedings of the National Academy of Sciences of the United States of America*, 2010, **107**, 11200-11204.

71. A. Borgoo, D. J. Tozer, P. Geerlings and F. De Proft, Influence of confinement on atomic and molecular reactivity indicators in DFT, *Physical Chemistry Chemical Physics*, 2008, **10**, 1406-1410.

72. S. Blügel, Two-Dimensional ferromagnetism of 3d, 4d, and 5d transition-metal monolayers on noble-metal (001) substrates, *Physical Review Letters*, 1992, **68**, 851-854.

73. S. Blügel, Ferromagnetism of 4d-metal monolayers on Ag, Au and Pd(001) surfaces, *Europhysics Letters*, 1992, **18**, 257-262.

74. S. Blügel and P. H. Dederichs, Ferromagnetism and antiferromagnetism of 3d metal overlayers on noble-metal substrates, *Europhysics Letters*, 1989, **9**, 597-602.

75. S. Blügel, B. Drittler, R. Zeller and P. H. Dederichs, Magnetic-properties of 3d transition-metal monolayers on metal substrates, *Applied Physics a-Materials Science & Processing*, 1989, **49**, 547-562.

76. D. Hennig, M. V. Ganduglia-Pirovano and M. Scheffler, Adlayer core-level shifts of admetal monolayers on tranistion-metal substrates and their relation to the surface chemical reactivity, *Physical Review B*, 1996, **53**, 10344-10347.

77. G. Liu, T. P. S. Clair and D. W. Goodman, An XPS study of the interaction of ultrathin Cu films with Pd(111), *Journal of Physical Chemistry B*, 1999, **103**, 8578-8582.

78. G. E. Ramirez-Caballero, Y. Ma, R. Callejas-Tovar and P. B. Balbuena, Surface segregation and stability of core-shell alloy catalysts for oxygen reduction in acid medium, *Physical Chemistry Chemical Physics*, 2010, **12**, 2209-2218.

79. J. M. Essen, J. Haubrich and C. Becker, Adsorption of ethene on Pt(111) and ordered PtxSn/Pt(111) surface alloys: A comparative HREELS and DFT investigation, *Surface Science*, 2007, **601**, 3472-3480.

80. R. Gomez, J. Solla-Gullon, J. M. Perez and A. Aldaz, Surface-enhanced Raman spectroscopy study of ethylene adsorbed on a Pt electrode decorated with Pt nanoparticles, *Chemphyschem*, 2005, **6**, 2017-2021.

81. T. Jacob and W. A. Goddard, Chemisorption of (CHx and C2Hy) hydrocarbons on Pt(111) clusters and surfaces from DFT studies, *Journal of Physical Chemistry B*, 2005, **109**, 297-311.

82. S. D. Bader, Magnetism in low dimensionality, *Surface Science*, 2002, **500**, 172-188.

83.   P. Ferriani, S. Heinze, G. Bihlmayer and S. Blügel, Unexpected trend of magnetic order of 3d transition-metal monolayers on W(001), *Physical Review B*, 2005, **72**, 024452.

84.   A. Kubetzka, P. Ferriani, M. Bode, S. Heinze, G. Bihlmayer, K. V. Bergmann, O. Pietzsch, S. Blügel and R. Wiesendanger, Revealing Antiferromagnetic Order of the Fe Monolayer on W(001): Spin-Polarized Scanning Tunneling Microscopy and First-Principles Calculations, *Physical Review Letters*, 2005, **94**, 087204.

85.   E. C. Stoner, Collective electron ferromagnetism II. Energy and specific heat, *Proceedings of the Royal Society of London Series a-Mathematical and Physical Sciences*, 1939, **169**, 0339-0371.

86.   E. C. Stoner, Collective electron ferromagnetism, *Proceedings of the Royal Society of London Series a-Mathematical and Physical Sciences*, 1938, **165**, 0372-0414.

87.   R. Zeller, Spin-Polarized DFT Calculations and Magnetism, in Computational Nanoscience: Do It Yourself!, J. Grotendorst, S. Blügel, and D. Marx, Editors, *John von Neumann Institute for Computing, NIC Series: Julich*, 2006, 419-445.

88.   J. G. Chen, C. A. Menning and M. B. Zellner, Monolayer bimetallic surfaces: Experimental and theoretical studies of trends in electronic and chemical properties, *Surface Science Reports*, 2008, **63**, 201-254.

89.   *The Physics and Chemistry of Materials,* J. I. Gersten and F. W. Smith, Jhon Wiley & Sons Inc, New York, 2001.

90.   J. F. Janak, Uniform susceptibilities of metallic elements, *Physical Review B*, 1977, **16**, 255-262.

91.   V. Bellini, N. Papanikolaou, R. Zeller and P. H. Dederichs, Magnetic 4d monoatomic rows on Ag vicinal surfaces, *Physical Review B*, 2001, **64**, 094403.

92.   T. Skotnicki, J. A. Hutchby, T. J. King, H. -S. P. Wong and F. Boeuf, The End of CMOS Scaling: Toward the Introduction of New Materials and Structural Changes to Improve MOSFET Performance, *IEEE Circuits and Devices Magazine*, 2005, **21**, 16-26.

93.   S. E. Thompson and S. Parthasarthy, Moore's law: the future of Si microelectronics, *Materials Today*, 2006, **9**, 20-25.

94.   K. Likharev, Single-electron transistors: Electrostatic analogs of the DC SQUIDS, *Magnetics IEEE transactions*, 1987, **23**, 1142-1145.

95.   T. A. Fulton and G. J. Dolan, Observation of single-electron charging effects in small tunnel junctions, *Physical Review Letters*, 1987, **59**, 109.

96.   J. R. Tucker, Complementary digital logic based on the "Coulomb Blockade", *Journal of Applied Physics*, 1992, **72**, 4399-4413.

97.   T. Wagner, W. Krech, B. Frank, H. Muhlig, H. -J. Fuchs and U. Hubner, Fabrication and measurement of metallic single electron transistors, *Applied Superconductivity IEEE Transactions*, 1999, **9**, 1051-8223.

98.   S. V. Rotkin and K. Hess, Principles of metallic field effect transistor, *in Technical Proceedings of the 2004 NSTI Nanotechnology Conference and Trade Show*, 2004.

99.   H. H. Cheng, C. N. Andrew and M. M. Alkaisi, The fabrication and characterisation of metallic nanotransistors, *Microelectronic Engineerin,* **83**, 1749-1752.

100.   G. E. Ramirez-Caballero and P. B. Balbuena, Dissolution-Resistant Core-Shell Materials for Acid Medium Oxygen Reduction Electrocatalysts, *Journal of Physical Chemistry Letters*, **1**, 724-728.

101. G. E. Ramirez-Caballero, P. Hirunsit and P. B. Balbuena, Shell-anchor-core structures for enhanced stability and catalytic oxygen reduction activity, *Journal of Chemical Physics*, 2010, **133**, 134705.

102. G. E. Ramirez-Caballero and P. B. Balbuena, Surface segregation of core atoms in core–shell structures, *Chemical Physics Letters*, 2008, **456**, 64-67.

103. G. E. Ramirez Caballero and P. B. Balbuena, Surface segregation phenomena in Pt–Pd nanoparticles: dependence on nanocluster size, *Molecular Simulation*, 2006, **32**, 297-303.

VITA

Name: Gustavo Emilio Ramirez Caballero

Address: Jack E. Brown Engineering Bldg,
                 3122 TAMU Room 620,
                 College Station, TX 77843-3122

Email Address: gwatara@gmail.com

Education: B.A., Universidad Industrial de Santander,
                 Bucaramanga, Colombia, 2006
                 Ph.D., Material Science and Engineering,
                 Texas A&M University, 2011